A model of large-scale instabilities in the Jovian troposphere

by

Yvan Orsolini

A thesis submitted in partial fulfillment
of the requirements for the degree of

Doctor of Philosophy

University of Washington

1991

Approved by _____
(Chairperson of Supervisory Committee)

_____

_____

Program Authorized
to Offer Degree GEOPHYSICS

Date July 15, 1991

Doctoral Dissertation

In presenting this dissertation in partial fulfillment of the requirements for the Doctoral degree at the University of Washington, I agree that the Library shall make its copies freely available for inspection. I further agree that extensive copying of this dissertation is allowable only for scholarly purposes, consistent with "fair use" as prescribed in the U.S. Copyright Law. Requests for copying or reproduction of this dissertation may be referred to University Microfilms, 300 North Zeeb Road, Ann Arbor, Michigan 48106, to whom the author has granted "the right to reproduce and sell (a) copies of the manuscript in microform and/or (b) printed copies of the manuscript made from microform."

Signature Joan T. Orsillo

Date July 15, 91

© Copyright 1991

Yvan J. Orsolini

University of Washington

Abstract

A MODEL OF LARGE-SCALE INSTABILITIES IN THE JOVIAN TROPOSPHERE

by Yvan Joseph Orsolini

Chairperson of Supervisory Committee : Professor Conway B. Leovy
Department of Atmospheric Sciences

The cloud-top circulation of Jupiter is characterized by latitudinal cloud bands and near-steady jets which decay with height. We developed a quasi-geostrophic mid-latitude beta-plane model to study whether the jet decay and meridional circulations are driven by large-scale instabilities of a deep zonal flow extending upward into the troposphere of Jupiter. Linear barotropic and baroclinic instabilities of simple analytic zonal flows thought to be representative of the Jovian tropospheric circulation are investigated.

When the vertical shear zones are not too thin, the shear confines disturbances which are essentially barotropic, and reduces their growth rates; the westward jets are the most unstable and the eastward jets are readily stabilized by a weak shear. The instabilities are associated with residual mean meridional circulations : they consist of a bottom cell with rising motions on the anticyclonic side of the jet, and an opposite cell stacked above it. The least unstable flows are shown to have a Burger number one at the most. A regime of baroclinic instability arises for narrower shear zones.

A quasi-linear model was also used to investigate how an initially barotropically unstable flow develops a steady shear zone in the lower scale heights as a result of the action of the eddy fluxes. The instabilities are then acting as a vertical drag term and the jets decay to a non-zero barotropic component. In the equilibrated state, the eddy to mean flow kinetic energy ratio is about 20 % for westward jets and less than 1% for eastward jets. For adjacent jets, unstable modes can propagate meridionally into the core of eastward jet and contribute to the jet decay even if it is stable.

We also introduce a Rayleigh drag, forcing the mean flow back to its unstable state, while the eddies are damped radiatively. When the forcing time scale is the same as the radiative damping time, we found an asymmetric life-cycle type of behavior, with the eddy energy growing quickly to saturation and decaying slowly. For faster forcings, the eddy energy can be steady, and there are time-averaged eddy fluxes which drive meridional circulations.

TABLE OF CONTENTS

Page

List of Figures.....v

List of Tables.....viii

Chapter 1 INTRODUCTION.....1

1.1. Statement of the problem.....1

1.2. Method and overview.....5

Chapter 2 OBSERVATIONAL CONSTRAINTS.....8

2.1. Introduction.....8

2.2. Composition.....9

2.3. Cloud Structure.....13

2.4. Thermal Structure.....19

2.4.1 Vertical Thermal Structure.....19

2.4.2. Horizontal Structure.....21

2.4.3. Radiative Time Constant.....22

2.5. Wind Observations.....23

2.6. Do we have a Picture of the Zone/Belt Structure?.....28

Chapter 3 LINEAR INSTABILITIES.....39

3.1. Introduction.....39

3.1.1. Previous Studies of the Instability Problem.....39

3.1.2. Model Description.....41

3.2. Barotropic Effects.....47

3.2.1. Barotropic Westward Jets.....47

3.2.2. Decaying Westward Jets.....51

3.2.3. Decaying Eastward Jets.....56

3.3. Barotropic and Baroclinic Effects.....57

3.3.1. Baroclinic Instability.....57

3.3.2. A Stability Parameter.....62

3.3.3. Transition Between Barotropic and Baroclinic Instabilities.....64

3.3.4. Pattern of Heat and Momentum Fluxes.....64

3.4. Discussion.....66

Chapter 4 QUASI-LINEAR MODELS.....97
4.1. Introduction.....97
4.1.1. Comments on the Use of Quasi-Linear Models.....97
4.1.2. Model Description.....100
4.2. Westward Jets.....103
4.2.1. Equilibration and Vacillations.....103
4.2.2. Comparison with Pirraglia.....104
4.2.2.1. Mean Zonal Velocities.....105
4.2.2.2. Eddy Velocities.....106
4.2.2.3. Eddy Energies and Energy Conversions.....106
4.2.2.4. Eddy Temperature.....107
4.2.2.5. Summary.....108
4.2.3. Vertical Scale Selection.....109
4.2.4. Residual Circulations and Eddy Drag.....109
4.2.5. Role of Forcing and Dissipation.....111
4.3. Eastward Jets.....114
4.4. Composite Jets.....115
4.4.1. Description of the Composite Jet Structure.....115
4.4.2. Jets that are far apart (y_1=2L).....117
4.4.3. Jets that are close (y_1=.75L).....117
4.5. Discussion.....119
4.5.1. Implications for the Energetics.....119
4.5.2. Implications for the Ortho/Para and Tracer Mixing Ratios.....121

Chapter 5 ROLE OF DAMPING AND FORCING.....151
5.1. Introduction.....151
5.2. Case of α^{-1} equal to t_R.....153
5.3. Case of $\alpha^{-1} < t_R$.....154
5.4. Eliassen-Palm Flux Divergence and Residual Circulation.....158
5.5. Implications.....163

Chapter 6 CONCLUSION.....179
6.1. Introduction.....179
6.2. Results of the Linear Modelling.....180
6.3. Results of the Quasi-Linear Modelling.....181
6.4. The Role of Forcing and Radiative Damping.....182
6.5. Future Directions.....182

Bibliography.....185

Appendix A FINITE DIFFERENCE FORMULATION.....194

Appendix B THE BOTTOM BOUNDARY CONDITION.....201

Appendix C ON THE POSSIBLE ROLE OF GRAVITY WAVES.....205

LIST OF FIGURES

Number Page

2.1 Temperature profiles from infrared and radio occultation data.....30
2.2 Cloud structure of Jupiter.....31
2.3 Zonal mean temperatures from infrared data.....32
2.4 Cross-section of the zonal mean temperature deviations.....33
2.5 Vertical profile of radiative damping time.....34
2.6 Cloud-top wind and thermal wind shear at 270 mbar.....35
2.7 Thermal wind shear at 270 mbar and 150 mbar 36
2.8 Standard deviation of 270-mbar temperatures and para-hydrogen retrievals.....37
2.9 Orange reflectivity and cloud-top wind.....38

3.1 Growth rate for westward jets.....69
3.2 Amplitude and fluxes of the most unstable mode for the westward jet ($\beta^* = -0.2$, k=20, m=100).....70
3.3 Cross-section of S_0 for the westward jet ($\beta^* = -0.2$, k=20, m=100).....73
3.4 Amplitude and fluxes of the most unstable mode for the westward jet ($\beta^* = -0.7$, k=18, m=100).....74
3.5 **A**) Growth rate as a function of k for various m. **B**) Phase speeds for various m.....77
3.6 Amplitude of the most unstable mode for the westward jet for m=1 and m=5.....78
3.7 Amplitude and fluxes of the most unstable mode for the westward jet ($\beta^* = -0.2$, k=20, m=2).....79
3.8 Growth rate as a function of log(m Bu).....82
3.9 Squared refractive index and zonal mean flow.....83
3.10 Cross-section of wind tendency for the westward jet ($\beta^* = -0.2$, k=20, m=2).....84
3.11 Amplitude and fluxes of the most unstable mode for the eastward jet ($\beta^* = 0.3$, k=20, m=10).....85
3.12 Amplitude and fluxes of the most unstable mode for the westward jet ($\beta^* = -0.2$, k=20, m=.25).....86

3.13 Vertical profiles of S_0 and F.....89
3.14 Amplitude and fluxes of the most unstable mode for the eastward jet ($\beta^* = 0.3$, k=20, m=.25).....90
3.15 Squared refractive index and eddy amplitude.....93
3.16 Growth rate for baroclinic westward jets.....94
3.17 Parameter **R** and growth rate as a function of m.....95
3.18 Cross-sections of F and χ^*.....96

4.1 Vertical profile of time-averaged mean flow.....125
4.2 Meridional profile of time-averaged mean flow.....126
4.3 Zonal velocities as a function of time.....127
4.4 Vertical profile of time-averaged mean flow.....128
4.5 Eddy meridional velocity.....129
4.6 Kinetic energies and conversion of kinetic energy 130
4.7 Conversions of kinetic energy at various heights.....131
4.8 Vertical profile of time-averaged conversion of kinetic energy 133
4.9 Vertical profile of eddy temperature.....134
4.10 Zonal mean flows from Pirraglia's model.....135
4.11 Vertical profile of time-averaged mean flow (weak jet).....136
4.12 Ratio of fv* to F.....137
4.13 Vertical shear 138
4.14 Kinetic energies (eastward jet).....139
4.15 Vertical profile of time-averaged mean flow (eastward jet).....140
4.16 Vertical profile of time-averaged eddy amplitude (eastward jet).....141
4.17 Meridional profiles of composite jets.....142
4.18 Meridional profiles of mean flow and eddy amplitude for composite jets (y_1=2L).....143
4.19 Vertical profile of time-averaged mean flow (y_1=2L).....144
4.20 Meridional profiles of mean flows for composite jets (y_1=.75L).....145
4.21 Eddy amplitude cross-section (y_1=.75L).....146
4.22 Refractive index and potential vorticity gradient (y_1=.75L).....147
4.23 Refractive index and potential vorticity gradient (y_1=2L).....148
4.24 Vertical profile of time-averaged mean flow (composite jets).....149
4.25 Kinetic energies (westward jet, 6H).....150

5.1 Kinetic energies ($t_R = \alpha^{-1} = 10$ days).....165
5.2 Kinetic energies for various α^{-1} ($t_R = 100$ days).....166
5.3 Meridional profile of eddy phase and mean flow ($t_R = \alpha^{-1} = 10$ days).....167
5.4 Meridional phase gradient as a function of time.....168
5.5 Eddy kinetic energy and meridional phase gradient as a function of time.....169
5.6 Vertical profile of time-averaged mean flows 170
5.7 Vertical profile of time-averaged eddy amplitude ($\alpha^{-1} = 10$ days).....171
5.8 Time-evolution of F and fv* for undamped case.....172
5.9 Time-evolution of F and fv* for $\alpha^{-1} = 20$ days.....173
5.10 Cross-sections of F.....174
5.11 Time-evolution of fv* for $\alpha^{-1} = 50$ days.....176
5.12 Cross-sections of χ^* for $\alpha^{-1} = 50$ days.....177
5.13 Cross-section of χ^* for $\alpha^{-1} = 20$ days.....178

6.1 Vertical profile of time-averaged zonal flow (L=1000 km) 184

A.1 Energies as a function of time for various resolutions.....200

LIST OF TABLES

Number page

3.1 Symmetric (S) and antisymmetric (A) quantities.....49
3.2 Burger number as a function of m.....54
3.3 Growth rate and phase speed when m=.25 59
3.4 Parameters D, Bu for various m in the westward jet case.....62

4.1 Typical zonal velocities in the troposphere and the stratosphere.....113
4.2 Typical periods of the fluctuations.....113
4.3 Energies at equilibration.....119

ACKNOWLEDGEMENTS

I would like to acknowledge my advisor, Professor Conway Leovy, for his advice, constant encouragements and many stimulating discusssions during the course of this work. I also would like to thank him for serving as the Chairperson of my Supervisory Committee and reading so carefully numerous drafts.

I wish to express my appreciation to Professors James Holton, Akira Ishimaru, George Parks and Peter Rhines for serving on my Supervisory Committee.

This work would not have been completed without the support of many friends and fellow graduate students; I want to thank especially John Vandecar, Bérengère Dubrulle, Von Walden and Jean-Frédéric Wagen. I want also to thank the staff of the Institute of Environmental Studies and of the Geophysics Program for their help and kindness.

I will always feel a debt a gratitude to Professor Jean Jeener for persuading me through his example to pursue a career as a physicist. Finally, the completion of this work would not have been possible without the love and support of Isabelle Tardy.

Much computer work was done on the Prime Computer from the Department of Atmospheric Sciences; most of the nonlinear simulations were run on a IBM 3090 of the Academic Computing Services.

This work was supported by the NASA Planetary Atmospheres Program through grant NSG-7085.

CHAPTER 1 : INTRODUCTION

1.1. STATEMENT OF THE PROBLEM.

The zonally averaged circulation of Jupiter at cloud-top level is characterized by a pattern of retrograde and prograde zonal jets. Major features are the broad equatorial jet, the strong midlatitude eastward jets and narrow weaker westward jets; in general, the jet magnitudes decrease with increasing latitude. The location of these jets has been quite steady over the period of the Voyager observations and the much longer period of groundbased observations (Ingersoll et al., 1979). Although the maximum speeds of these jets can be even higher than 100 ms^{-1}, the deviation of the zonal wind velocities from their time-mean in Voyager measurements is small, only being of the order of a few ms^{-1} (Limaye, 1986). This steadiness is remarkable in view of the vigorous eddy activity seen at these levels in Voyager images. In contrast, the large-scale latitudinal cloud bands, known as the zones and belts, that girdle the planet and that are so characteristic of the visible and infrared images of Jupiter, have displayed some variability over the years of groundbased and space observations (Owen and Terrile, 1981); their existence may be linked with the zonal jets, as the zone/belt boundaries correlate with the positions of jet maxima.

Although winds are only measured at cloud-tops, temperature retrievals have been used to infer the vertical wind shears in the upper troposphere through use of the thermal wind relationship. At several altitudes, meridional temperature differences on the scale of the jets have been observed (Pirraglia et al., 1981). The corresponding shears correlate negatively with the cloud-top zonal velocities so that the winds are decaying with height; moreover shears are very similar at several levels in the upper troposphere (Gierasch et al., 1986) which suggests that the vertical decay is monotonic. The shears appear to be as strong for the westward jets as for the eastward jets. If the jets would decay to zero, the westward jets would do so over a smaller height interval, since westward jets are generally weaker than eastward jets.

The observation that there are meridional temperature gradients in the upper-troposphere on the scale of the jets have motivated some authors to associate these variations with adiabatic cooling/warming arising from large-scale dynamical motions. It has been suggested that there are mean meridional circulations (MMC) with upwelling in regions of anticyclonic shear (Conrath and Pirraglia, 1983; Gierasch et al., 1986). Such circulations had been conjectured long ago to explain the origin of the bright zones and dark belts; through rising motions cloud condensates were postulated to form in the zones, creating a cloud cover of high visible albedo, and to be removed through precipitation, making the belts appear depleted (Hess and Panofsky, 1951).

Two fundamental questions concerning the general circulation of the Jovian atmosphere are : what generates and what maintains the jet system and the meridional circulations.

Two classes of dynamical models have been proposed to explain the origin of the zonal jets. The first class consists of the shallow-layer models which rely on a body of theories developed to study the atmosphere of the Earth and the other terrestrial planets; the jets are supposed to be contained in a shallow "weather" layer in a state of hydrostatic balance and approximate geostrophic balance, bounded at the bottom by a rigid surface as on the Earth. The second class consists of the deep-layer models which resemble models of stellar interior circulations, in which the jets originate in the deep convective interior of the rotating body.

Various types of linear instabilities have been investigated in the shallow-layer models, as well as nonlinear processes associated with two-dimensional turbulence responsible for energy decascade toward zonal motions. Numerical calculations (Williams, 1978; 1979) have been successful at reproducing an alternating jet pattern with appropriate scales but the origin and characteristic scales of the forcing are somewhat unclear. Barotropic models require stochastic stirring, the meridional scale of which may obscurely be linked to the meridional scale of the

produced jets; baroclinic models require meridional temperature gradients that are not observed on Jupiter.

Many attempts have been made to describe how convection constrained by strong rotation could generate zonal flows in a deep planetary interior. A broad range of methods have been used from analytical linear and weakly nonlinear analyses (Busse, 1976; 1983), numerical stability analyses of appropriate conservation laws (Ingersoll and Pollard, 1982; Ingersoll and Miller, 1986) to numerical simulations of the full hydrodynamical equations (Glatzmaier and Gilman, 1981). There have also been several laboratory investigations of convection in rotating spherical or cylindrical shells (Busse and Hood, 1982; Hart et al., 1986). Linear theories predict the most unstable modes to be of the form of columnar eddies aligned with the axis of rotation, and that the associated Reynolds stresses could accelerate the zonal flows; numerical simulations of Gilman and his coworkers show that these motions and their strong coherence along the axis of rotation exist in the nonlinear regime and that zonal flows are indeed generated. Either corotating zonal flows or counterotating ones were simulated in separate experiments, but an alternating pattern of jets as seen from cloud-top observations of Jupiter has not been reproduced.

These theories of the deep circulation provide a qualitative explanation for the axisymmetric circulation of the low and midlatitudes. However, the maintenance of such a circulation is problematic as convective eddy velocities based on the traditional mixing length hypothesis, would rapidly dissipate zonal energy. Ingersoll and Pollard (1982) provided a diagnostic scaling analysis whereby differential rotation and convection coexist and eddy velocities are reduced considerably over mixing length estimates. It led them to suggest that zonal jets can be sustained in the interior and to derive a criterion for their stability. Interestingly enough, this criterion is similar to the barotropic stability criterion for a shallow atmosphere, familiar to meteorologists. A full numerical simulation of these processes is lacking at this stage.

The dynamical origin of the meridional circulations has been investigated

since Voyager measurements became available. The picture of a dissipative upper-troposphere forced from below by deep jets was outlined by Conrath and Pirraglia (1983). An adhoc Rayleigh drag could give qualitative agreement with the observations : the jets would decay with height and associated meridional circulations, with upwelling in regions of anticyclonic shear, would arise. Busse (1983) sketched how this could be tied in with the deep origin of the jets and suggested that the jets might decay in the troposphere perhaps because of Ekman dissipation or radiative processes. Gierasch et al. (1986) draw a more quantitative picture while keeping a Rayleigh drag as momentum dissipation.

The nature of the drag is not revealed in these models but it was clear from these studies that further investigations of in-situ instabilities were greatly desirable. In this thesis, we will pursue the idea that the jet decay and meridional circulations are driven by large-scale instabilities of a deeper flow extending into the upper troposphere. The idea that large-scale inviscid instabilities could provide such a drag effect was tested by Pirraglia (1989) and independent results, developed in this dissertation, were presented by Orsolini and Leovy (1989a).

We pursue here the development of a capping layer model for the Jovian tropospere as outlined by Leovy (1986). Our purpose is to investigate the extent to which instabilities of a deep jet structure could be responsible for the maintenance of the tropospheric vertical shear zone. More precisely, we suppose that the jets originate in the deep interior where they reach a stable state. As the jets penetrate into the statically stable upper troposphere, their extensions into this layer are barotropically unstable and generate mean meridional circulations and eddy fluxes. We model a shallow atmospheric layer, the stably stratified portion of the atmosphere, but the forcing comes from the deep layer motions; the source of energy for the tropospheric eddies is then thought to be the unstable deep jets. We also assume that the troposphere, which we take to mean the region extending upward from the convective zone to the tropopause, is statically stable and governed by quasi-geostrophic dynamics.

Our basic picture of Jovian dynamics is similar to that recently published by Pirraglia (1989) who used a truncated nonlinear model to examine the role of unstable eddies in jet decay.

1.2. METHOD AND OVERVIEW.

In the first stage, we address the linear problem of characterizing the instabilities of decaying jets. The jets have a simple analytical profile with characteristic parameters in agreement with observed winds. The observation that cloud level zonal winds violate the barotropic instability criterion for flow in a shallow atmosphere (Ingersoll et al., 1984) motivates our investigation of barotropically unstable jets. The thermal wind observations noted above suggest a decay scale of at least one scale height. Our analysis shows that, in this regime, instability is indeed barotropic with important effects introduced by the vertical decay of the jets. Previous instability studies of the Jovian troposphere have not focused on the barotropic instabilities of vertically decaying jets (Conrath et al.,1981; Gierasch et al., 1979; Read, 1988). In addition to the study of the barotropic regime, we will present some results on the baroclinic regime for the sake of completeness.

The quasi-geostrophic equation for the perturbation potential vorticity is solved for a wave of given zonal wavenumber by the well-known initial value approach. That method has been extensively used in the study of the terrestrial atmospheric circulations (Geisler and Garcia, 1976; Matsuno, 1979; Pfister, 1979)

The main role of these instabilities is to spread the zonal momentum horizontally thereby stabilizing the jets which gave rise to them; however due to the three-dimensional nature of the problem, they also contribute to the jet decay with height, at least in the jet cores. We will analyze the growth rate, structure and fluxes of these linear instabilities, as well as the residual mean meridional circulations they drive.

In the second stage, the growth of these perturbations to a finite amplitude

regime is investigated through numerical experiments with a quasi-linear model. In this approach, the most unstable wave can feed back on the mean flow, while interaction between waves of different zonal wavenumbers is not included. Again, such a wave-mean flow method has been widely used in atmospheric dynamics. An initially unstable barotropic flow is shown to develop linear instabilities which then grow and saturate at the end of an equilibration stage during which the initial jet broadens and vertical shear develops. During the stabilization, mean kinetic energy is released into a finite amplitude eddy. In such an inviscid experiment, overshoot and vacillations are also encountered, the periods and amplitude of which depend on the model truncation and the supercriticality of the initial mean flow. Nevertheless, the mean flow is shown to develop a near-steady shear zone in the lower scale heights. Comparisons are made with the results of Pirraglia (1989) and results of the linear study. The cases of westward and eastward jets are separately examined as well as the case of a composite jet structure consisting of neighbouring westward and eastward jets.

In the presence of radiative damping acting on them, the eddies decay after the source of eddy energy is switched off once equilibration has been achieved. Radiative damping will also tend to suppress vertical shears, thereby forcing the mean flow back toward its initial unstable state. Gravity wave may also provide a mean flow forcing, possibly acting on a faster time scale. A model combining both forcing and damping which is also simple enough to allow relatively simple interpretation of its dynamical behavior is used in which a Rayleigh forcing to the initial state is applied to the mean momentum equation. The time scale of that forcing is critical for determining the dynamical behavior of the system. In some cases, a balance can be achieved with steady eddy and residual mean meridional circulations, the structure of which can be compared with the results of the linear study.

There are obviously severe limitations in the applicability of this study to the real Jovian atmosphere. The zonal truncation at one wavenumber is introduced merely as a way to simplify the wave-mean flow problem. As

perturbations grow, the jet structure changes and the most unstable mode of this new jet may have a wavenumber different from that of the initial jet. Moreover, wave-wave interactions may become important and instrumental in generating waves of higher zonal wavenumber. Such wave-mean flow decompositions have been applied widely in studies of the terrestrial stratosphere, a situation where it is frequently assumed that the atmospheric flow can be well represented by a zonal flow distorted by a few waves. The quasi-linear models are able to capture some important features of these circulation systems. The relevance of these models to flows which are more reminiscent of fully developed turbulence, like the apparent Jovian circulation, is more questionable. Certain predictions of these quasi-linear models are most certainly model-dependent; such are the ubiquitous vacillations. Nevertheless, we believe that these models describe well the gross effects of instabilities on the mean flow. In this sense, the time-averaged mean flow profiles derived from these computations should be compared with observations. Concerning the eddies themselves, the amount of eddy energy, the relevant wavenumbers at which energy is fed through these instabilities, the magnitude of the temperature or velocity perturbations are all relevant quantities to be checked with the observations.

From these comparisons, we hope to determine whether the hypothesis of the capping layer model, that the vertical shear of the zonal wind, the gross properties of the eddies and the mean meridional circulations are governed by the instability of the extension into the troposphere of a deep zonal jet structure, is sufficiently promising to merit further investigations with more sophisticated models.

CHAPTER 2 : OBSERVATIONAL CONSTRAINTS

2.1. INTRODUCTION.

Observations of the composition, thermal structure and large-scale atmospheric circulation of Jupiter are briefly reviewed. We only mention here observations pertinent to the understanding of the topic of this dissertation; namely we present together with necessary background information, observational evidences for a near-steady zonal jet system and meridional circulations in the troposphere.

Several review papers have appeared in the literature during the recent years (Ingersoll et al., 1984; Flasar, 1986 and 1987; Hunten and al., 1986; Encrenaz, 1990) and we will often rely on them, without necessarily referring to the original papers.

The Outer Planets (Jupiter, Saturn, Uranus and Neptune) of the solar system have common characteristics; they are fluid objects essentially composed of a mixture of hydrogen and helium; their cloud chemistry involves ammonia, methane, sulfur and water vapor. Their heat balance is governed by both solar heating and emission of internal heat remnant of the epoch of their formation. Saturn and Jupiter are the most alike not only because of their size and composition but also in the similarity of their cloud-top atmospheric circulation and their global heat budgets (they have nearly the same ratio of emitted thermal power to absorbed solar power, about 1.6). Our knowledge of these bodies has been tremendously increased by the Voyager missions; a considerable amount of data on their meteorology is just being unveiled. Due to the limited scope of this dissertation, we will focus exclusively on Jupiter, but it is likely that similar mechanisms should operate on both planets. The following brief review bears almost exclusively on Jupiter.

The averaged thermal structure of Jupiter shows a tropopause slightly below 100 mbar and a near adiabatic profile below 600 mbar (Figure 2.1a

and b). Our study concerns the Jovian troposphere and lower stratosphere, namely the stably stratified atmospheric layer bounded from below by the convective planetary interior, where heat is transported upward by convection and the temperature profile is expected to be close to adiabatic.

2.2. COMPOSITION.

The two main constituents of the Jovian atmosphere, hydrogen (H) and helium (He), have near-solar abundance; the determination of He abundance in the Giant Planets comes from inversion of their thermal-infrared spectrum and spacecraft radio-occultation experiments. Recent values for the mass fraction of He are .18±.04 for Jupiter and .06±.05 for Saturn (Gautier and Owen, 89).

These abundances are compatible with ideas about the formation of the Giant Planets whereby elements distributed with proto-solar abundances condense according to the local nebular temperature. At the heliocentric distance of the Giant Planets, carbon (C), nitrogen (N) and oxygen (O) condense as well as the rocks and metals that form the cores of the terrestrial planets. This scenario is consistent with the idea that the core of the Giant Planets are more massive than the core of terrestrial planets; they are in fact sufficiently massive to bind and retain forever a primordial gaseous atmosphere of He and H. The departure of the composition of the gaseous envelope from the proto-solar composition results from differentiation between inner and outer layers and atmospheric enrichments from degassing/capture. The smaller He abundance on Saturn is interpreted as a depletion of the upper layers through gravitational sinking of He; as the planet cools, He becomes immiscible with metallic hydrogen at pressures greater than 3 Mbar and sinks. Planetary evolution models consistent with the value of the excess thermal energy flux of Jupiter, predict that, having started at warmer temperatures, Jupiter has started differentiation more recently, so that its He/H ratio is intermediate beween the proto-solar and Saturn value (Gautier and Owen, 1989).

The main atmospheric component, molecular hydrogen (H_2), under the Jovian atmospheric conditions, exists in two nearly-decoupled forms, ortho and para, which differ in the relative orientation of the nuclear spins. The thermodynamics of an H_2 gas depends on their relative abundance through a strong dependence of the heat capacity at constant pressure, Cp; a consequence is that the adiabatic temperature gradient also depends on the ortho-para ratio. The infrared opacity of the atmosphere is also affected by the relative abundance. The sensitivity of the absorption coefficient in the infrared is actually used to derive that abundance from measurements. The thermal infrared spectrum of Jupiter is dominated by the collision-broadened dipolar transitions of H_2, the S(0) and S(1) lines, superposed on the translational continuum excited by the H-He collisions. The infrared absorption depends on the ortho-para ratio in a frequency-dependent way; measurements in a spectral region where the absorption is nearly independent of the ortho-para ratio (near 520 cm^{-1}) in conjunction with measurements in a region of strong dependence on the ortho-para ratio (near 320 cm^{-1}) has allowed the determination of the ortho-para relative abundances (Conrath, 1986).

Nuclear spins are parallel in the ortho form and antiparallel in the para form. In the high temperature approximation, the fractional abundance is given by its statistical weight of 3 to 1 (this is also referred to as the normal abundance). The relative abundance of ortho and para hydrogen is often expressed by the para fraction f_p, which in the normal high-temperature case is f_p=.25. Transitions with ΔJ=1 are highly forbidden in a pure H_2 gas so that thermal ortho-para equilibration is prohibited; ortho hydrogen is linked to the odd rotational levels, para to the even levels. The S(0) line corresponds to the transitions between para states while the S(1) line corresponds to ortho transitions. The exchange rate between the two forms is expected to be very slow due to the weakness of the paramagnetic interactions in a pure H_2 gas; the exchange time constant is estimated to be 10^9 s at a pressure of .5 bar. But this is still subject to debate; the presence of paramagnetic molecules or paramagnetic sites on solid surfaces could considerably shorten the time scale and it has been suggested that catalytic processes upon aerosol particles could provide such a mechanism (Massie

and Hunten, 82). It is fair to say that considerable uncertainty exists due to the lack of knowledge of the appropriate equilibration rates in atmospheres of Jovian composition. If the equilibration time is long, maybe as large as 10^9 s, then the ortho-para fraction has the potential of being used as a tracer of atmospheric motions occuring on shorter time scales.

Temperature adiabats depend on the f_p ratio. Normal adiabats are those for which f_p is frozen to its normal value. When the f_p ratio is in equilibrium at the local temperature, one has a class of adiabats called equilibrium adiabats; this would happen if the H_2 gas instantly relaxes to equilibrium f_p at the local temperature. As temperature decreases, the equilibrium ratio becomes greater than .25. Due to the exothermic conversion, these adiabats are less steep than the normal ones. For atmospheric temperatures of about 150 K, like the ones encountered on Jupiter, the release of energy caused by equilibration of normal H_2 can yield horizontal temperature contrasts up to 4-5 K, and this obviously would be higher for colder temperatures.

On Jupiter, Conrath and Gierasch (1984) have shown that the ortho/para ratio is not in equilibrium in the upper troposphere at the 300 mbar level; a large scale variation from equator to pole exists with near equilibrium values reached toward the pole. They offer the explanation that there is upwelling in the equatorial region and that, at the equator, one sees hydrogen with a low f_p, closer to the normal ratio, characteristic of deeper and hotter regions. The upwelling in the equatorial regions would be on a time scale faster that the equilibration time scale. Such an upward motion could be associated with a meridional circulation on the hemispheric scale; a poleward return flow in the upper troposphere would explain why f_p becomes closer to the equilibrium ratio as latitude increases. We do not see such an hemispheric variation in the temperature field (see later), so that the overturning time should be between the radiative time scale, $5\ 10^7$ s, and the equilibration time scale, presumably 10^9 s, as for pure hydrogen gas.

There are hints of meridional variations in the ortho-para ratio on the

scale of the jets at the 270 mbar level from a recent study (Gierasch and al., 1986), although the uncertainties are quite large. In this case, there are correlations between these variations and the temperature field, which may happen if the overturning times are shorter.

The other most abundant elements are carbon (C), nitrogen (N) and oxygen (O). An enrichment by a factor 2 of carbon, mainly in the form of methane (CH_4), over proto-solar values is observed on both Jupiter and Saturn. This is expected for Giants Planets having cores containing ices (which include CH_4, NH_3, H_2O) enriching their atmospheres through outgassing of the core. Nitrogen and oxygen are mostly in the form of NH_3 and H_2O; these constituents do not have constant mixing ratio due to condensation and photodissociation effects. These will be discussed later; nevertheless, below its condensation level, NH_3 is also enriched by a factor 2 over proto-solar values, a result derived from observations at centimetric wavelengths (de Pater, 1986). For oxygen, the situation is still a puzzle; water has been detected on Jupiter only. Below its condensation level, H_20 seems depleted by a factor 50 over proto-solar values as derived from measurements at 5 μm (Bjoraker et al., 1986). More will be said about these problems in the section on the cloud structure.

Many other trace constituents have been detected by ground-based as well as spaceborne spectroscopy. A detailed account can be found in Drossart et al. (1987). A first class is includes products of methane and ammonia photodissociation, such as C_2H_2, C_2H_6, HCN; they are essentially found in the stratosphere. In the auroral zones of Jupiter other compounds of this type have been identified (C_2H_4,C_3H_4, C_3H_8). Minor compounds of other elements in hydrogenated form belong to a second class. Among those, phosphine (PH_3), arsine (AsH_3) and germane (GeH_4) are interesting because they are desequilibrium species, probably brought into the upper troposphere by vertical motions on a time scale shorter than their destruction time scale. Although they are potential candidates for tracers of atmospheric motions, little work has been carried out to exploit their spatial variability.

2.3. CLOUD STRUCTURE.

Although the composition of the Jovian atmosphere is well-constrained by available data, our understanding of the cloud structure is still quite speculative. The foundations of our understanding come from a series of papers by Lewis and collaborators based on the idea of condensation of an atmosphere of near-solar composition in thermochemical equilibrium (Lewis, 1969; Weidenschilling and Lewis, 1973; see also West et al., 1986); they predicted a 3-layer cloud structure schematized in figure 2.2; the highest cloud of NH_3 ice has a base at a temperature of about 150 K (i.e. in the 500-700 mbar range); an ammonia hydrosulfide (NH_4SH) cloud at about 205 K, and a bottom cloud consisting of an aqueous solution of NH_3 at 270 K are also predicted. The location of the cloud bases depends slightly on assumptions about the temperature profile and the exact composition. The thicknesses of these clouds may depend strongly on dynamical and microphysical processes but from these thermochemical considerations only, one can deduce a vertical scale as the distance over which the cloud density decays by, let us say, a factor 100 : for the NH_3 cloud, the thickness would be less than about 10 km, and for the NH_4SH cloud it would be slightly more than 10 km (Atreya and Romani, 1985).

None of these clouds has been unequivocally identified. Clues about the NH_3 cloud appear in the vertical distribution of gaseous NH_3. NH_3 is not uniformly mixed above 700 mbar due to a combination of photochemical, microphysical and dynamical effects. Evidence for a cloud exists in the depletion pattern of NH_3 in the 500-700 mbar range. At visible wavelengths, the appearance of Jupiter consists of an alternation of bright white latitudinal bands, called the zones, and darker bands, called the belts. This banded appearance persists up to a latitude of 45°. At higher latitudes, this fairly regular pattern gives way to more irregular eddies. It seems that Hess and Panofsky (1956) were the first to suggest that the zones are regions of rising gas, with condensation of NH_3 giving rise to the white clouds. The belts were thought to be areas of sinking motions, devoid of NH_3 cloud so that one sees deeper through the atmosphere presumably down to a deeper cloud layer. This interpetation is supported by the thermal mapping of

Jupiter at 5 μm. Indeed, correlation of groundbased images at 5 μm with Voyager photographs led Owen and Terrile (1981) to associate the zones with regions of low brightness temperature, supporting the idea that these cold zones are regions of upwelling motions; on the other hand, the belts are hotter and therefore presumably deeper regions. More recently, Gierasch et al. (Gierasch et al., 1986) further supported that picture with analysis of NH_3 abundance in the upper troposphere from the Voyager infrared spectra. These observations of low NH_3 in belts at 680 mbar correlate closely with the cloud optical depth derived from the same data as well as with ortho-para-hydrogen variations, although the noise levels are quite high in this last retrieval. A possible interpretation of these findings is that the zones are regions of upwelling, large optical depths and large NH_3 abundance due to the trapping of gaseous NH_3 in ice clouds with downwelling of NH_3-depleted gas in the belts. This model however implies some microphysical removal of condensates in the zones; it is to be remarked that photodissociation of NH_3 alone cannot account for the undersaturation of NH_3 below 300 mbar (de Pater, 1986). The correlations derived by Gierasch et al. (1986) involve quantities representative of different atmospheric levels (NH_3 at 680 mbar, f_p at 270 mbar) so that the vertical velocity field generating the zones could extend from the tropopause down to the cloud base.

Similarly, there is only indirect evidence for the existence of the NH_4SH cloud. The seeming absence of sulfur in the upper troposphere suggests trapping of that element in such a cloud component. It has also been suggested that the reflection of sunlight on solid NH_4SH particles could produce the yellow/brown colors of the belts (see Hunten, 1986).

Even deeper, at levels of 2 bars, a recent analysis of Voyager infrared data at 5 μm with improved laboratory data on NH_3 absorption at low temperature shows a correlation between the cloud opacity, probably of the NH_4SH cloud, and NH_3 abundance (Lelouch et al., 1989). The correlation is such that NH_3 is less abundant where the cloud is more transparent. This is an extension to deeper levels of the correlations found by Gierasch et al. (1986).

At these depths, there is additional evidence for a belt/zone structure from ground-based remote sensing (de Pater, 1986). Between .5 and 10 bar, gaseous NH_3 is the main absorber at radiowavelengths. Through analyses of high resolution (1/30 of the disc) Very Large Array observations at 1.3, 2., 6.1 and 20 cm, de Pater (1986) showed the existence of bright bands whose positions correlate with the bands seen in optical data. At pressure greater than 2 bars, ammonia has a uniform abundance of $2.5\ 10^{-4}$ but shows vertical and latitudinal variability above that level. Above 2 bars, NH_3 is strongly depleted with respect to the near-solar value and changes in two steps : first it decreases in a layer where the postulated NH_4SH cloud is expected to form, then it stays constant up to the NH_3 cloud base at about .7 bar. At higher levels, NH_3 progressively decreases in a manner compatible with the photodissociation processes. The meridional structures appear above 2 bars and the contrast between zones and belts is most pronounced in the .6-2 bar region; NH_3 is more depleted in the belts by a factor of 2 and the NH_4SH cloud seems thicker in the zones. The vertical resolution of the zone/belt structures is still uncertain as it relies on a very few measurements but nevertheless brightness contrasts at the different wavelengths indicate that this structure is indeed real and extends between 2 and .6 bar. The interpretation of these spectra depends though on the assumption that temperature profiles are identical in the belts and the zones. Although the horizontal resolution is much poorer at these radio wavelengths, there is partial agreement with the Voyager infrared data in the relative latitudinal variations of NH_3 within 30° of the equator. Although these data sets do not agree in the absolute values of the NH_3 abundance (Flasar, 1987), they tend to support the view that the zone/belt contrast, possibly due to vertical motions, extends from the upper troposphere down to the 2 bar level. de Pater speculates that the origin of the belt/zone structure lies in the NH_4SH cloud layer where it would be supported by release of latent heat of condensation. Condensation enhances buoyancy and saturated adiabats are steeper than the dry adiabatic ones. However for an atmosphere of solar composition the saturated lapse rate deviates from the dry adiabatic one by no more than .1 °K/km (Flasar, 86).

This simple picture of cloud bands has to be made more complex in several ways. First of all, it is not quite a steady structure as confirmed by the changing visual appearances of Jupiter.

Earth-based observations conducted over more than a century (Peek, 1958), have documented the changing appearance of the Jovian disc; such useful observations are still conducted today (Sanchez-La Vega, 1987). Changes are sometimes gradual, spanning several terrestrial years. This is also, perhaps coincidentally, the seasonal time scale (the orbital period is slightly less than 12 years). But the radiative time scale is also of the order of a few years. Pictures shown in Flasar (1987) taken at the Lowell Observatory illustrate such changes during a 5 year-period before the Voyager encounters. On the other hand, there can be dramatic events on a scale of several days. Often these events involve sudden apparition of a bright spotlike disturbance becoming sheared by the zonal flow thereafter (Sanchez-La Vega, 1987).

Some information on this aspect has also been collected by the space missions. The clouding up of a northern hemisphere belt in between the Pioneer and Voyager encounters is well documented as well as the narrowing of a zone by a factor 2 in the southern hemisphere at latitudes of 12-24° (Ingersoll et al., 1979).

Overall, these variations on a scale of a few years may come from intrinsic variations in the dynamical forcing, from unknown seasonal effects or from a cyclic nature of the cloud formation processes. The rapid changes are more likely to result from penetrative convection.

West et al. (1986) reviewed both the infrared retrievals and the reflected sunlight measurements and favored the following view : there is a high cloud layer of small particles (1 μm or less) over both belts and zones extending up to the tropopause. This would have a thickness of several optical depths and would be a mixture of NH_3 and chromophores. The nature of these chromophores has not yet been identified, although sulfur and phosphorus compounds have been proposed as candidates. At deeper

level there would be a cloud of larger particles (3 to 100 μm) with a base at the condensation level of NH_3; it would be a fraction of a scale height thick. The existence of a similar two-cloud component system was also proposed by Gierasch et al. (1986) through analysis of infrared optical depths. The component with large particle sizes correlates with NH_3 abundance, while the other cloud is uniform over belts and zones and is composed of smaller particulates. The existence of such a uniform haze layer has interesting dynamical implications; according to West et al. (1986), it could put a constraint on the location of the horizontal mixing through the return flow of the upwelling in the zones; they put this level of horizontal mixing at 300 mbar.

There is also considerable literature on stratospheric haze layers (see West et al., 1986).

Finally, the existence of the deep H_2O cloud is also problematical. The water vapor cloud for a Jovian atmosphere model of solar composition is located at the 5 bar level and the deep water vapor mixing ratio should be about $2\ 10^{-3}$. This ratio should be constant up to about the 5-bar level where condensation should occur. Measurements challenge several predictions of this model. High spectral resolution disc-averaged observations from the Kuiper Airborne Observatory in the 5 μm range and the IRIS observations were compared by Bjoraker and al. (1986). From this analysis, the H_2O abundance has been estimated to be $3\ 10^{-5}$ at the 6 bar level, and about $3\ 10^{-6}$ throughout the 2 to 4 bar layer with a saturation value above 2 bars. Bjoraker's results are thus incompatible with the presence of a H_2O cloud at the 5-bar level and imply a depletion in oxygen compared to the solar value by the factor 50. Observations of other oxygenated compounds, such as CO, as well as theoretical constraints on the O abundance resulting from the non-observability of SiH_4, (presumably trapped by chemical reactions with water) have led, however, to a near-solar value of the oxygen concentration (Fegley and Prinn, 1987). The puzzling problem of the water depletion has been further studied by Lunine and Hunten (1987); they proposed a convection model, driven by condensation of water vapor in the 2 to 6 bar layer, with slow large (horizontal scale of 100 to 1000 km)

downdrafts and rapid narrow (10 to 100 km) updrafts of saturated gas. This model preserves the near-solar value of the H_2O mixing ratio below 6 bars and is compatible with Bjoraker's disc-averaged results. The apparently low abundance of water could be explained by the difference in the scales of the convective cells; the saturation representative of the cloud forming regions is not seen in the data as these regions represent a few percent of the disc. In the downdrafts, the H_2O abundance is characteristic of the overturning level of 2 bars. Their model was developed to explain the disc-averaged profiles of Bjoraker et al. (1986) and this postulated convective pattern is assumed to bear no relationship with the zone/belt structure.

There is a large number of local cloud features visible in the Voyager images (Hatzes et al., 1981; Ingersoll et al., 1979; Ingersoll et al., 1981). The famous Great Red Spot is the most prominent one, but there are numerous other cyclonic and anticyclonic vortices in both hemispheres ranging from scales of 25000 km down to less than 500 km. These spots were observed during both Voyager encounters; the Great Red Spot itself has been known for three centuries. An anticyclonic vortex located in an anticyclonic shear zone at about 22.5 ° S, it extends quite high vertically, with a cold top located in the lower stratosphere. Its color might be due to upwelling of deep out-of-equilibrium materials. There are other anticyclonic vortices; the White Ovals have been observed for several decades in the anticyclonic zone south of the Great Read Spot (at 33 ° S). A belt of smaller White Ovals can be found in the next anticyclonic shear zone further south around 41 ° S. The Voyager photographs also reveal cyclonic vortices; these last ones are seen hotter at 5 μm and might be deeper. They also seem more compact with a dark core (known as the brown barges). These long-lived cyclonic and anticyclonic vortices have some common features : they coexist with strongly turbulent motions and they are found in a region of (meridional) shear of the same sign as the vortex. Except for the larger spots which are alone at their latitude, the other spots often form a chain spreading along a latitude circle (this is especially noticeable at 41 ° S).

In the equatorial regions, one also observes plumes, probably of convective nature.

2.4. THERMAL STRUCTURE.

2.4.1 VERTICAL THERMAL STRUCTURE.

Information about the thermal structure of Jupiter has been obtained through remote sensing experiments in the thermal infrared and at radio frequencies.

Thermal radiation comes mainly from the atmospheric layer where the optical depth is unity. The more absorbing the atmospheric constituent at a given wavelength, the higher are the levels probed at that wavelength. In the thermal infrared, one probes levels between 1 mbar and a few bars. Local thermodynamical equilibrium is assumed to prevail, and the flux of infrared radiation is expressed as a function of the vertical profile of temperature and a vertical distribution of the absorber. A double iterative method is then used to determine the temperature profile and the H_2/He ratio from the infrared measurements.

Inversion of the measurements from the instruments carried by Voyager 1 and 2 yielded spatially resolved data sets which have been extensively analysed (Ingersoll 84, Hanel 79a and 79b, Gierasch et al., 86). They completed and extended previous analyses using groundbased data and the Pioneer data. Observations were in the 100-2500 cm^{-1} region where opacity is principally dominated by the broad S(0) and S(1) pressure-induced rotation lines and translational continuum of H_2; the upper tropospheric structure from 80 mbar to cloud-top was retrieved with these observations (Pirraglia et al., 81) with a nominal error of .5 K on individual spectra and a vertical resolution of about half a scale height.

Observations were also taken around 1034 cm^{-1} in the υ_4 vibration band of CH_4. Inversion of these measurements provided the stratospheric temperature structure in the region from 10 to 1 mbar. The Voyager temperature profiles were interpolated in the lower stratosphere.

Radio-occultation from a spacecraft is another method for probing a planetary atmosphere. Typically, it allows determination of two profiles of temperature per flyby as the spacecraft passes behind the planet and later emerges. The ratio of temperature to mean molecular weight is actually retrieved so that an hypothesis has to be made about the atmospheric composition, i.e. in the case of interest here, the H_2/He ratio. Occultations of Voyager 1 and 2 have been used to derive the temperature of the atmosphere between pressure levels of a few mbar to slightly more than 1 bar (Eshleman et al., 1979). These occultation profiles represent specific locations, generally in the equatorial regions on the planet but their vertical resolution is quite sharp, about one kilometer in the troposphere, increasing to 10 kilometers at the highest levels. Later, more accurate methods were derived by combining infrared and radio-occultation measurements (Flasar et al., 1987).

The infrared and radio occultation data sets show very good agreement, except in the lower stratosphere where the infrared measurements were interpolated. This is illustrated on figure 2.1. The averaged thermal structure shows a tropopause slightly below the 100 mbar level. Above it, the temperature increases with height, but no stratopause has been identified so far. From the tropopause down to 600 mbar the profiles derived from infrared and radio-occultation measurements agree closely. The infrared measurements probably contain uncertainties below that level due to the haze and cloud layer contributions, but the radio-occultation profiles extend down to about 1 bar, showing a near adiabatic profile below 600 mbar. Such an adiabatic temperature profile is expected in the Jovian interior where the heat is transported upward by convection. With the high temperatures encountered in the Jovian troposphere, the normal and equilibrium adiabats are nearly identical and their difference falls within the experimental errors. In the lower stratosphere, the radio-occultation profiles show a lot of vertical variability : measurements show wavelike structures, with regions of near-adiabatic gradients alternating with temperature inversions. Vertically propagating waves might break and create such structures, but variations in aerosol distributions affecting solar heating might also be responsible. This is still an open question.

At much deeper levels, heat is expected to be transported upward by convection. Convective transport being very efficient, only slightly superadiabatic temperature gradients are required according to mixing length theories. The existence of an internal heat source has been confirmed by analysis of the planetary radiative balance. It was early observed that Jupiter emits more in the infrared than it absorbs from solar radiation; this was also confirmed by the Voyager data (Hanel and al., 1979). The magnitude of that internal energy flux is about 14 W/m^2. The ratio of the emitted thermal power to the absorbed power is believed to about 1.6 (Conrath and Gautier, 1989).

2.4.2. HORIZONTAL STRUCTURE.

Of great interest is the existence in the troposphere of small meridional temperature variations at the zone/belt scale as mostly revealed by the Voyager data (figure 2.3). There are no significant variations from the pole to equator in the troposphere; an hemispheric asymmetry in temperature has been observed in the Jovian stratosphere (Hanel et al., 1979) with a typical difference of 10 K between the northern and the southern hemispheres. This was interpreted to be a response to the seasonally varying solar heating (Caldwell, 1981).

The thermal emission is independent on latitude despite the fact that the solar heating is strongly dependent of latitude; this requires a mechanism for redistribution of heat. However there are relatively small but clear variations at several levels in the upper troposphere on the scale of the zone/belt structure. How this could be related to dynamical motions on the scale of the jets will be examined in a later section. The magnitude of these variations is 2-3 K, as one can see from the cross-sections shown on figure 2.4 assembled with about 150 spectra by Pirraglia et al. (1981). These variations are not well correlated with the zonal wind or albedo variations at 500 mbar. This is thought to be due to condensates whose meridional distribution can induce opacity variations not taken into account in the retrievals. Above that, at pressure levels of 270 mbar and 150 mbar, where

retrievals were performed, there is a good correlation with the wind structure and the albedo within the formal pointing error of 1-3 ° latitude. The correlation with the albedo is such as that bright areas are associated with low temperatures. The meridional temperature variations have the sign required for a jet decay with altitude; this implication for the wind structure will be discussed in a following section.

Interestingly enough, in the stratosphere above 10 mbar, there are temperature variations of 3-4 K which are negatively correlated with the tropopause variations. This was observed above the Great Red Spot and in the Northern Equatorial Belt (Flasar, 86). This certainly deserves further investigation.

There is little information on the time dependence of the temperature structure. Four months separate the Voyager 1 from the Voyager 2 observations. There are some difference in the profiles, namely in the equatorial regions, of the order of 1-2 K but the contribution of pointing errors is not well assessed. As mentioned before, the North Temperate Belt (25 ° N) was dark at the time of the Pioneer encounters but had a high albedo during the Voyager flybys. At the time of the Voyager flybys, the upper troposphere temperatures were still relatively high however - corresponding to a belt -, indicating that the temperature field might not have had time to adjust.

2.4.3. RADIATIVE TIME CONSTANT.

The response of an atmosphere to radiative forcing is governed by its radiative time constant t_R. As we shall see, this constant is very large (over 1.2 terrestrial years) in the troposphere of Jupiter, so that the temperature distribution responds strongly to dynamical phenomena such as upwelling.

As indicated before, the infrared opacity in the troposphere is mainly due to molecular hydrogen, while in the lower stratosphere hydrocarbons play an important role. The well-mixed gaseous CH_4 is actually the main absorber of solar radiation; to reproduce the high stratospheric

temperatures of Jupiter, it was found that absorption of solar energy by aerosols also had to be included in model calculations.

The radiative time constant is shown as a function of height on figure 2.5 (in that figure, it is denoted as τ_R). At the emission-to-space level (near 300 mbar), where t_R reaches its minimum, t_R is about 4 10^7 s. At greater depths, t_R increases due to the increase in density and reaches 10^8 s at a depth of 1 bar. It also increases to 10^8 s at about 10 mbar.

With such a long radiative time constant, no diurnal changes are expected. The orbital time constant, T_{orb}, (the orbital period divided by 2π) is about 2 terrestrial years, and therefore is of the order of t_R at the tropopause. At the 10-mbar level, t_R has increased up to 2 times T_{orb}. Seasonal effects could be important; although the obliquity of the planet is only 3°, the ellipticity of the orbit causes a 20% change in the amount of solar radiation received. This is the basis on which the inter-hemispheric antisymmetry in the stratospheric temperatures has been interpreted as a response to the varying seasonal forcing (Caldwell, 1981).

2.5. WIND OBSERVATIONS.

Although the zonal currents of Jupiter had been observed for over a century (Peek, 1958), by far the most accurate measurements of the zonal wind speeds were derived from cloud-tracking analyses of the Voyager images. The cloud-top flow is predominantly zonal; major features are the strong prograde equatorial jets and alternating eastward and westward jets extending up to 60° or more, getting weaker as latitude increases.

In the early Voyager studies (Ingersoll et al., 1981), the zonal velocities were derived by measuring the displacement of cloud features, 100-200 km in size, usually over 1 to 3 rotation periods; tracking was done also over a 2-hour time interval to check compatibility of the results. The latitudinal resolution of the zonal mean flow profiles was 1° latitude.

More recent studies (Limaye, 1986; 1987) improved that resolution by a

factor five at least. A new method of digital pattern matching on pairs of cylindrical mosaîc images was used; an extended set of Voyager images in the violet and blue filters was analysed. This technique made it possible to have a time resolution of one Jovian rotation period. The zonal wind cloud-top profile based on Limaye's data is shown on figure 2.6, where it has been smoothed over 3° latitude to compare it with the lower resolution vertical shear data.

Extensive comparisons were also made with intensive groundbased measurements made over the five years preceding the Voyager encounters (Beebe, 1979). Comparisons with earlier results are more difficult because the latitudes were not measured accurately. The Voyager results tend to have larger zonal speeds than groundbased observations because groundbased observers tend to track major long-lived clouds, which tend to lie in between zonal jets in regions of slow zonal flow.

A major conclusion that emerged from these studies is that the meridional locations of these zonal jets appear to be constant to quite a high degree, not only on the four-month interval separating the two Voyager encounters but also over much longer times based on groundbased observations. There is excellent agreement with the two studies of Ingersoll et al. (1981) and Limaye (1987) between 60°N and 60°S. These Voyager 1 and 2 images provided nearly identical profiles except for a small latitude drift of .15° thought to be navigational.

The zonal winds are remarkably constant between Voyager encounters; the root-mean-square deviations from the zonally averaged values have been estimated to be less than 7 ms^{-1} at most latitudes (Limaye, 1986). In a later study (1987), Limaye showed a histogram of all deviations from the time-mean for all latitudes together; the data span over 300 rotations. It shows a sharply peaked symmetric distribution with most of the temporal eddies within a 5-10 ms^{-1} amplitude range

Limaye also displayed time series of zonal wind velocity based on the Voyager 2 data for a few latitudes (Limaye, 1987). At 22°S, they show a slow

variation of amplitude of 15 ms^{-1} over a 100 rotations period and additional variability of few ms^{-1} on a time scale of 12 rotations.

If the zonal jets appear to be quite steady, on the contrary, the appearance of the Jovian cloud bands has been reported to vary over a scale of a few years (Ingersoll and al., 79), as mentioned before. There is also vigorous eddy activity at the cloud-top at the small scales as seen in the Voyager images. Bright features are seen punching through the cloud layer and getting sheared by the mean flow on the time scale of a few rotations.

Horizontal temperature gradients are linked to vertical wind shears through the thermal wind relation. Although the wind profile has only been derived at cloud-top, the vertical wind shear can then be inferred at several heights to give information on the three-dimensional wind structure. For a rotating fluid in hydrostatic and geostrophic balance, this relationship between the zonal mean flow $\overline{u}$ and the zonal mean temperature $\overline{T}$ implies that

$$\overline{u}_z = - R\overline{T}_\phi \; / \; aHf$$

where ϕ is the latitude, z the altitude, R the gas constant, H the pressure scale height, a the planetary radius and f the Coriolis parameter.

As indicated before, the temperature has been retrieved in the upper-troposphere at 150 mbar and 270 mbar (Pirraglia et al., 1981; Gierasch et al., 1986); there are no reliable temperature retrievals at the cloud-top level. The derived thermal wind shears indicate a decay with height of the cloud-top velocities : the vertical shears derived from the thermal wind relationship are anticorrelated with the cloud-top wind (figure 2.6). This is true for both eastward and westward jets. The thermal wind relation breaks down at the equator but data shows that equatorial jets are also decaying a few degrees of latitude away from the equator. The inferred shears have the same meridional scale as the jets. The shears are of order of 10 ms^{-1} per scale height but these may be lower limits because of the

finite resolution of the measurements; the temperature field may vary over scales too small to be resolved.

The great similarity between shears retrieved at 150 and 270 mbar (Gierasch et al., 1986) appears to indicate that the jets decay monotonically in the upper-troposphere (figure 2.7). Maintenance of the inferred shears over two or more scale heights would be necessary to reduce winds to zero. This characteristic scale seems to be independent of the latitude.

Two noteworthy problems are the presence of a very strong vertical shear at 18°S, in an area characterized by an unusually broad westward jet scale. At 25°N, there is a good correlation between jets and vertical shears, and not with the albedo. This is the region which clouded up between the Pioneer and Voyager encounters as mentioned before.

The stability of the Voyager derived cloud-top wind profile has been investigated by Ingersoll et al. (1979). The stability criterion for thin atmospheres states that a necessary condition for instability of a zonal flow is that the potential vorticity (PV) gradient changes sign in the domain. The barotropic (two-dimensional) PV gradient in the β-plane approximation is written as

$$\overline{q}_y = \beta - \overline{u}_{yy},$$

where β is the meridional gradient of the Coriolis parameter. β is a positive quantity everywhere; the curvatures measured from the wind observations exceed β at many locations, specially in the cores of the westward jets, so that the vorticity gradient becomes negative; this suggests that the wind profile may be barotropically unstable. That work improved earlier conclusions derived with Earth-based data (Ingersoll and Cuzzi, 1969).

The temperature variance along a latitude circle, characterizing departures from the zonal mean, also depends on latitude as shown of figure 2.8 (Gierasch et al., 1986). At the 270-mbar level, the RMS deviations are large, of order 1-3 K, and are of large-scale. They are the largest over

the westward jets and somewhat smaller but still large over the stronger eastward jets. This fact, along with the stability considerations of the zonal flow, suggests that barotropic instabilities may play a role in the dynamics of the Jovian troposphere.

Early analyses from Ingersoll et al. (1981) computed an upgradient eddy momentum transport $\overline{u'v'}$, with eddies transporting momentum toward latitudes where the zonal flow is largest in magnitude. This positive correlation between $\overline{u'v'}$ and $\overline{u}_y$ indicates kinetic energy conversion from eddy to mean flow. By comparing the global conversion coefficient with the zonal mean kinetic energy, Ingersoll and coworkers suggest a conversion time scale of the order of 75 days. When the correlation between $\overline{u'v'}$ and $\overline{u}_y$, was computed for latitudinal bins 1° wide, the correlation coefficient was about .4 (Ingersoll et al., 1984). Srovmoski et al. (1985) show that correlation coefficients range between .3 and .54 for the differents data sets from Voyager 1 or Voyager 2; however the noisier data sets were shown to have the higher correlation coefficients. Srovmoski and coworkers (1982) found a negligible coefficient when they used a data set from images at four times poorer resolution. They used a "one feature per grid point" sampling method on a uniform latitude/longitude grid to find a negligible correlation; it suggests that uneven or incomplete sampling in longitude could explain the higher correlation found by Ingersoll, provided it is consistently biased. This could be true because in the earlier studies, prominent large eddies were oversampled. Such a momentum transport from eddies to mean flow would be incompatible with barotropic conversion resulting from jet instability.

As noticed by Flasar (1986), the contribution of cloud measurements with the product $\overline{u'v'}\ \overline{u}_y$) being negative nearly cancel the contribution of those with $\overline{u'v'}\ \overline{u}_y$) positive, so that the positive correlation results from less than 10% of the measurements. More will be said about the implications of these eddy fluxes later.

Difficulties arise when trying to compute a zonal mean momentum budget within latitude bands. The major eddy contribution, $\partial_y(\overline{u'v'})$, cannot be

accurately computed because of the relatively large errors in $\overline{u'v'}$. Also, eddy fluxes tend to induce mean meridional circulations which act to counter the fluxes of heat and momentum by the eddies; meridional velocities at the cloud tops on Jupiter are difficult to measure, although they could be inferred from a knowledge of eddy transports and diabatic heating rates (Flasar, 1986).

2.6. DO WE HAVE A PICTURE OF THE ZONE/BELT STRUCTURE ?

As mentioned before, there was an early interpretation of the zones as cloudy regions of rising motions with condensing NH_3 and belts as cloud-free regions of subsidence. No such simple picture of the cloud structure is clearly emerging. But from NH_3 abundances at various levels and also from the reflectivity maps (figure 2.10), it seems that there is agreement on the fact that the zones are bright and optically thick (high optical depth) and the belts depleted in NH_3 . That zone/belt structure disappears below two bars and there is a cloud component which spans both belts and zones just below the tropopause.

Gierasch et al. (1986) derived a meridional profile of the vertical velocity, $\overline{w}^*$, associated with the residual mean meridional circulation, from the thermodynamical equation applied to the temperature data at 270 mbar; they assumed constant values for radiative time constant t_R, static stability N^2 and radiative equilibrium temperature $\overline{T}_e$, so that $\overline{w}^*$ is essentially linearly proportional to $\overline{T}$. The argument of Gierasch et al. (1986) was essentially to suppose that the balance for the zonal mean temperature $\overline{T}$ is

$$\overline{w}^* (N^2 H/R) \sim -(\overline{T} - \overline{T}_e)/ t_R.$$

In this formula, H is the scale height and R the gas constant; the radiative time scale is typically 10^8 sec in the troposphere. On the jet scale, this implies meridional temperature contrast

$$\Delta T \sim (N^2 H/R)\ w^*\ t_R$$

where w* is an estimate of the vertical velocity. A ΔT of order 1 K imposes $w^* \sim 10^{-9}$ H/s. The meridional profile of $\overline{w}^*$ derived by Gierasch et al. (1986) coincides nicely with variations of ammonia concentration at cloud-top levels, ortho-para ratio and cloud optical depth. This derivation of a dynamical quantity together with the temperature retrievals provide a consistent basis to the abundance and albedo-derived conjectures about the meridional circulations.

The dynamical aspects will be examined in a later chapter, but we want to mention at this point that people have sought to link the belt/zone cloud structure with a vertical velocity field having roots in the jet dynamics. It was early recognised that meridional circulations would be associated with the vertical decay of the jets in a dissipative upper troposphere (Conrath and Pirraglia, 1983; Busse, 1983). In the more detailed modeling undertaken by Gierasch et al. (1986), the meridional circulation was driven by a linear drag on the mean momentum; they showed that the circulation induced by such a drag in the .680-.150 mbar layer is compatible with observations.

The nature of the drag is not revealed by these models but it is clear from these studies that further investigations of in-situ instabilities are greatly desirable. In this thesis, we will pursue the idea that the jet decay and meridional circulations are driven by large-scale instabilities of a deeper flow extending over the upper troposphere. The idea that large-scale inviscid instabilities could provide such a drag effect was tested by Pirraglia (1989) and independent results were presented by Orsolini and Leovy (1989a). How such instabilities could drive meridional circulations was first analysed by Orsolini and Leovy (1989b).

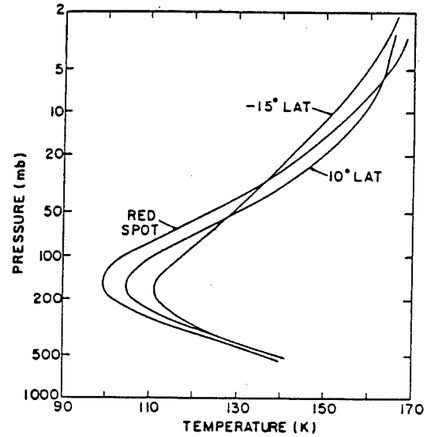

A

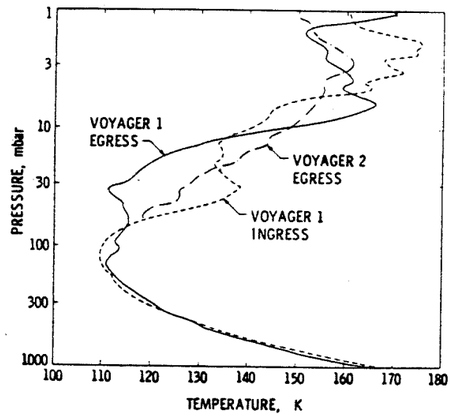

B

Figure 2.1: **A)** Temperature profiles of Jupiter retrieved from the infrared data of Voyager 1. The figure is taken from Encrenaz (1990) and is originally from Hanel et al. (1979). **B)** Temperature profiles from the radio occultation data from Voyager 1 and 2. The figure is taken from Flasar (1986) and is originally from Lindal et al. (1981).

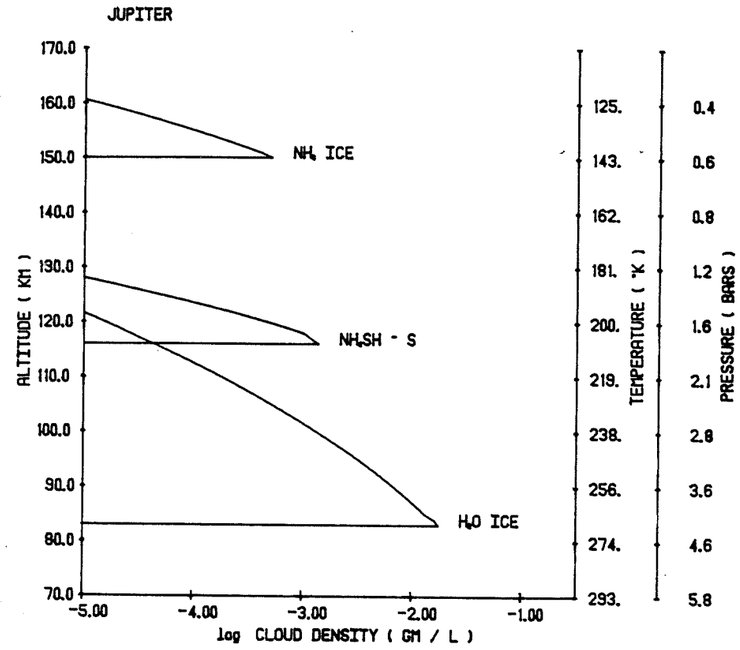

Figure 2.2: Cloud structure of Jupiter for a solar composition atmosphere and thermal profile from Voyager data. Altitudes are relative to the 200 bars level. The figure is taken from Atreya and Romani (1985).

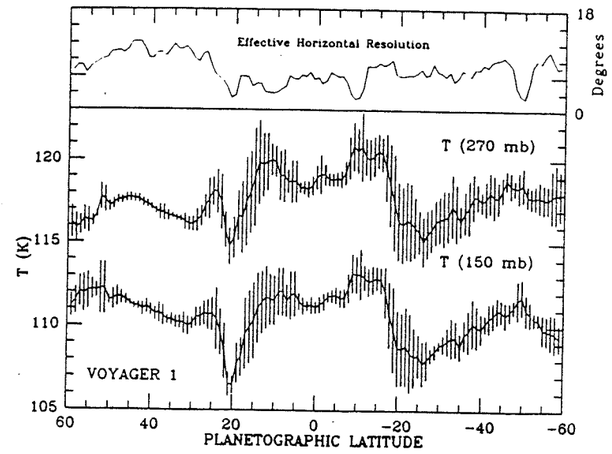

Figure 2.3: Zonal mean temperatures at 150 mb and 270 mb retrieved from the infrared data of Voyager 1. The figure is taken from Gierasch et al. (1986).

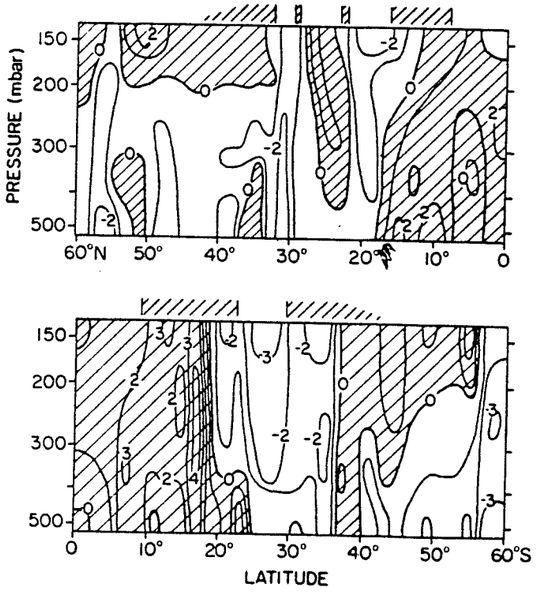

Figure 2.4: Cross-section of the zonal mean temperature deviations from the latitudinal mean as measured by Voyager 1. Top panel is the Jovian northern hemisphere and bottom panel is the southern hemisphere. The figure is taken from Pirraglia et al. (1981).

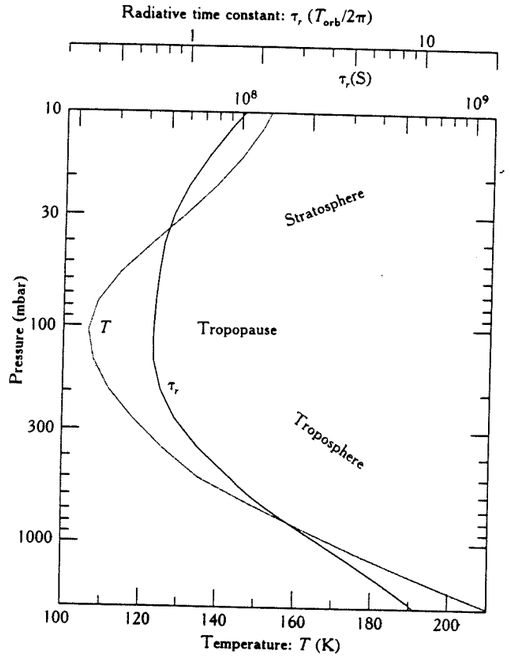

Figure 2.5: Radiative damping time, τ_r, as a function of pressure for a typical profile of temperature. The figure is taken from Flasar (1987).

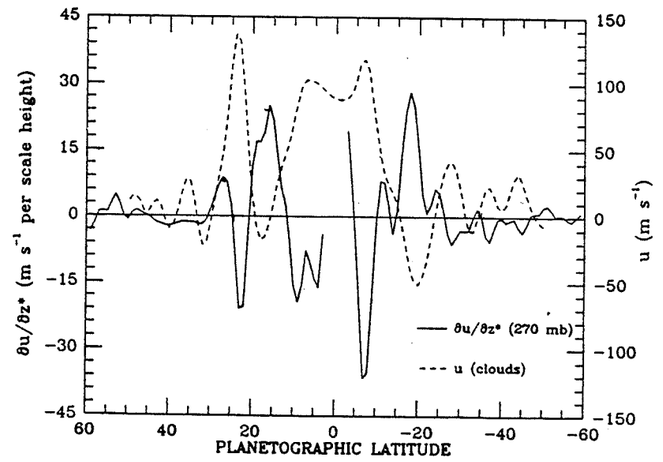

Figure 2.6: Zonal mean cloud-top wind and thermal wind shear at 270 mb as a function of latitude. The figure is taken from Gierasch et al. (1986).

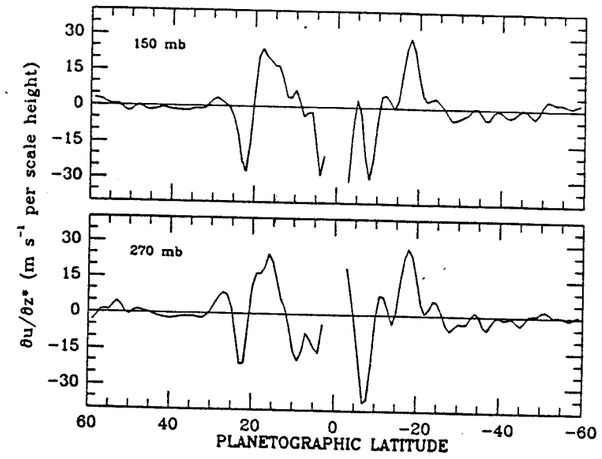

Figure 2.7: Zonal mean thermal wind shear at 270 mb and 150 mb as a function of latitude derived from Voyager 1 temperatures. The figure is taken from Gierasch et al. (1986).

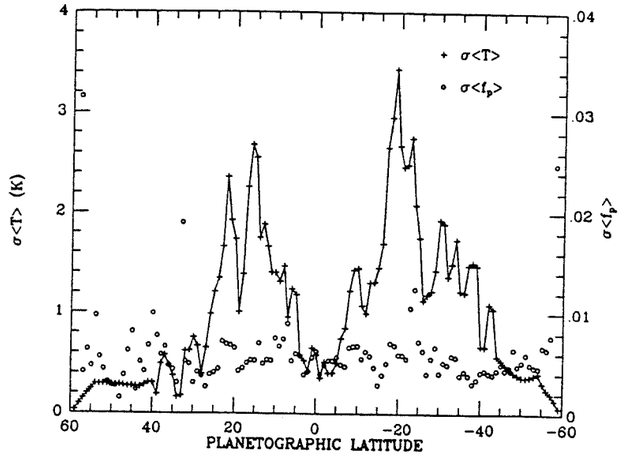

Figure 2.8: Standard deviation of Voyager 1 270-mb temperatures and para-hydrogen retrievals as a function of latitude. The figure is taken from Gierasch et al. (1986).

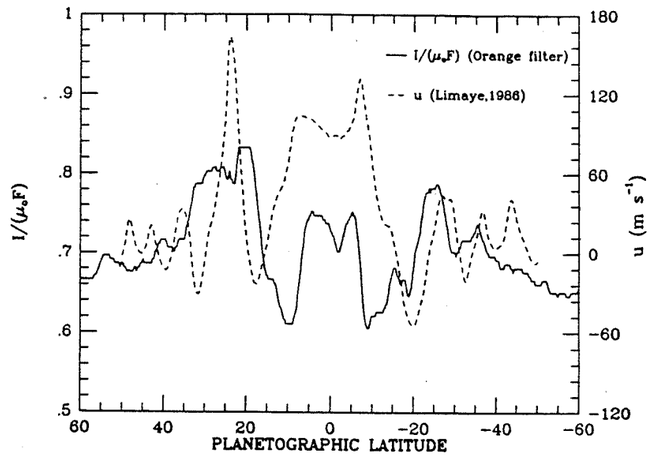

Figure 2.9: Orange reflectivity and cloud-top wind from Voyager 1 images. The figure is taken from Gierasch et al. (1986).

CHAPTER 3 : LINEAR INSTABILITIES

3.1. INTRODUCTION.

3.1.1. PREVIOUS STUDIES OF THE INSTABILITY PROBLEM.

Previous attempts have been made to characterize the linear instabilities of the Jovian troposphere within quite different sets of hypotheses.

Some models were based on generalizations of the well-known Eady model of baroclinic instability. Gierasch (Gierasch et al., 1979) investigated the baroclinic stability problem for Jovian atmospheres with a model that kept some of the features of the Eady model, such as a zonal flow increasing linearly with height on an f-plane, but instead of a rigid lower boundary condition, they introduced a lower fluid layer, supposed very deep, hydrostatic, motionless and of low static stability. The continuity boundary condition at the interface had the effect of reducing considerably the Eady growth rates. They further generalized his model by relaxing the hydrostatic balance in the lower layer. In that calculation, growth rates were again reduced.

In another generalization of the Eady model, Read (Read, 1988) introduced the effect of compressibility to assess its influence on motions extending over many scale heights, the relevance to Jovian atmospheres being that disturbances might extend from the tropopause down to below the cloud deck. He kept the features of the Eady model, in particular the rigid lower boundary condition, and the role of compressibility was examined as a function of the domain vertical extent. When the domain extended over more than three scale heights, disturbances were less unstable than in the incompressible Eady model.

The relevance of the Eady problem to the stability of the Jovian atmosphere is questionable : observations suggest that the vertical shears are such that

zonal flows are decaying with height and that meridional shears are important. Moreover, the applicability of the model clearly depends on the kinematic condition applied at the lower boundary. As in Gierasch et al. (1979), Conrath et al. (1981) argued that a boundary condition of zero amplitude for the disturbance geopotential would be more appropriate when a deep adiabatic layer is present. The Eady modes are then strongly suppressed as mentioned above. Other types of instabilities could be of some importance: other boundary-induced instabilities have been examined by Conrath et al. (1981). In a model of mixed barotropic-baroclinic instabilities, they included a jet-like profile in the meridional plane along with a vertically sheared flow. A zero amplitude boundary condition was applied at the bottom and a rigid one at the top. Instabilities were triggered by the kinematic boundary condition at the top; they were caused by the β-effect in analogy with the usual Charney modes but operated on the westward jets only. Barotropic instability was also operating, preferentially on the westward jets when meridional extent was narrow enough.

Instabilities of the internal type were also proposed as being relevant to the Jovian circulation (Read, 1988; James and Hoskins, 1985). They appear relevant for the Jovian atmosphere problem as the zonal flow has strong meridional curvatures and vertical shears and no solid boundaries.

In the context of the stability of the terrestrial atmosphere, internal instabilities of a vertical shear-zone were examined by Dickinson (1973). He studied a pure baroclinic problem, not allowing barotropic instability and noticed that negative shear zones, for example the decay zones above the cores of the eastward jets, were more unstable in the sense that the instability domain extended over a wider range of shears and larger growth rates were obtained than for the positive shear zones. This effect was due to the stabilizing effect of the vertical shear in the positive shear zones on scales which are of order of the scale height. In the Jovian stability problem, meridional curvatures of the westward jets will modify this picture, as the westward jets are barotropically more unstable. Dickinson also pointed out the existence of radiating instabilities at long wavelengths, extending in the vertical over many scale heights in the region of relative

eastward flow.

Three-dimensional internal instabilities were examined by Pfister (1979) for jet profiles representative of the terrestrial stratospheric circulation. He defined a Burger number, Bu, from the mean flow scales as :

$$Bu = (fL / ND)^2$$

where f is the Coriolis parameter, N the static stability parameter, L the mean flow meridional scale and D the mean flow vertical scale. He investigated a small Burger number regime, with vertical shear modulating essentially barotropic instabilities. Also, the Boussinesq approximation was used.

We introduce hereafter a model to study internal instabilities of mean flows representative of the Jovian atmosphere; they are similar to Pfister's (1979) flows but the effect of compressibility is included and boundary conditions are appropriately modified. The parameter space is also different : we look at cases where the Burger number is not necessarily small. We study westward as well as eastward jets; eddy fluxes and the residual mean meridional circulations they drive are investigated in more detail than in Pfister (1979). The model extends from the convective/radiative boundary up to the tropopause and above, and the waves have zero amplitude at the bottom following the suggestions of Gierasch et al. (1979) and Conrath et al. (1981). We should also stress the point that the problem is non-separable, the mean flow being a function of both vertical and horizontal directions. One then needs to resort to numerical techniques to solve the linear stability problem.

3.1.2. MODEL DESCRIPTION.

We hereafter suppose that the large-scale dynamics of the Jovian troposphere obeys quasi-geostrophic scaling. This dynamical regime corresponds to regimes of many planetary flows. For representative horizontal scale, L, and velocity, U, this regime corresponds to :

1°) small aspect ratio H/L, where H is the pressure scale height, for the hydrostatic balance to be respected.

2°) small Rossby number Ro = U/fL, where f is the Coriolis parameter. This condition insures that we are concerned with large-scale motions characterized by a time scale long compared to the rotation time scale.

3°) large Richardson number $Ri = (NH/U)^{1/2}$, where N is the static stability parameter. This imposes the condition that the fluid is strongly stably stratified.

4°) the quasi-geostrophic regime studied here corresponds to $RoRi^2$ not too small, i.e. that the Rossby radius, NH/f, is not too small compared to L.

For the Jupiter troposphere, one has $L \approx 2000$ km, $U \approx 30$ ms^{-1}, $H \approx 20$ km, $f \approx 10^{-4}$ s^{-1}. The static stability for the upper troposphere is estimated by Gierasch et al. (1986) to be $N \approx 0.016$ s^{-1}. One can see that the aspect ratio is about 10^{-2}, the Rossby number $1.5\ 10^{-1}$, the Richardson number $Ri \approx 3$, and the Rossby radius of the order of 3000 km. The only condition which is only weakly verified is condition 3°. The static stability parameter is not well constrained below the cloud-top either and could be considerably smaller. This has led to preliminary studies of the large-scale dynamics of weakly stratified flows (Allison and Gierasch, 1982). Nevertheless, we will assume that the flow is stably stratified in the usual sense for large-scale quasi-geostrophic motions.

We consider the quasi-geostrophic perturbation vorticity equation on a mid-latitude β-plane :

$$(\partial_t + ik\,\overline{u})\ \mathbf{L}_k(\psi) + ik\,\overline{q}_y\,\psi = D$$

where

$$\overline{q}_y = \beta - \overline{u}_{yy} - \varepsilon \mathbf{L}_z(\overline{u}_z)$$

$$\mathbf{L}_k = (-k^2 + \partial_{yy}) + \varepsilon (\partial_{zz} - 1/4H^2)$$

$$\mathbf{L}_z = \rho^{-1}\partial_z(\rho),$$

$$\varepsilon = f^2/N^2$$

$$\rho = \rho_0 \exp\{-z/H\}.$$

D is a radiative damping term and N is the constant static stability; the unknown ψ is related to the geopotential perturbation ϕ by

$$\phi(x,y,z,t) / f = \mathrm{Re}\,[\, \psi(y,z,t) \exp\{z/2H\} \exp\{-ikx\} \,] .$$

The quasi-geostrophic perturbation vorticity equation is solved using finite differences in the vertical and meridional directions. The inversion of the elliptic operators was done using the Lindzen-Kuo scheme (Lindzen and Kuo, 1969) and is explained in greater detail in the appendix A. The well-known initial value approach was used (Geisler and Garcia, 1976), by which the time integration of that equation, with $\psi(y,z,t)$ as the unknown, was pursued until an initially small perturbation converges toward the most unstable mode. $\psi(y,z,t)$ factorizes then as :

$$\psi(y,z,t) = \Psi(y,z) \exp\{-ikct\},$$

$c=c_r+ic_i$ being the complex phase speed and $\Psi(y,z)$ the complex mode structure. The growth rate of the perturbation is then $\sigma = kc_i$ and the phase speed is c_r. Once the most unstable mode has been isolated, we compute its meridional fluxes of momentum, $\overline{u'v'}$, and of heat $\overline{v'T'}$; the Eliassen-Palm flux divergence divided by the density (EPFD), which we will write F, is also an important dynamical quantity as it represents the eddy driving of the zonal mean momentum. As usual, the eddy velocities are simply given by

$$u' = \phi_y / f,$$
$$v' = - \phi_x / f.$$

One has therefore :

$$\overline{u'v'} = - \phi_x \phi_y / f^2$$

$$= -k/2 \exp\{z/H\} (\psi_i \partial_y \psi_r - \psi_r \partial_y \psi_i)$$

and similarly

$$\overline{v'T'} = - k/2 \exp\{z/H\} (\psi_i \partial_z \psi_r - \psi_r \partial_z \psi_i).$$

where $\psi = \psi_r + i \psi_i$. The Eliassen-Palm flux divergence per unit mass is written as

$$F = - \partial_y (\overline{u'v'}) + \varepsilon \mathbf{L}_z (\overline{v'T'})$$

or

$$F = -k/2 \exp\{z/H\} \{ [\psi_i \partial_{yy} \psi_r + \varepsilon (\psi_i \partial_{zz} \psi_r)] - [\psi_r \partial_{yy} \psi_i + \varepsilon (\psi_r \partial_{zz} \psi_i)] \}.$$

This quantity acts as a wave-induced source in the mean momentum equation. In order to facilitate the study of the wave-mean flow problem, we use the transformed Eulerian-mean (TEM) formalism (Andrews, Holton and Leovy, 1987). The main advantage of the TEM formalism is that, while the eddy-forcing terms appear explicitly in the mean momentum equation, they do not appear in the thermodynamic equation. A quantity that we name S_0, defined by the relation

$$S_0 = - (f/N^2) \rho_0 \partial_z F,$$

acts as a source term for the residual mean meridional circulation (RMMC) streamfunction $\overline{\chi}^*$. Throughout the rest of this dissertation, the *-

quantities have to be understood as quantities in the TEM formalism. As we are interested in processes on the meridional scale of the jet, it seems reasonable to assume that the heating rate has a negligible meridional gradient. Neglecting then the radiative processes, the equation for the streamfunction is

$$[\,\partial_{yy} + \varepsilon\,\rho_0\,\partial_z\,(\rho_0^{-1}\partial_z)\,]\,\overline{\chi}^* = S_0.$$

The equation for $\overline{\chi}^*$ is elliptic; the response to a localized forcing is then non-local and the aspect ratio of the induced streamfunction is essentially the Burger number. It should be again emphasized that it is essentially the vertical derivative of the Eliassen-Palm flux divergence that acts as a source of the streamfunction $\overline{\chi}^*$, i.e. it is the vertical shear in the mean momentum source that creates mean meridional circulations. The associated meridional and vertical velocities are respectively,

$$\overline{v}^* = \rho 0^{-1}\ \partial_z\,\overline{\chi}^*$$

and

$$\overline{w}^* = -\,\rho 0^{-1}\ \partial_y\,\overline{\chi}^*.$$

The equation for the streamfunction was solved using the Lindzen-Kuo scheme taking advantage of the fact that the elliptic operator to be inverted had many common matrix elements with the operator inverted while solving the perturbation equation for the geopotential.

We investigated the class of flows

$$\overline{u}(y,z) = U_0\ \mathrm{sech}^2\,(y/L)\ \ \mathrm{sech}^2\,(z/mH).$$

The mean flow has no vertical shear at the lower boundary at z=0 where it overlies the assumed barotropic convective zone but it decays over a height range of several scale heights as measured by the parameter m. In a first

round of calculations, we have ignored any radiative damping. One should remark that although the mean flow is a product of a function of y by a function of z, the partial differential equation for the geopotential perturbation is not separable.

The pure barotropic instability of the Bickley jet

$$\overline{u}(y) = U_0 \, \mathrm{sech}^2 (y/L)$$

has been extensively studied (Haltiner and Williams, 1980); the jet being symmetric in y, unstable modes are either symmetric or antisymmetric. The symmetric mode is sometimes referred to as the sinuous mode and the antisymmetric one as the varicose mode. In the linear analysis, the symmetric modes are the most unstable. This is a general property of inviscid parallel shear flows (Drazin and Howard, 1966) when β=0; this property holds when β is non-zero. This is confirmed for the Bickley jet in the presence of a β-effect by the numerical results of Kwon and Mak (1988) in the case of the westward jet. For the eastward jet, the complete stability diagram of the antisymmetric modes when β is non-zero seems to be lacking in the literature, but Lipps (1962) has shown that the symmetric modes have a wider instability domain and that in the vicinity of the neutral curves the symmetric modes have larger growth rates than the antisymmetric modes. Accordingly, we have restricted our study to the sinuous modes.

This allows us to restrict the computational domain to a half-jet and to impose a boundary condition of symmetry at the jet center. This also implies that the EPFD is symmetric at the jet center. The perturbation is set to zero at the other meridional limit of the computational domain. The vertical boundary conditions were that the wave has zero amplitude at the top and the bottom as previously discussed. The source term S_0 being symmetric about the jet core, the appropriate boundary conditions on the streamfunction $\overline{\chi}^*$ were that it was symmetric at the jet center and goes to zero at other boundaries. This implies that the meridional velocity derived from $\overline{\chi}^*$ is symmetric while the vertical velocity is antisymmetric. Table 3.1

shows which variables are symmetric at y=0 and which ones are antisymmetric. Details on the numerical method are given in Appendix 1.

Table 3.1: Symmetric (S) and antisymmetric (A) quantities

ψ	S
v'	S
u'	A
F	S
$\overline{u'v'}$	A
$\overline{v'T'}$	S
$\overline{\chi^*}$	S
$\overline{w^*}$	A
$\overline{v^*}$	S

We chose values for atmospheric parameters that are representative of the Jovian midlatitudes; $N = .016\ s^{-1}$ as representative of the upper troposphere (Gierasch et al., 1986), $H = 22$ km, $f = 1.2029\ 10^{-4}\ s^{-1}$, $\beta = 4.623\ 10^{-12}\ m^{-1}s^{-1}$.

3.2. BAROTROPIC EFFECTS.

3.2.1. BAROTROPIC WESTWARD JETS.

As a first case study, we will focus in this section on barotropic westward jets. This is a simple problem which makes it possible to outline some characteristics which will be useful latter. The key parameter in the pure barotropic instability case is

$$\beta^* = \beta L^2 / U_0,$$

L being the mean flow meridional scale. We know that westward jets are unstable for β^* in the range (0,-2); this is the instability domain for the symmetric modes (Kuo, 1973). Observations can constraint the choice of U_0 and L; if ones takes U_0 as the representative cloud-top jet intensity and L its

representative length scale, one can see that the observed jets are well in the range of unstable jets as computation of the vorticity gradient from observed velocities had suggested (Ingersoll et al., 82). We desire to make the least assumptions about the deep jet structure; consequently, we only assume that the jets are stronger at deeper levels and decay above to magnitudes typical of the observed cloud-tops. We chose to take jet intensities of the order of 100 ms^{-1} for both eastward and westward jets.

We ran the model for Bickley jets with the parameters U_0 and L representative of a strong jet case : U_0 = - 90 m/s and L = 2000 km, which gives β^* = - 0.2. We also considered a weak jet case : U_0 = -25 m/s and L = 2000 km, which gives β^* = -0.7. The barotropic case considered in this section corresponds to the parameter m being very large and it proved sufficient to take m = 100.

Figure 3.1 shows the growth rate as a function of the wavenumber k for both β^* = -0.2 (strong jet case) and β^* =-0.7 (weak jet case). Here k is an integer giving the number of wavelengths at the chosen latitude circle (20° in this case). For β^* = -0.2, one has a maximum growth rate around k = 30. For β^* = - 0.7, the growth rate curve has a maximum around k = 40; in that case, there is also a secondary maximum around k = 18. The model results agree very well with values indicated in Haltiner and Williams (1980). For β^* = - 0.7, a growth rate of about σ = 0.18 day^{-1} is predicted at the wavenumber of maximum instability, i.e. around k = 40. This corresponds to a nondimensional wavenumber kL= 1.4 and the asymptotic growth rate agrees well with the 0.17 value of Haltiner and Williams.

The maximum growth rate corresponds to trapped modes which have their amplitude confined to the jet core; it is well known that when β^* is sufficiently large in magnitude, there is a secundary maximum in the growth rate curve which corresponds to radiating modes whose amplitude can extend to large distances away from the jet core (Haltiner and Williams, 1980). In the following, we will first concentrate on describing the properties of trapped modes, which are the most important modes because of their larger growth rate.

density weighting and boundary conditions. Indeed in the Boussinesq limit where H goes to infinity, all quantities would be either symmetric or antisymmetric in the vertical; the EPFD term and the zonal wind tendency would be $\cong \sin^2 \pi z/z_2$; $S_0 \cong -2 \sin(\pi z/z_2) \cos(\pi z/z_2)$ creating a clockwise cell in the upper half and a counterclockwise cell in the bottom half. The meridional velocity $\overline{v}^*$ would be symmetic in the vertical with the poleward (direction of increasing y) branch at midlevel.

The phase speed of the most unstable mode is about .6 of the jet maximum, i.e. $c_r = .6\ U_0$.

The modes around the primary maximum of the growth rate curve were trapped in the meridional direction, extending over a distance comparable to the jet scale. For lower wavenumbers and β^* sufficiently large in magnitude, modes were found which extend long distance away from the jet center. Such modes are often called radiating modes and are the equivalent of the Green modes of some baroclinic stability problems. These modes correspond to destabilized Rossby waves in the far-field (where the mean flow has decayed to zero) and are excited by the instability in the core of the jet under appropriate phase speed matching conditions (McIntyre and Weisman, 1978), i.e. when phase speeds of the instabilities match phase speeds of Rossby waves in the far-field. In this case, the meridional boundary condition at a finite distance from the jet core confines the meridional extent of the mode amplitude.

As an example, the radiating mode for $\beta^* = -0.7$ and k=18 is displayed on figure 3.4. The amplitude decays fast in the core of the jet and is meridionally radiating away from the jet at great distances compared to the jet scale (figure 3.4a). Away from the jet, the momentum flux is decaying meridionally at a rate twice as fast as the wavefunction. In our example, the envelope of the amplitude has a characteristic meridional scale of at least 10 L; therefore, on the poleward side of its minimum, the momentum flux is smeared over a broad region of width 5 L. The EPFD is still positive in a region of width L/2 in the core of the jet, but becomes very small away from it (figure 3.4e). This is to be contrasted with the large negative area for

the trapped modes. It is because the envelope of Ψ is slowly decaying that the EPFD term is negligible. Consequently, the source term S_0 is reduced on the poleward side of the jet core. This creates a streamfunction pattern in which the clockwise cell can expand to greater distance away from the core (figure 3.4h); this dictates the pattern of vertical velocities which is shown to expand to a distance 2 L away from the jet. The growth rate for this mode is about one third of the growth rate of the most unstable mode.

We have not further investigated radiating modes because they have smaller growth rates and will consequently have little role in the wave-mean flow problem.

3.2.2. DECAYING WESTWARD JETS.

The next step is to introduce vertical shear by reducing m progressively. Note that the scale parameter m is the distance over which the wind decays to about 40% of its maximum value, measured in units of scale heights. We focus on the trapped instabilities of westward jets in this section. Also, we explore the regime where instabilities are of barotropic nature, leaving the baroclinic ones for a later section. The parameter m took the following values : 100,10,5,2,1.

The resulting growth rate spectrum is shown on figure 3.5a for the various shear zone thicknesses and β^*= -0.2 (corresponding to U_0 = -90 ms^{-1} and L=2000 km); k is again the zonal wavenumber expressed as the number of wavelengths on the Jovian latitude circle. One can see that for the displayed range of m, the vertical shear is stabilizing: the domain of instability is shrinking and the magnitude of the growth rates decreases. The phase speed keeps nearly the barotropic value whatever the value of m (figure 3.5b).

The shear has also the effect of confining the wave vertically; the vertical dependence of the wave amplitude is no longer of the type of $\sin(\pi z/z2)$ as in the m=100 case, but peaks below the middle of the domain. This is illustrated in figure 3.6 for m= 5 and 1. We associate a Burger number with

the mean flow scales :

$$Bu = (fL / mNH)^2.$$

Note that there are various definitions of the Burger number in the literature. Sometimes, the inverse of the above quantity is defined as Burger number; we took the definition of Pfister (1979) : a small Burger number corresponds to nearly barotropic instability. Table 3.2 shows the Burger numbers for the mean flows corresponding to various values of m.

Table 3.2 : Burger number as a function of m

m	Bu
100	$44\ 10^{-6}$
10	0.0044
5	0.017
2	0.11
1	0.44
0.5	1.76
0.25	7.00

We examine the case m=2 and look at the structure and properties of the most unstable mode (figure 3.7) which has a wavenumber k=20. The vertical structure is strongly influenced by the vertical shear, with the mode being confined by the shear layer and the associated critical surface. The critical surface is defined as the curve where the mean flow equals the wave phase speed. The critical surface is shown on figure 3.7a and its role in confining the mode amplitude will be examine latter.

The most unstable modes have the meridional structure of a barotropic wave trapped by the jet; the amplitude peaks at the jet core and decays away from the jet, while the phase has the meridional tilt necessary to ensure energy conversion from the mean flow to the wave as in the pure barotropic case. Correspondingly, the momentum flux $\overline{u'v'}$ has the dipolar structure necessary to flatten the jets (figure 3.7f), and the heat flux is two orders of magnitude smaller than the momentum flux which dominates the EPFD

term (figure 3.7d and e). The wave Eliassen-Palm flux divergence per unit mass, F, has the required structure to smooth the jet meridionally and to reduce the jet amplitude at all heights, at least in the jet core. It also drives a clockwise RMMC with ascending motions on poleward side of the jet center (figure 3.7g,i). A subsiding cell is stacked above the rising cell.

Figure 3.8 shows how the growth rate depends on the vertical scale m for k=20. It shows the decrease of σ from the pure barotropic value down to a value of σ=.1 corresponding to a minimal instability when

$$mBu \sim 1.$$

This behavior results from the fact that for westward jets the vertical shear is stabilizing and offsets the meridional curvature. Indeed, these two terms in the $\overline{q}_y$ expression scale as

$$\varepsilon \overline{u}_z / H \overline{u}_{yy} \sim \varepsilon L^2 / mH^2 \sim mBu.$$

For the barotropic cases, mBu is small ($\sim 10^{-2}$). As m decreases, mBu increases and minimal instability occurs when the two terms compensate each other at mBu ~ 1. Baroclinic effects start becoming important for m less than 1 with growth rates increasing as vertical curvatures generate baroclinic instability. These instabilities are described in a separate section. The balance that dictates the condition mBu ~ 1 is therefore approximate and will be further refined at a later stage.

How the presence of vertical shear acts to decrease the growth rate of the most unstable mode was put forward by Pfister (1979). The growth rate can be shown to be the ratio of the mean-to-eddy energy conversion (mainly barotropic) to the total wave energy. A decaying wind profile reduces that ratio.

The origin of the vertical wave trapping can be related to the morphology of the critical line and propagation theorems. One can readily see that the wave propagates in a region where the mean flow is westward relative to

the wave phase speed. This may seem at first contrary to the Charney-Drazin theorem, but these waves originate in instabilities and more general propagation theorems have to be considered (Andrews, Holton and Leovy, 1987).

For one-dimensional problems, insight into vertical propagation has been gained by using a refractive index n; the vertical propagation equation then reads

$$\Psi_{zz} + (n^2/\varepsilon)\,\Psi = 0,$$

where n is the complex refractive index given by :

$$n^2 = -\varepsilon/4H^2 + \overline{q}_y / (\overline{u}-c) - k^2.$$

In dealing with instabilities, n is complex because of the complex phase speed c. Looking at the real part of n^2 gives information on the propagation characteristics as it does for neutral modes. In the latter case, n^2 is real and the wave can be trapped by regions in which $n^2<0$.

The situation can be further analysed when the mean flow is constant. We find it useful to introduce the complex number $x + i\,y = -n^2$. One can easily show that we have propagating modes when

$$x = \varepsilon/4H^2 - \overline{q}_y\,(\overline{u}-c_r)\,/\,|\overline{u}-c|^2 + k^2 < 0.$$

For neutral modes, this implies that

$$\overline{q}_y\,/\,(\overline{u}-c_r) \;>\; k^2 + \varepsilon/4H^2$$

which is the condition of the Charney-Drazin theorem as $\overline{q}_y$ then reduces to β. One then has

$$0 < \overline{u} - c_r < \overline{u}_c = \beta/(k^2 + \varepsilon/4H^2),$$

so that the wave can only propagate in regions where the mean flow speed is relatively eastward and not too large. In regions where $x < 0$, one can write ψ as a Rossby wave, while in regions where $x > 0$, it is a trapped wave with no vertical tilt (Holton, Andrews and Leovy, 1987). The condition $x<0$ also holds when n^2 is complex. By applying a similar condition, one can also rederive the criterion for the existence of radiating unstable modes (Charney and Pedlosky, 1963; Holton, 1974).

Although this analysis is derived for a constant wind, one can apply the same condition on the sign of n^2 when the wind -and consequently the refractive index- varies with height (Holton, Andrews and Leovy, 1987). This approximation is used in geometrical optics and acoustics. Although our problem is two-dimensional and not separable, these conditions on vertical propagation have proven useful in interpreting the results.

Looking at the vertical profile of n^2 at the jet core for the case of the westward decaying jets, one has a propagating region below the critical surface. The quantity x is then negative because $\overline{q}_y < 0$ and $\overline{u} - c_r < 0$. The negative sign of $\overline{q}_y$, due to the large contribution of the meridional curvature, explains why the wave propagates although the mean flow is westward relative to the wave phase speed.

Above the propagation region, one has $x > 0$ because one still has $\overline{q}_y < 0$ while $(\overline{u} - c_r) > 0$. This is clearly a trapping region; at some height, $\overline{q}_y > 0$ and $(\overline{u} - c_r) > 0$, but the inequality $x < 0$ still holds. This is illustrated in figure 3.9a which shows the vertical profile of $Re\{n^2\}$ as well as the profile of $\overline{u}$ for reference. The dip where $Re\{n^2\}$ becomes zero is where $\overline{u} \approx c_r$. Above it, at about z=1.8H, the wave is trapped. Although the real part and the imaginary part are of the same order of magnitude, it is the zero-crossing of $Re\{n^2\}$ which matters for propagation.

A cautionary remark is that n^2 obviously depends on c_r. Whether one has a trapping or a propagating region depends on the wave phase speed. A region can still sustain Rossby wave when β is non-zero; these can be excited under appropriate phase speed matching conditions and radiating

instabilities are found in these circumstances. For unstable modes, one cannot have purely radiating modes even where n^2 is constant; as a consequence of the imaginary part of n^2 being non-zero, there is always some amount of decay. The distinction between radiating mode and trapped mode has to rest on the comparison of the decay scale to the vertical wavelength.

A look at the zonal wind tendency for m=2 (figure 3.10) shows that the instabilities tend to broaden the jet. This is due to the contribution of the EPFD which is at least an order of magnitude higher than the contribution of the term $f\overline{v}^*$. The EPFD term acts essentially as a smoother in the meridional direction, although it also acts as a vertical drag term, at least in the core of the jet. One can remark that the effect of the instability is to smooth out the $\overline{q}_y$ profile as well. The necessary condition for an instability to occur is that $\overline{q}_y$ changes sign over the domain. The barotropic instabilities of westward jets are associated with the pockets of negative $\overline{q}_y$ in the cores of the jets. The instabilities act on the $\overline{q}_y$ field in a similar fashion : they tend to increase $\overline{q}_y$ in the core, and to decrease it in the wings. This could be seen from the following simple considerations :

$$\overline{u}_t \approx F$$

$$\overline{q}_{yt} \approx - F_{yy}.$$

Taking into account that the meridional profile of F is very approximately sinusoidal, one can see that $\overline{u}_t$ behaves as $\overline{q}_{yt}$.

3.2.3. DECAYING EASTWARD JETS.

Growth rates for eastward jets are also shown on figure 3.5 for $\beta^*=0.3$ ($U_0=150$ ms^{-1}, L=3125 km) well in the range of pure barotropic instability : $0 < \beta^* < 2/3$. From inspection of figure 3.8, one can see that a weak vertical shear readily stabilizes the jet. In contrast to the westward jets which have minimal instability at m Bu ~ 1, the eastward jets are stabilized by much smaller vertical shears, a result also found by Pfister (1979). In this case,

the phase speed is : $c_r \sim 0.4\ U_0$. The structure of the mode for m=10 is shown on figure 3.11; as for westward jets, the waves are trapped below the shear zone; however, maximum amplitude and fluxes for the eastward jet case occur at higher levels where barotropic energy conversion is weak. Again the eddy fluxes tend to smooth the jet horizontally and these fluxes then drive stacked cells of the RMMC to maintain the geostrophic balance. The lower cell has rising motions on the equatorward side of the jet; this still corresponds to rising motions in areas of anticyclonic shear, i.e. a zone-like behavior.

In terms of the propagation theorems, the smaller value of c_r/U_0, allows the wave to propagate to higher levels as can be seen from the diagram of $Re\{n^2\}$ in figure 3.9b. As the wave amplitude peaks at a higher level, the conversion is weaker.

3.3. BAROTROPIC AND BAROCLINIC EFFECTS.

3.3.1. BAROCLINIC INSTABILITY.

Figure 3.8 shows that the growth rate increases when m decreases below some value. One enters a parameter regime where the vertical curvature of the mean flow becomes the source of energy for the disturbance. The results for m=.25 are shown on Table 3.3.

Table 3.3 : Growth rate and phase speed when m=.25

U_0	m	σ	c_r/U_0
-90	.25	.18	.6
150	.25	.34	.6

In the barotropic regime, one has $F \approx -\overline{(u'v')}_y$; as the instabilities tend to smooth the jet horizontally, u'v' is always negative on the poleward side of the westward jet and has a single lobe structure, so that F has the structure

of a dipole oriented in the horizontal direction, which we may call the "active direction". When m = .25, one has a baroclinic case with $F \approx L_z$ $(\overline{v'T'})$; now, z is the "active direction" and the instabilities tend to smooth the jet in the vertical. Note that the domain vertical extent is much smaller than in the barotropic regime previously described. Figure 3.12 displays the mode for the westward jet case and m=.25; the EPFD term has now a dipolar structure oriented along the vertical. The baroclinic nature of the instability can also be traced back in the conventional fashion to the vertical tilt of the phase of ψ.

Baroclinic instabilities now drive a main RMMC with rising motions in areas of cyclonic shears. This is not compatible with the traditional interpretation of the zones as regions of upwelling and anticyclonic shears. In the barotropic case, the vertical structure of the EPFD drives two sources for the RMMC; consequently, one has two cells with opposite circulations stacked upon each other. In the baroclinic case however, the EPFD term is dipolar in the vertical. The source of the RMMC has a more complex structure but drives a single broad cell; this cell corresponds to a tendency for suppressing the vertical shear which is the origin of the instability. A look at the source for the RMMC for the westward jet case (figure 3.13) shows that the positive peak which drives the upper cell is much greater than the negative peak which drives the bottom cell. In the barotropic cases, the peaks were of the same amplitude. The total RMMC is the linear superposition of the cells driven by the sources, and in the baroclinic case, the lower cell is not visible but for its effect on confining the upper cell. In both barotropic and baroclinic cases, the RMMC appears as a response to the eddy-induced vertical shearing in order to keep the thermal wind balance; in the baroclinic case, the dominant upper cell is induced in the region where the vertical shear tends to be suppressed. There is a sign reversal between the westward jet case and the eastward jet case. Figure 3.14 shows the eastward baroclinic case (m=.25).

The vertical structure of the mode can be understood in terms of the refractive index introduced before. Figure 3.15 shows the squared refractive index, n^2, along with the modal structure for the westward and

eastward cases and m=.25. The dip where n^2 becomes negative corresponds to the critical line. However, in this case the region above the critical line corresponds to a propagating region. This is due to the fact that $\overline{q}_y$ and $(\overline{u}-c)$ change sign at neighbouring altitudes. The wave is then able to tunnel through this other propagating region and peaks above the critical line. One can also remark that the wave for the westward jet case peaks at higher levels than the eastward jet case, contrary to the barotropic cases studied before. For the eastward jet, n^2 is negative above z=.75 H, so that the wave is more trapped than for the westward jet for which n^2 is small and positive at z=.75 H and becomes only weakly negative above.

Some insight into the effect of the vertical shear and curvature might be gained by looking at the potential vorticity gradient :

$$\overline{q}_y = \beta - \overline{u}_{yy} - \varepsilon\, \overline{u}_{zz} + \varepsilon\, \overline{u}_z / H.$$

The relative contribution of the different terms are expressed by a few nondimensional numbers; they scale as

$$\beta / \overline{u}_{yy} \sim \beta L^2 / U \approx \beta^*$$

$$\varepsilon\, \overline{u}_{zz} / \overline{u}_{yy} \sim \varepsilon L^2 / m^2 H^2 \sim Bu$$

$$\varepsilon\, \overline{u}_z / H\, \overline{u}_{yy} \sim \varepsilon L^2 / mH^2 \sim mBu$$

where Bu is a Burger number constructed with the mean flow scale. Let us call $\delta = m^{-1}$; note that δ is the ratio of the vertical curvature to the vertical shear term. When m = 0.25, δ = 4 so that the baroclinic instability comes mainly from the curvature term. To pursue the analogy with the barotropic instability, one can introduce a parameter $\mathbf{D} = \beta L_D^2 / U_0$ (Dickinson, 1973), where L_D is the deformation radius constructed with the mean flow scale $L_D = NmH/f$. Note that in this case, the two parameters **D** and β^* are related to the Burger number, $Bu = L^2 / L_D^2$, because $\beta^* = Bu\, \mathbf{D}$. The relevant parameters in the westward jet case ($U_0 = -90$ ms^{-1}, $\beta^* = -0.2$) are shown in Table 3.4.

Table 3.4 : Parameters D, Bu for various m in the westward jet case

m	Bu	**D**
2	.11	-1.81
1	.44	-.45
.5	1.76	-.11
.25	7	-.028

In the limit of large L and large δ, i.e. when the barotropic effects are unimportant and when the vertical shear term can also be neglected, the problem is formally equivalent to the barotropic instability of a Bickley jet. One can see that **D** has a similar role for internal baroclinic instability as β^* for the barotropic one. The flow is then baroclinically unstable to symmetric modes for $0 > \mathbf{D} > -2$. The vertical structure of the mode is then equivalent to the antisymmetric (varicose) mode of the Bickley jet because of the vertical boundary conditions. The examples shown for $k = 20$ do not correspond to the most unstable modes. We did investigate numerically the growth rate as a function of k for the baroclinic case $m = 0.25$ and found that indeed the mode of maximum growth rate appears at $k = 40$ (figure 3.16); that figure also shows that the most unstable mode has wavenumber near $k = 100$ when $m = 0.1$. In the case of the barotropic instability of a Bickley jet for small β^*, we know that the wavelength of maximum instability for the sinuous mode is $2\pi L$, where L is the jet half-width; for the varicose mode, the wavelength is about .6 times $2\pi L$ as can be seen from the numerical study of Kwon and Mak (1988). In the analogous baroclinic problem, L has to be replaced by $mH\varepsilon^{-1/2}$. The corresponding wavenumber is then about 120. The location of the maximum instability for m=.1 indicates that this scale estimation is quite correct, taking into account that δ and L are not infinite and β^* is not exactly zero.

In the barotropic regime, the westward jets are more unstable than the eastward jets, but the trend reverses for small value of m as shown on figure 3.8 (Orsolini and Leovy, 1989b) and table 3.3. The reason is not very clear. In a related study of internal baroclinic instability, Dickinson has shown that negative shear zones (i.e. when the wind becomes more westward with height) are more unstable (Dickinson, 1973); consequently, decaying eastward jets should be more unstable. However, this was an effect due to the vertical shear in a situation where δ is not large. Indeed, when the domain extent is small compared to a scale height, there is no difference between negative and positive shear zones for the hyperbolic tangent profile he used. This is analogous to a well-known property of the problem of the barotropic instability of the hyperbolic tangent shear flow that the growth rate is independent of the basic flow direction. For our problem, the analogy with the barotropic instability of the Bickley jet seems to indicate that the westward jets should be more unstable than the eastward jets for such a small **D**. In the case of the barotropic instability of the Bickley jet, the westward jets are more unstable than the eastward jets; not only do they attain higher growth rates, but their instability domain covers a wider parameter regime. However, this finding is based on a property of the most unstable symmetric mode; in our calculations, the growth rate is the one of an antisymmetric mode and a comparison between the eastward and westward jets for those modes is not known to this author and it could be that the growth rate of the varicose mode of the eastward jet is higher than the varicose mode of the westward jet. Note that there is no contradiction with the basic property stated earlier that the symmetric mode is always the most unstable for a given set of parameter, i.e. also a given direction.

The relevance of these baroclinic modes to the Jovian atmosphere is uncertain. When m = .25, the mean flow decreases from 100 ms^{-1} to zero in half a scale height, so that the shears implied are an order of magnitude larger than those suggested by the Voyager data. Also they drive meridional circulations which are opposite to the zone/belt picture (which rising motions in regions of anticyclonic shears). One can note that in

these cases the most unstable mode has a zonal wavenumber around 40 (for m = 0.25) and a phase speed $c_r/U_0 = 0.7$. Also the momentum fluxes at a given height are not of uniform sign, so that the fluxes switch from downgradient to upgradient away from the jet core.

3.3.2. A STABILITY PARAMETER.

One can finally remark that in this problem, the stabilizing effect of the vertical shear is offset by the curvature terms : meridional curvature in the barotropic regime and vertical one in the baroclinic regime. In absence of jets, the potential vorticity gradient reduces to the positive term β; a necessary condition of instability is that this gradient changes sign in the domain. This is not a sufficient condition, but , for westward jets, instabilities are associated with a pocket of negative potential vorticity gradient in the core of the jets. The meridional and vertical curvatures tend to create such negative values of the potential vorticity gradient.

We found an empirical rule that to have the most stable situation, one needs to have the largest possible stabilizing contributions (the stabilizing term is the vertical shear term), and the the smallest possible destabilizing contributions (the destabilizing terms are the curvatures terms). This means that the ratio **R** of the stabilizing term to the destabilizing terms has to be maximum, i.e.

$$\mathbf{R} = \text{(vertical shear) / (curvatures terms)}$$

has to be maximum. In nondimensional form, this ratio **R** is written :

$$\mathbf{R} = mBu \; / \; (1+Bu).$$

The value of m which gives the maximum value of **R** is found by taking $\partial \mathbf{R}/\partial m = 0$. This implies that

$$(1 + Bu)\; \partial_m (mBu) \; - \; mBu\, (\partial_m Bu) \; = \; 0.$$

One can find the following root :

$$m = (L/L_D)$$

This value of m should give an estimate of the amount of vertical shear you need to stabilize the flow against barotropic instability without creating baroclinic instability. The vertical shear zone of the neutral flow should have the scale mH. This also means that the mean flow has Bu ~ 1. This is the appropriate generalization of the condition mBu ~ 1 that was described earlier. For the case we have examined numerically, we had $\beta^* = -.2$ and $L/L_D \sim 0.66$ so that this rule of thumb gives

$$m = 0.66$$

A plot of the growth rates for the westward jet shows that the computed minimal instability corresponds indeed quite well to the maximum **R** reached at m=.66 (figure 3.17a). This is quite remarkable that the growth rate curve computed from a numerical stability analysis of Bickley jets agreed so well with a simple curve drawn from the characteristic parameters of the problem. Also note that the criterion is independent of the magnitude of the jet.

For the eastward jet, we had $\beta^* = .3$ and $L/L_D \sim 1.041$; again, a plot of the growth rates for the that case shows that the computed minimal instability is not incompatible with the criterion of maximum **R** (figure 3.17b); however, the growth rates becomes very small as soon as m is less than 5, and the growth rate curve is very flat in a wide region of the parameter m. This amount of vertical shear predicted by the criterion $m = L/L_D$ has to be understood as an upper bound. Stabilization might occur with less vertical shear as in the case of the eastward jets; stability of a flow is afterall a global property of the flow.

3.3.3. TRANSITION BETWEEN BAROTROPIC AND BAROCLINIC INSTABILITIES.

For the westward jet case, the transition is between m=.75 and m=.5. In the case m=.75, the source of instability is still barotropic; this can be seen in the EPFD term which is still a dipole oriented in the horizontal direction, or in the pattern of χ^* which has the barotropic pattern with a lower cell of rising motions on the poleward side of the jet core (figure 3.18a,b). For m=.5, one has definitely a baroclinic source as can be seen from the diagrams of the EPFD and the RMMC (figure 3.18c,d). The growth rate curves can be thought of as made of two branches. This corresponds to a transition from an instability driven by meridional curvature to an instability driven by vertical curvature. The role of the vertical shear is to influence strongly the propagation characteristics of the wave and consequently its growth rate. These plots of the parameter R serve as a mere illustration of the balances involved; they do not contain information on the wavenumber of the most unstable mode or the magnitude of the growth rate nor do they show the asymmetry in growth rate between the westward and the eastward jets.

3.3.4. PATTERN OF HEAT AND MOMENTUM FLUXES.

Let us consider the pattern of eddy fluxes in the westward jet case. In the barotropic regime, the heat flux $\overline{v'T'}$ is much smaller than the momentum flux $\overline{u'v'}$; the latter is downgradient so as to transfer the eastward zonal momentum into the jet core and to spread the jet horizontally; it can be seen from the figures, for example figure 3.2f, that $\overline{u'v'}$ is negative on the poleward side of the jet. The energy conversions are related to the eddy fluxes in the following manner :

$$CKE = - < \rho \ \overline{u'v'} \ \overline{u}_y >$$

$$CAPE = < \rho \ \overline{v'T'} \ \overline{u}_z >$$

where CKE is the mean-to-eddy kinetic energy conversion and CAPE the mean-to-eddy available potential energy conversion; brackets denote domain integration. For the westward jets, one has $\overline{u}_y > 0$, and $\overline{u'v'} < 0$ so that, as expected, CKE > 0. The Eliassen-Palm flux divergence (EPFD) term is dominated by the momentum flux contribution; this implies that the latter term governs the time evolution of the vertical shear. Recall that in the TEM formalism used here in absence of radiative damping, one has

$$\overline{T}_{yt} \approx - \overline{w}^*_y$$

so that the isentropes and their slopes change through the RMMC and not explicitly by the heat flux term. Initially, $\overline{T}_y$ is negative across the westward jets so that it is hotter on the equatorial side of the jets; this is true at all heights and the jets decay with height throughout the domain. The bottom cell of $\overline{\chi}^*$ is slope-steepening; by that, we mean that the meridional slopes of the potential temperature have a negative tendency ($\overline{T}_{yt} < 0$). The region where this cell is located is a region of vertical shear increase ($\overline{u}_{zt} > 0$), corresponding to a drag-like effect. Physically, the upwelling and its associated adiabatic cooling ($\overline{w}^* > 0$) provide the mechanism for that slope steepening effect. The upper branch of the residual mean meridional circulation has downward motion on the poleward side of the jet, so that it is slope-flattening. In that problem, heat-fluxes follow the same pattern: there is a bottom region where $\overline{v'T'}$ is equatorward, so that it is also slope-steepening; the heat flux reverses sign at a height where the RMMC cell reversal occurs. This provides an overall consistent picture in which there is a region of vertical shear increase at the bottom on which is superposed a region of shear decrease. This is how the barotropic eddies simulate a vertical drag on the zonal mean flow.

In the baroclinic regime, $\overline{v'T'}$ is much larger than $\overline{u'v'}$; in this case CAPE is positive as $\overline{u}_z > 0$ and $\overline{v'T'} > 0$. The RMMC has a major cell of $\overline{\chi}^*$ with downward motion on the poleward side and so is a slope-flattening cell; in agreement with what we expect from baroclinic instability, it reduces the vertical shear. In that case, one has a small momentum flux which is poleward associated with a negative barotropic conversion.

The eastward jet case can be treated in a completely analogous manner.

3.4. DISCUSSION.

This simple model cannot describe the characteristics of fully developed eddies observed in Jovian clouds nor the interaction between unstable eddies and the mean flow maintained by deep interior processes. Nevertheless, the linearly unstable eddies have properties that invite comparison with observations of Jupiter.

1) Barotropic instabilities provide a mechanism of vertical drag through their vorticity transports. Eastward jets are stabilized by much weaker vertical shears than the westward jets, so they may penetrate further through the statically stable upper troposphere. Since the bottom of the stable layer is somewhere below the cloud tops, this could explain why the observed cloud top westward jets are less intense than the eastward jet. The westward jets are stabilized when Bu ~ 1, a condition which does not depend on the jet intensity. This may select the vertical shear scale m in the real equilibrated situation, a possibility that will be investigated in the next chapter.

2) The most unstable eddies are trapped meridionally by the jet and have a zonal wavelength $\lambda=2\pi La$ where a is a number of order one. Its precise value depends on m Bu as shown in figure 3.8. It also depends on β^* with a increasing as the magnitude of β^* increases (Haltiner and Williams, 1980). Because of the barotropic instability condition, λ corresponds approximately to the Rhines wavenumber $k_\beta = (\beta/U)^{1/2}$. Mitchell (1982) performed Fourier analysis of the eddy zonal winds and showed that the turbulent kinetic energy is large at zonal wavenumbers k_β or lower. For westward jets and L=2000 km, the range of λ is typically 10^4 to 1.5 10^4 km, which is compatible with the characteristic scale separating vortex cores in the westward jets, as can be especially well seen in the Voyager images of the southern hemisphere south of the Great Red Spot. This scale could be the remnant

scale forced by the instability of the deep jets. This does not preclude energy input at the Rossby radius through some other forcing, like small-scale convection, which could be accompanied by reverse energy cascade up to wavenumbers kβ; energy input at the Rossby radius, at wavenumbers over 100, due to baroclinic instability would however require stronger vertical shears than those suggested by the Voyager temperature data. Barotropic unstable eddies are also trapped vertically by the shear zone; the instabilities of eastward jets are able to extend to higher levels than these of westward jets.

3) Due to the jet barotropic instability, the eddy momentum flux always acts to broaden and smooth the jets horizontally; for example, these unstable eddies transfer eastward momentum into westward jets. This is contrary to the result of Ingersoll et al. (1981), but this result has been questioned on observational grounds. Sromovski et al. (1982; 1985) argued that the high eddy-to-mean-flow conversion rate of Ingersoll et al. could result from a bias in the sampling procedure, as we discussed in chapter 2. However, the momentum flux observations do not have enough resolution to be compared with our numerical results; the width scales of our jets are in the range of 1500-2000 km, i.e. 1-2° latitude; the momentum flux should go to zero at the jet core and reach a maximum at about a jet width from the core. The data from Ingersoll and al. have a meridional resolution of 1° which is not enough to resolve sharp changes in momentum fluxes shown by our models.

4) In the upper troposphere, we expect the radiatively driven RMMC to be negligible compared to the jet-driven RMMC (Conrath et al., 1989). In our model, the lower cell of the RMMC is characterized by subsidence in regions of cyclonic shear in agreement with the old belt/zone picture, but a countercell is stacked above the main cell and the circulations produced are more complex than those driven by Rayleigh damping of zonal momentum. In the baroclinic cases, the upper cell is dominant.

Clearly, our calculations depend on a certain number of unknown parameters. We specified the jet intensity U_0 and meridional scale L, these

two parameters entering β^*. The magnitude of L is constrained by the observed jet profile but the jet maximum intensity below the cloud-top U_0 is an unknown. The growth rate would decrease for weaker jets and the maximum growth wavelength λ also depends weakly on β^*, with λ increasing for weaker jets.

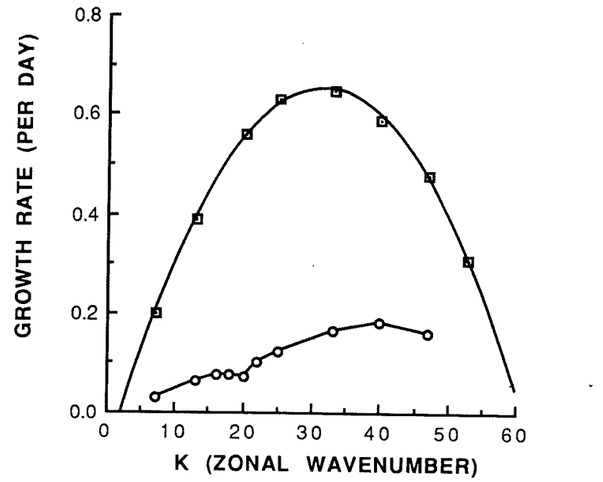

Figure 3.1: Growth rate (per day) as a function of zonal wavenumber for the westward jet with β^*= -.2 (squares) and for the westward jet with β^*= -.7 (circles).#

Unless specified otherwise, all quantities are normalized and the contour increment is 0.1 in contour plots; contours corresponding to negative values are dashed. A negative contour for a stream function corresponds to clockwise motion. Z is the height in units of scale height H, and Y is the meridional coordinate in units of L, the jet width defined in the text. A growth rate of 1 corresponds to an e-folding time of 1 (terrestrial) day which is about 2.4 Jovian rotation periods. The phase is expressed in radians and then normalized. All units are in the MKS system except where indicated otherwise.

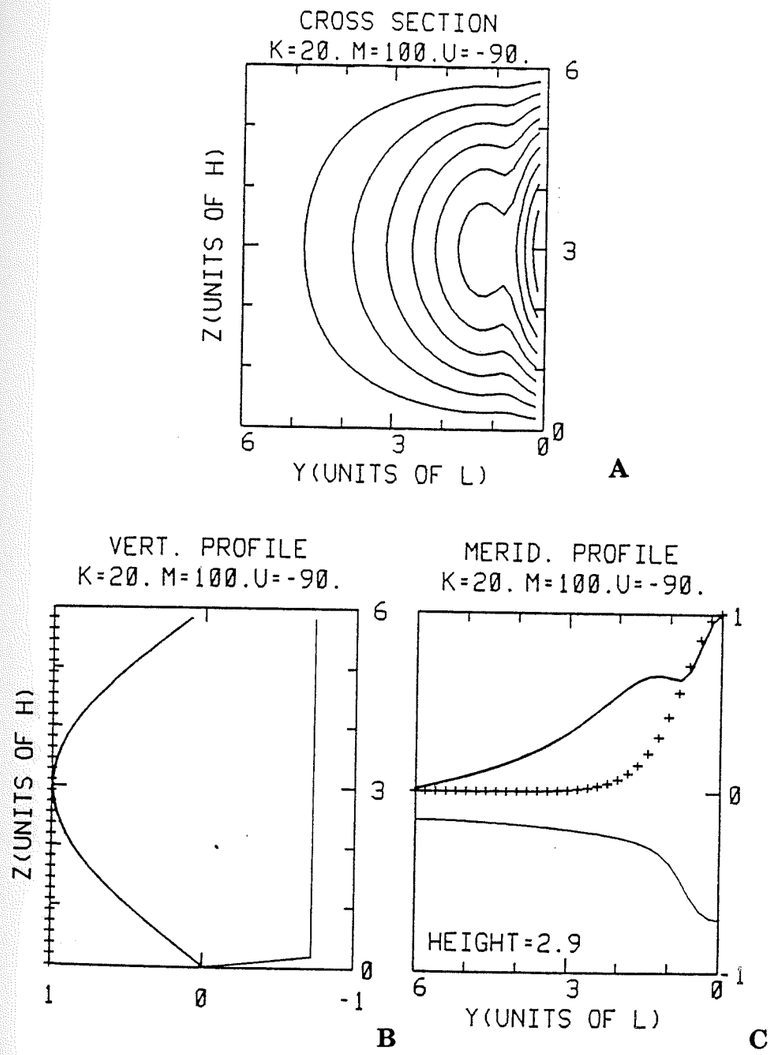

Figure 3.2: Amplitude and fluxes for most unstable mode for the westward jet (β^*=-.2) and k=20, m=100. **A)** Amplitude cross-section in the y-z plane. **B)** Vertical profile at the jet core of mode amplitude (full line) and phase (thin line). **C)** Meridional profile of the same quantities compared to the mean flow (crossed line). The height of these profiles is 2.9 H. **D)** Cross-section of heat flux. **E)** Cross-section of F. **F)** Cross-section of momentum flux. **G)** Cross-section of $-\overline{w}^*$ **H)** Cross-section of $\overline{\chi}^*$ **I)** Cross-section of $\overline{v}^*$.

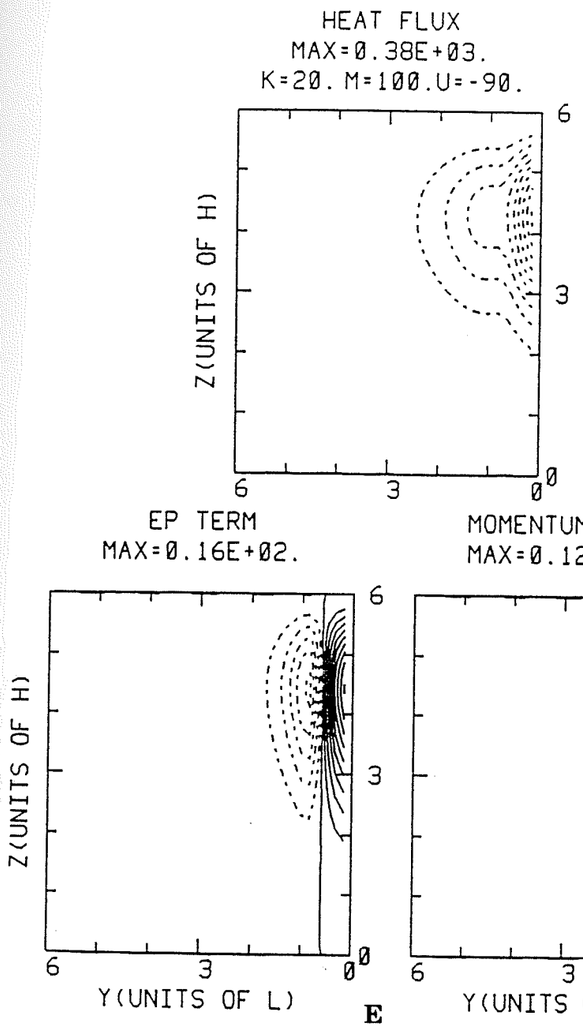

Figure 3.2: (continued)

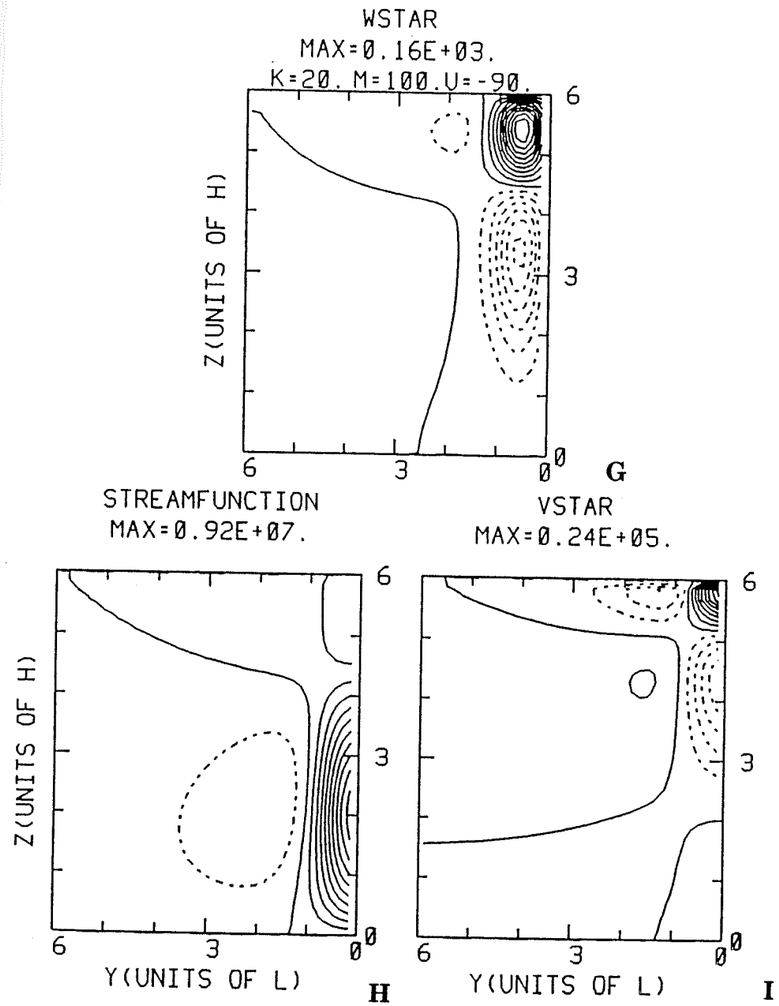

Figure 3.2: (continued)

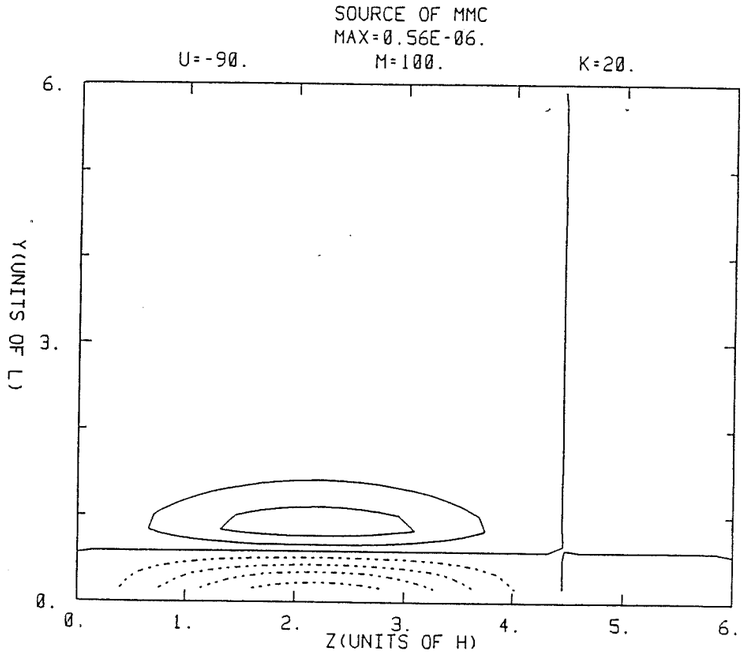

Figure 3.3: Cross-section of S_0 for the westward jet (β^*=-.2) and k=20, m=100. The contour increment is 0.2

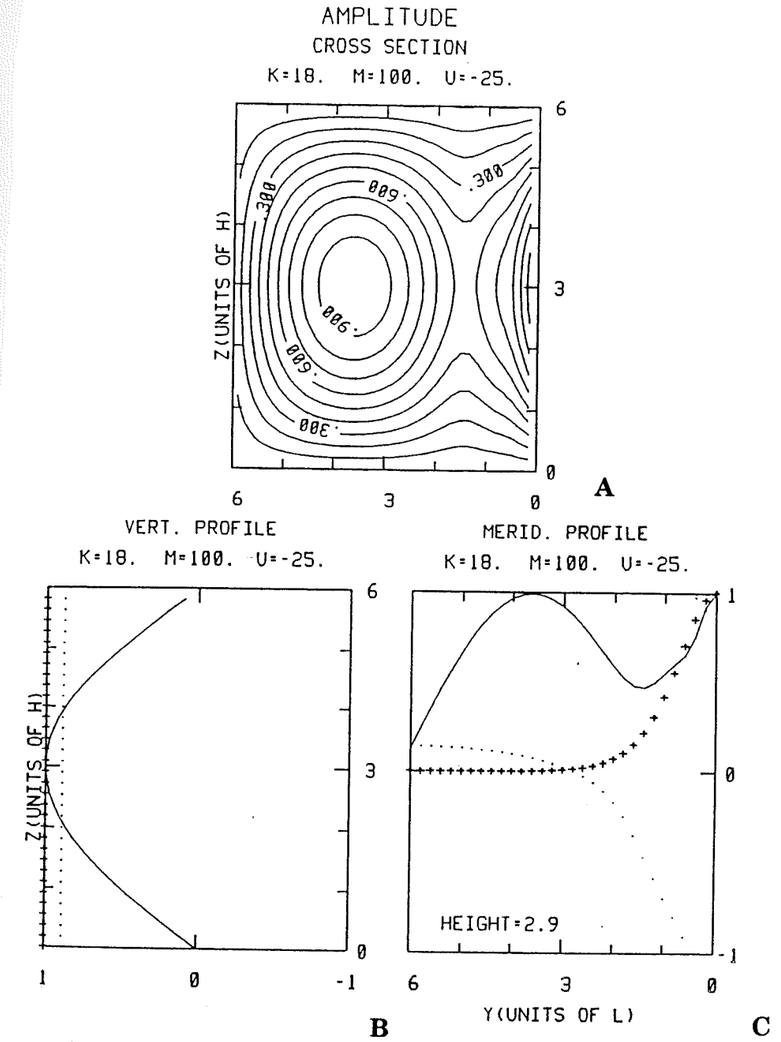

Figure 3.4: Amplitude and fluxes for most unstable mode for the weak westward jet (β^*=-.7) and k=18, m=100. **A)** Amplitude cross-section in the y-z plane.
B) Vertical profile at the jet core of mode amplitude (full line) and phase (dotted line).
C) Meridional profile of the same quantities compared to the mean flow (crossed line). The height of these profiles is 2.9 H.
D) Cross-section of heat flux. **E)** Cross-section of F. **F)** Cross-section of momentum flux. **G)** Cross-section of $-\overline{w}^*$ **H)** Cross-section of $\overline{\chi}^*$ **I)** Cross-section of $\overline{v}^*$

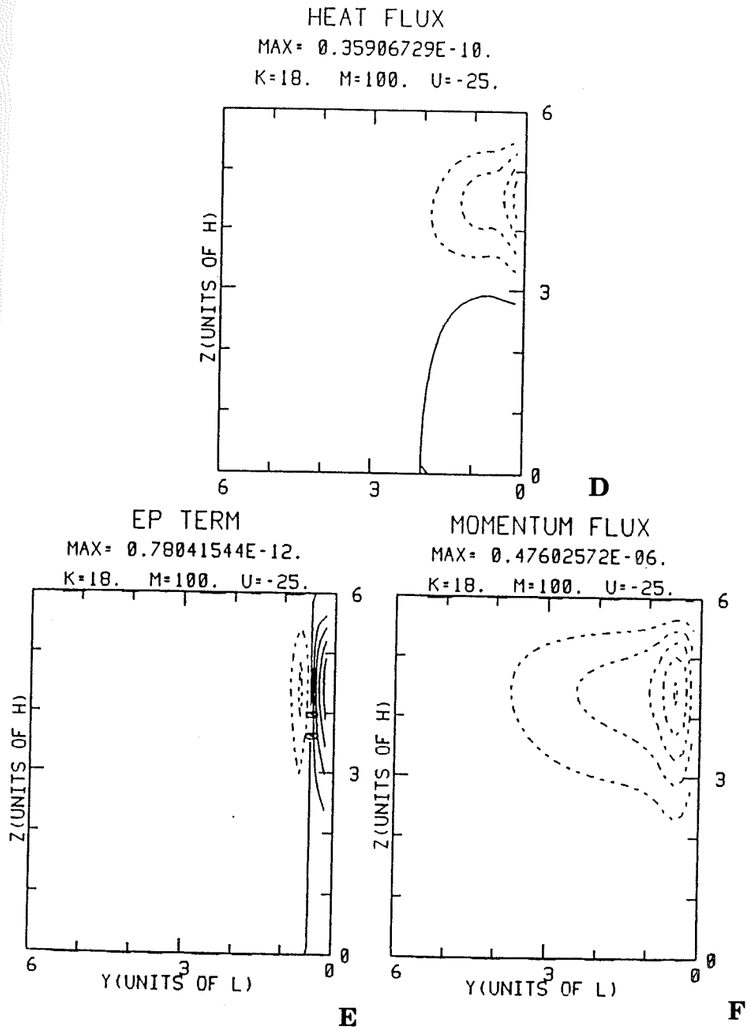

Figure 3.4: (continued)

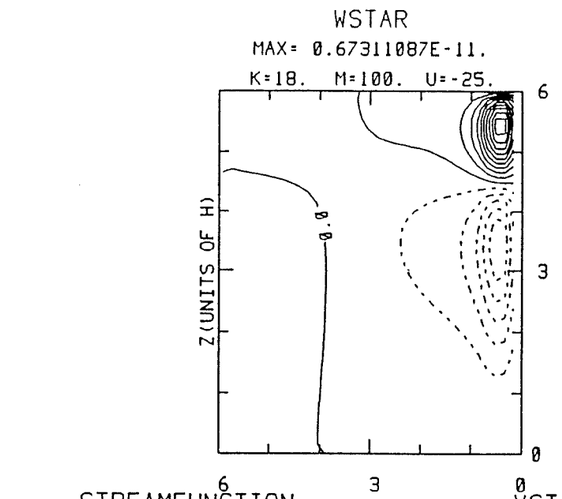

Figure 3.4: (continued)

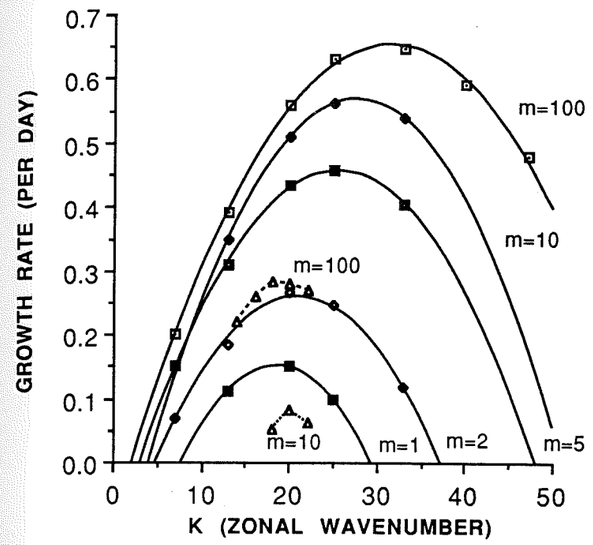

A

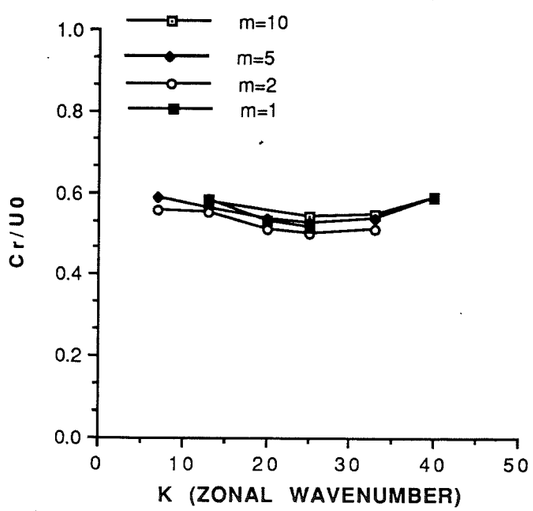

B

Figure 3.5: **A)** Growth rate as a function of zonal wavenumber for various m : for the westward jet (β^*=-.2) (full lines) and for the eastward jet (β^*=.3) (dotted lines). **B)** Phase speeds (normalized to U_0) for the westward jets (β^*=-.2) for various m.

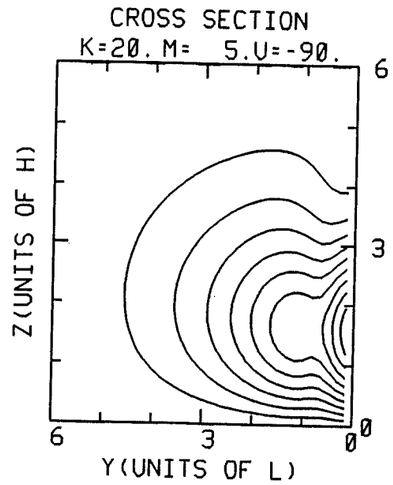

A

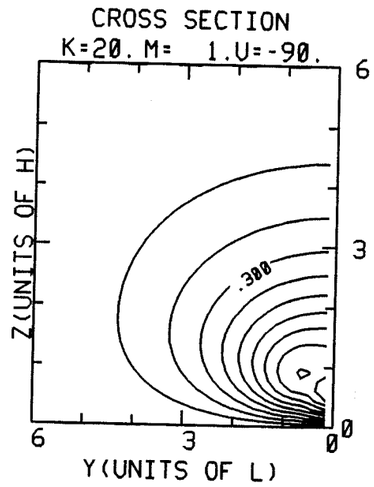

B

Figure 3.6: Amplitude of the most unstable mode for the westward jet (β^*=-.2) and k=20: **A)** m=5. **B)** m=1.

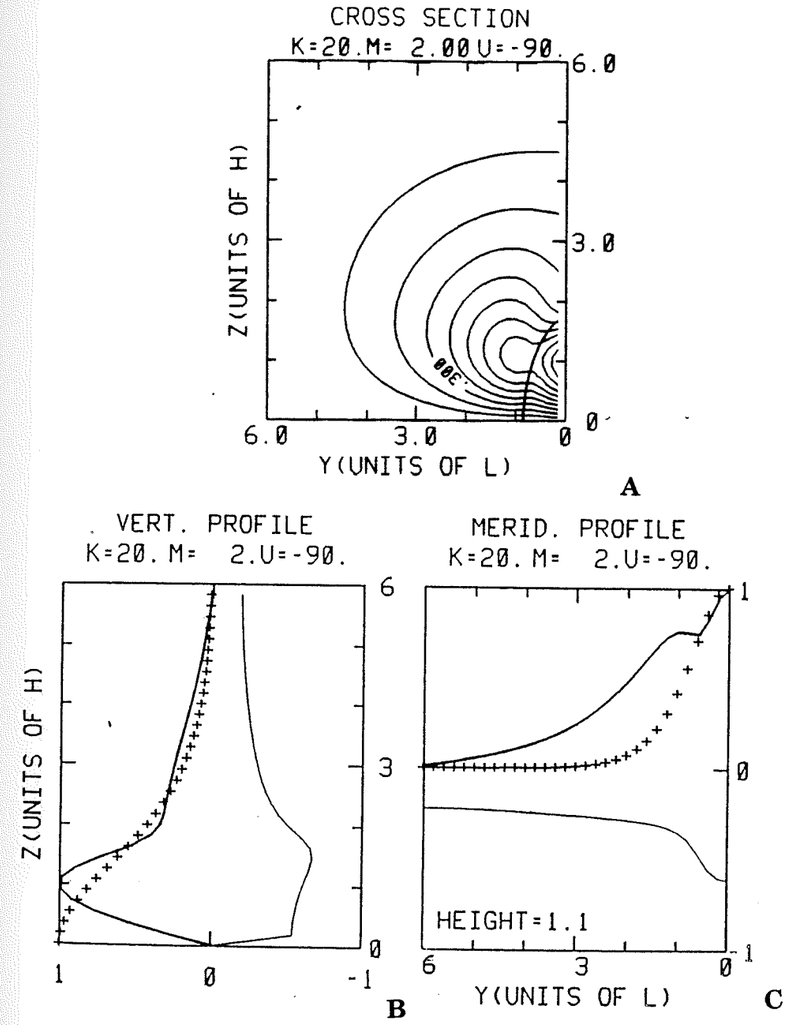

Figure 3.7: Amplitude and fluxes for most unstable mode for the westward jet (β^*=-.2) and k=20, m=2. **A)** Amplitude cross-section in the y-z plane. The critical line is also shown (thick line). **B)** Vertical profile at the jet center of mode amplitude (full line) and phase (thin line) compared to the mean flow (crossed line). **C)** Meridional profile of the same quantities. The height of these profiles is 1.1 H **D)** Cross-section of heat flux. **E)** Cross-section of F. **F)** Cross-section of momentum flux. **G)** Cross-section of - $\overline{w}^*$ **H)** Cross-section of $\overline{\chi}^*$ **I)** Cross-section of $\overline{v}^*$

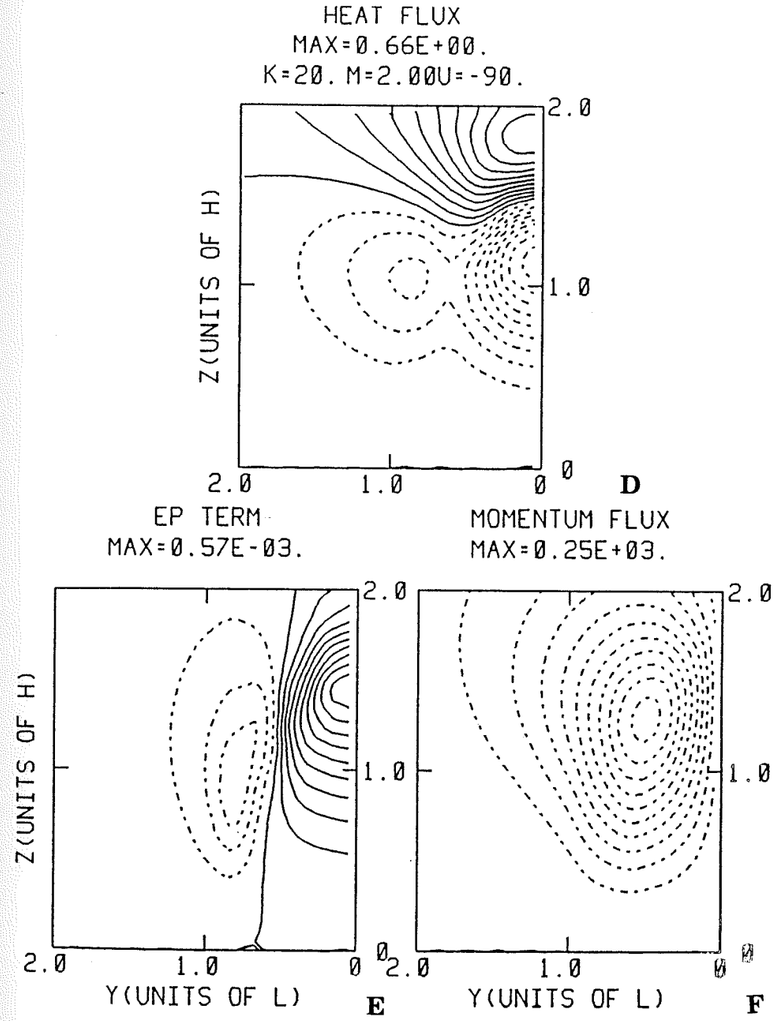

Figure 3.7: (continued)

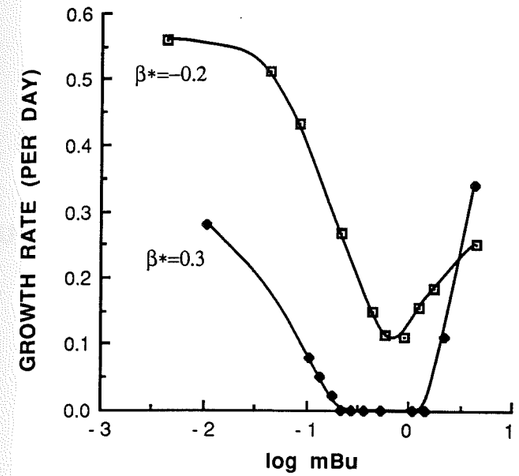

Figure 3.8: Growth rate (per day) as a function of log(m Bu) for westward jet (β^*=-0.2) and for the eastward jet (β^*=0.3); the zonal wavenumber is k=20.

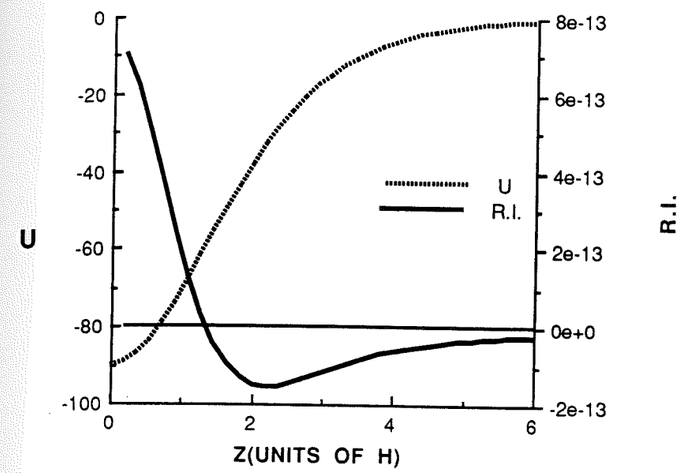

A

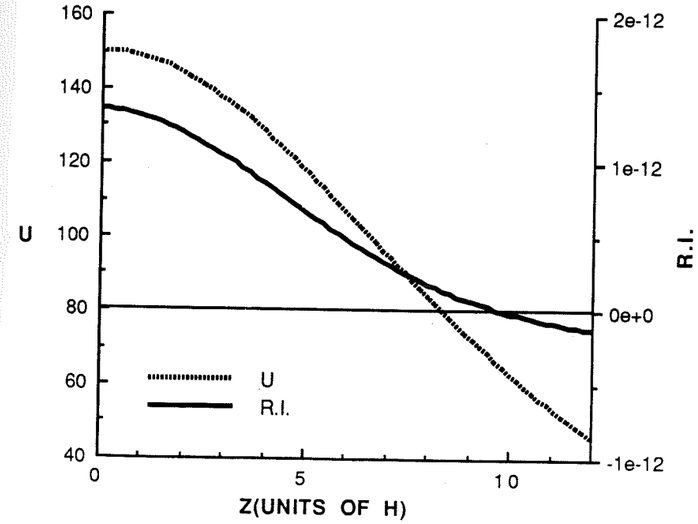

B

Figure 3.9: **A)** Real part of the squared refractive index (R.I.) and zonal mean flow (U) as a function of height at the jet core for β^*=-0.2, k=20, m=2. **B)** same for β^*=0.3, k=20, m=10.

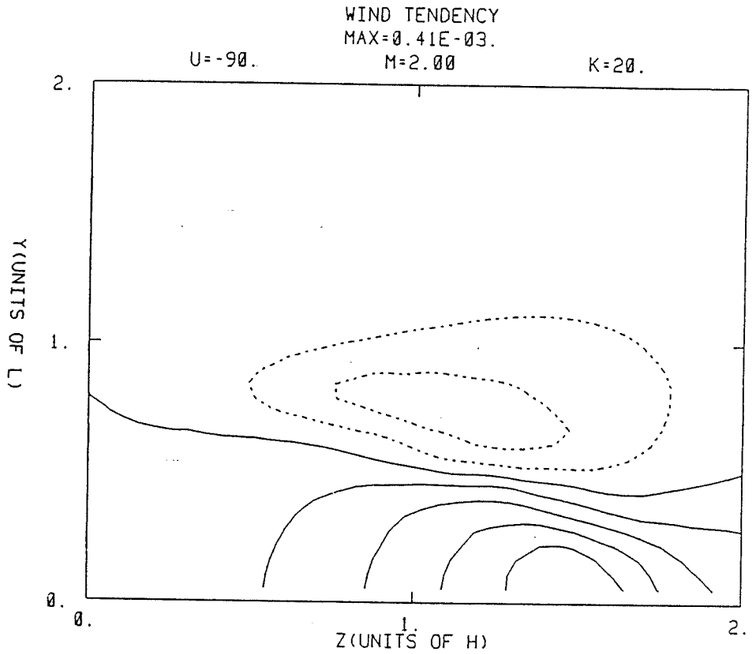

Figure 3.10: Cross-section of $\bar{u}_t$ for the westward jet (β^*=-.2) and k=20, m=2. The contour increment is 0.2

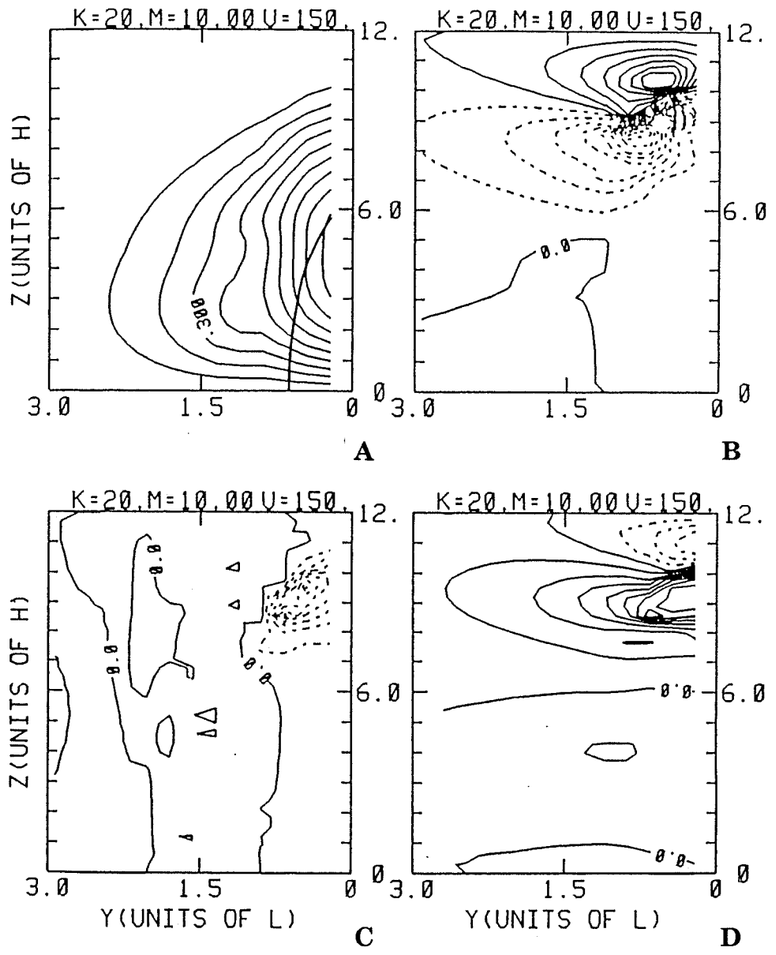

Figure 3.11: Amplitude and fluxes for most unstable mode for the eastward jet (β^*= .3) and k=20, m=10. **A)** Amplitude cross-section in the y-z plane. **B)** Cross-section of $\overline{v}^*$. **C)** Cross-section of F. **D)** Cross-section of $\overline{w}^*$.

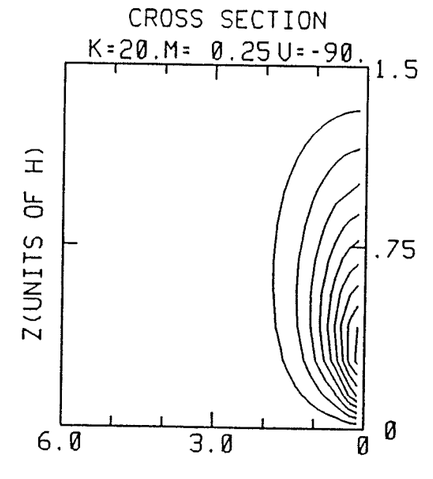

A

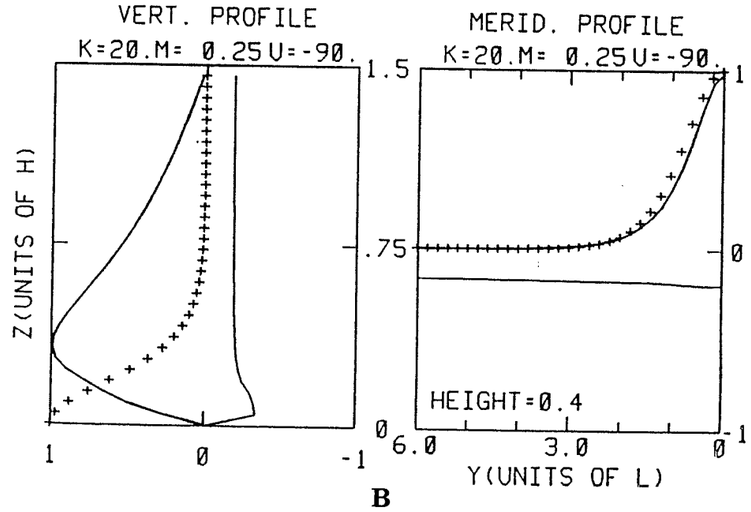

B C

Figure 3.12: Amplitude and fluxes for most unstable mode for the westward jet (β^*=-.2) and k=20, m=.25. **A)** Amplitude cross-section in the y-z plane. **B)** Vertical profile at the jet center of mode amplitude (full line) and phase (thin line) compared to the mean flow (crossed line). **C)** Meridional profile of the same quantities. The height of these profiles is .4 H **D)** Cross-section of heat flux. **E)** Cross-section of F. **F)** Cross-section of momentum flux. **G)** Cross-section of $\overline{w}^*$. **H)** Cross-section of $\overline{\chi}^*$. **I)** Cross-section of $\overline{v}^*$

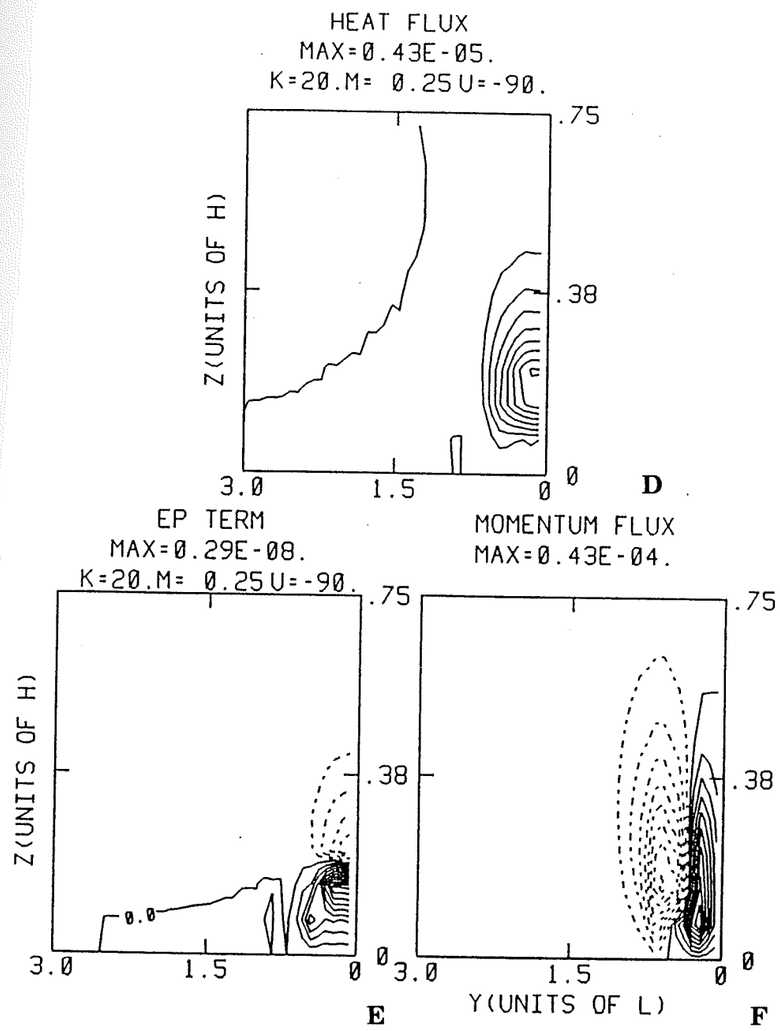

Figure 3.12: (continued)

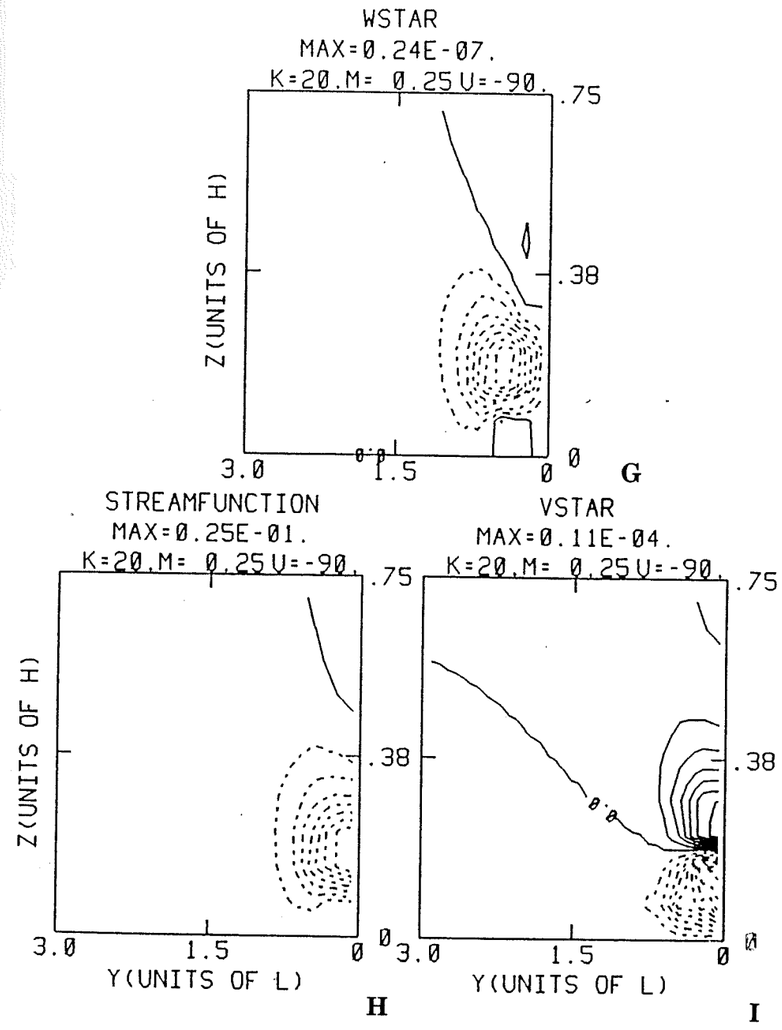

Figure 3.12: (continued)

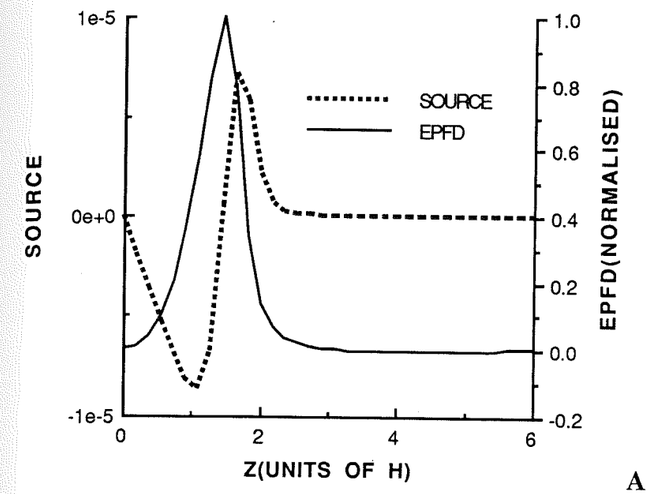

A

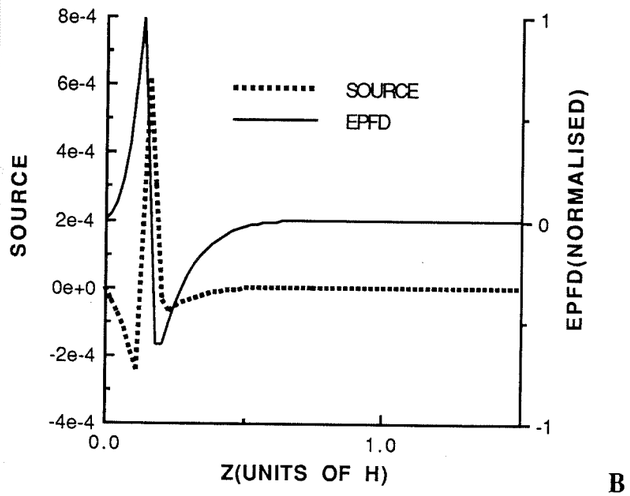

B

Figure 3.13: Source of the RMMC (S_0) and F at the jet core as a function of height: **A)** for β^*=-0.2, k=20, m=2 **B)** for β^*=-0.2, k=20, m=.25

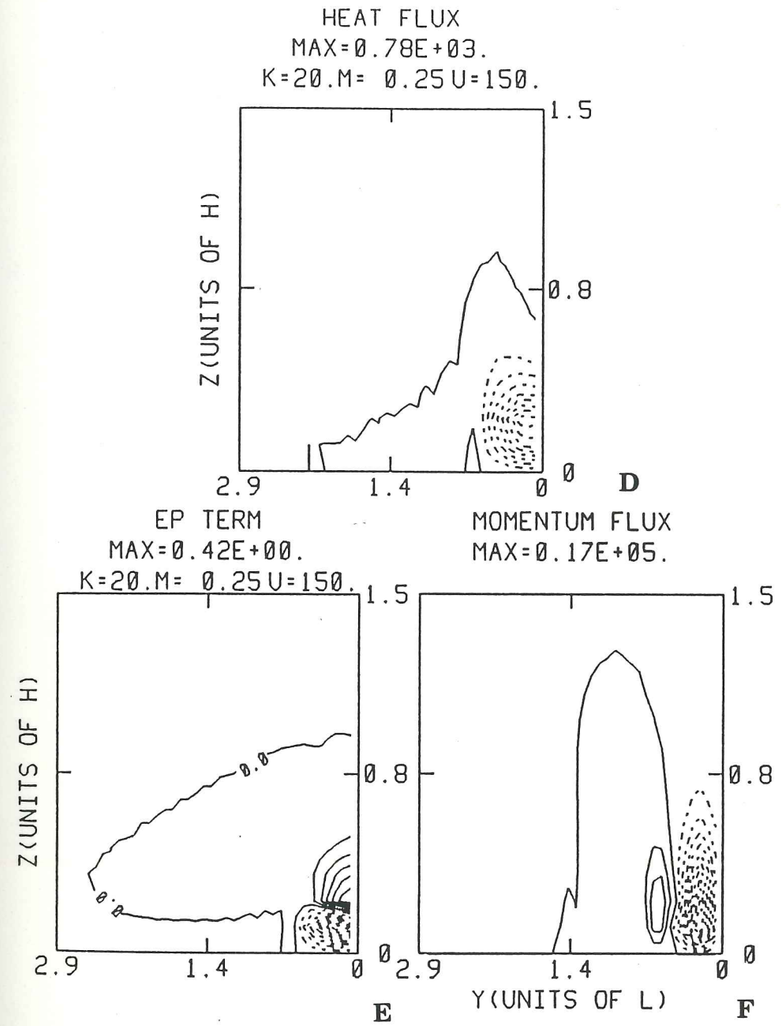

Figure 3.14: (continued)

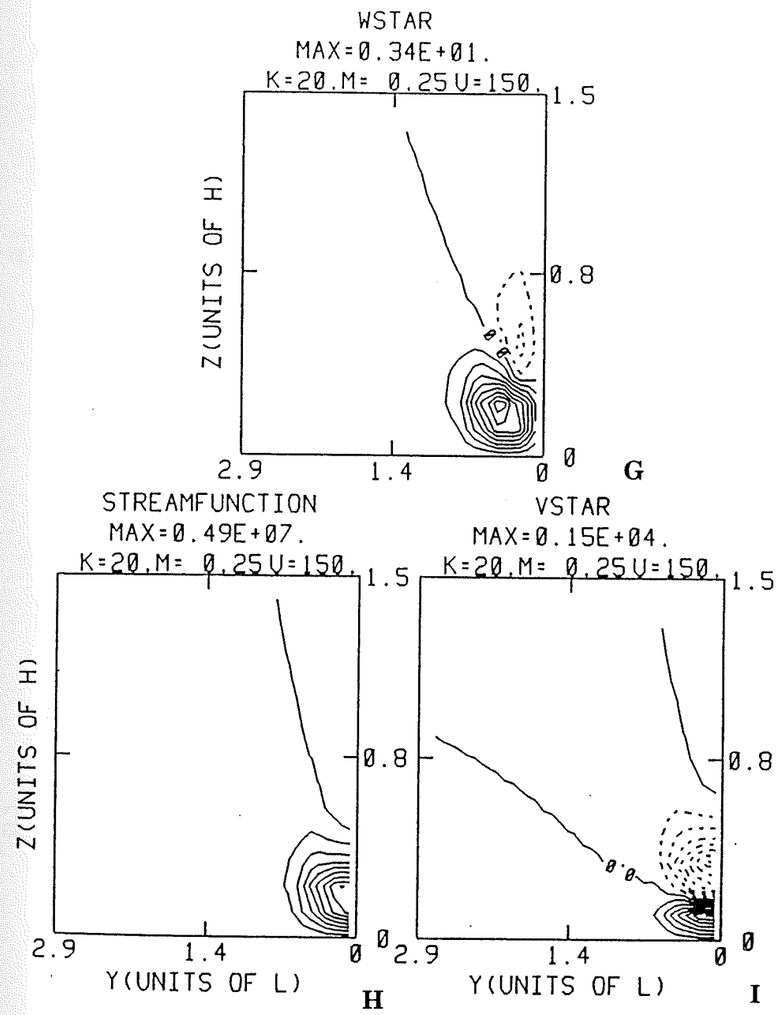

Figure 3.14: (continued)

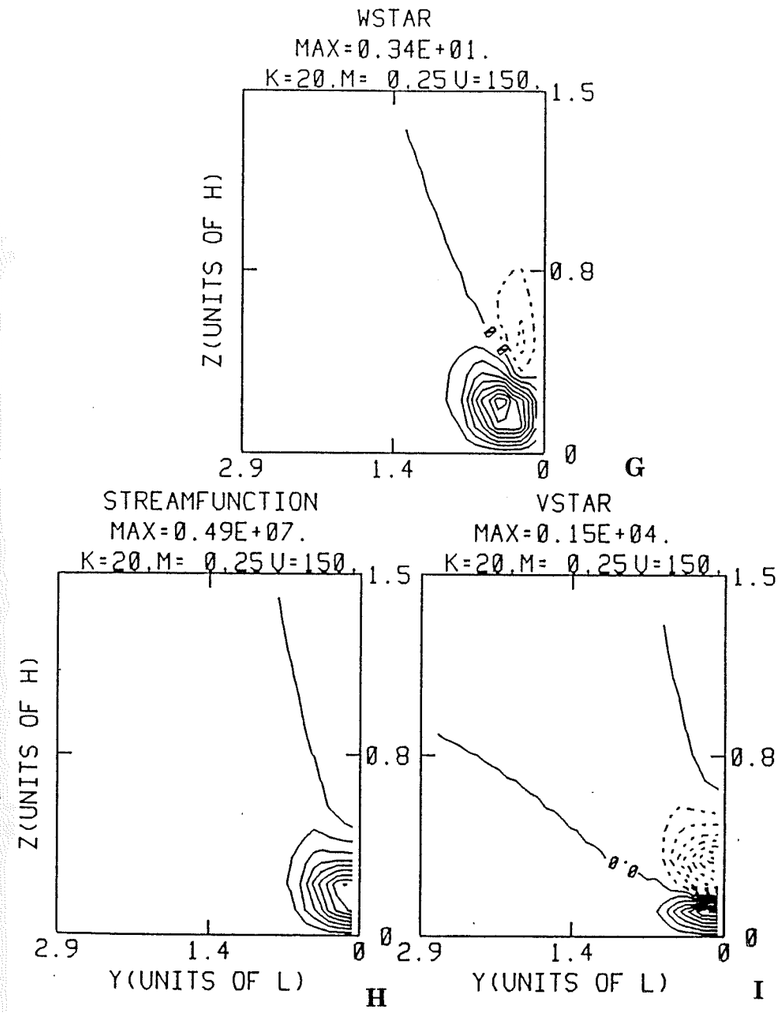

Figure 3.14: (continued)

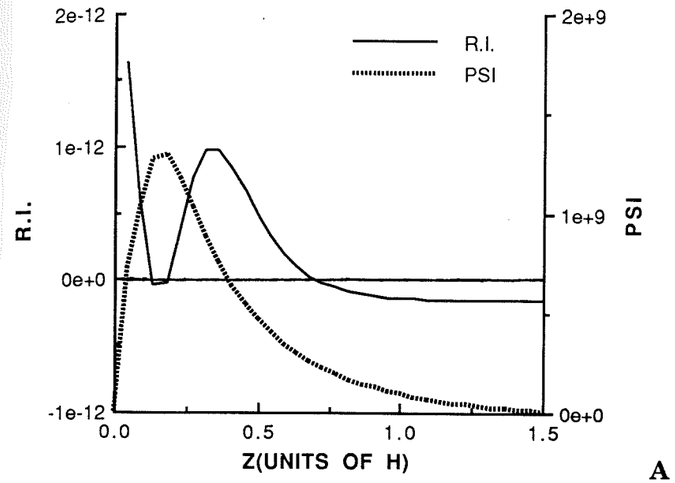

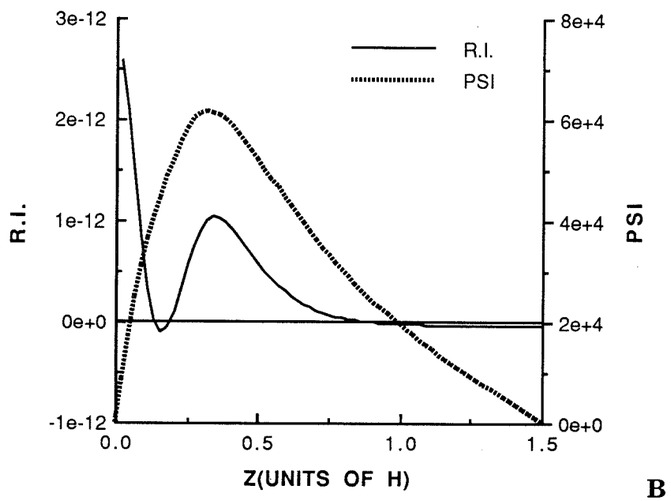

Figure 3.15: Real part of the squared refractive index (R.I.) and eddy amplitude ($|\Psi|$) as a function of height at the jet core : **A)** β^*=0.3, k=20, m=.25. **B)** β^*=-0.2, k=20, m=.25.

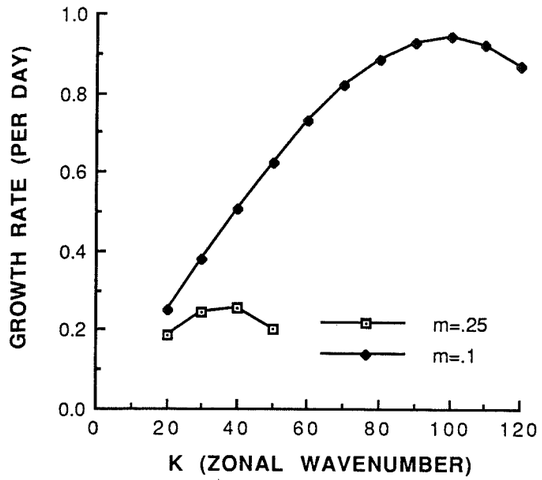

Figure 3.16: Growth rate (per day) as a function of zonal wavenumber for the baroclinic westward jets for m=0.1 and m=0.25

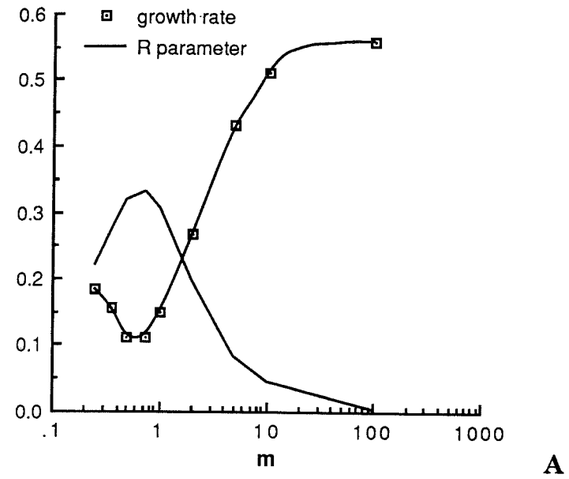

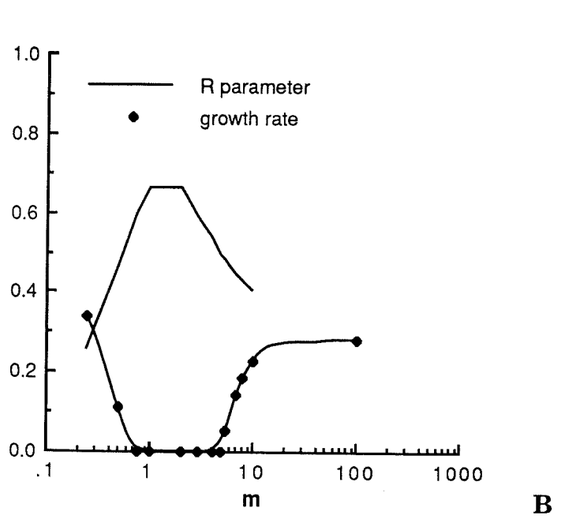

Figure 3.17: Parameter **R** and growth rate (per day) as a function of m. **A)** For westward jet (β^*=-0.2) **B)** For the eastward jet (β^*=0.3).

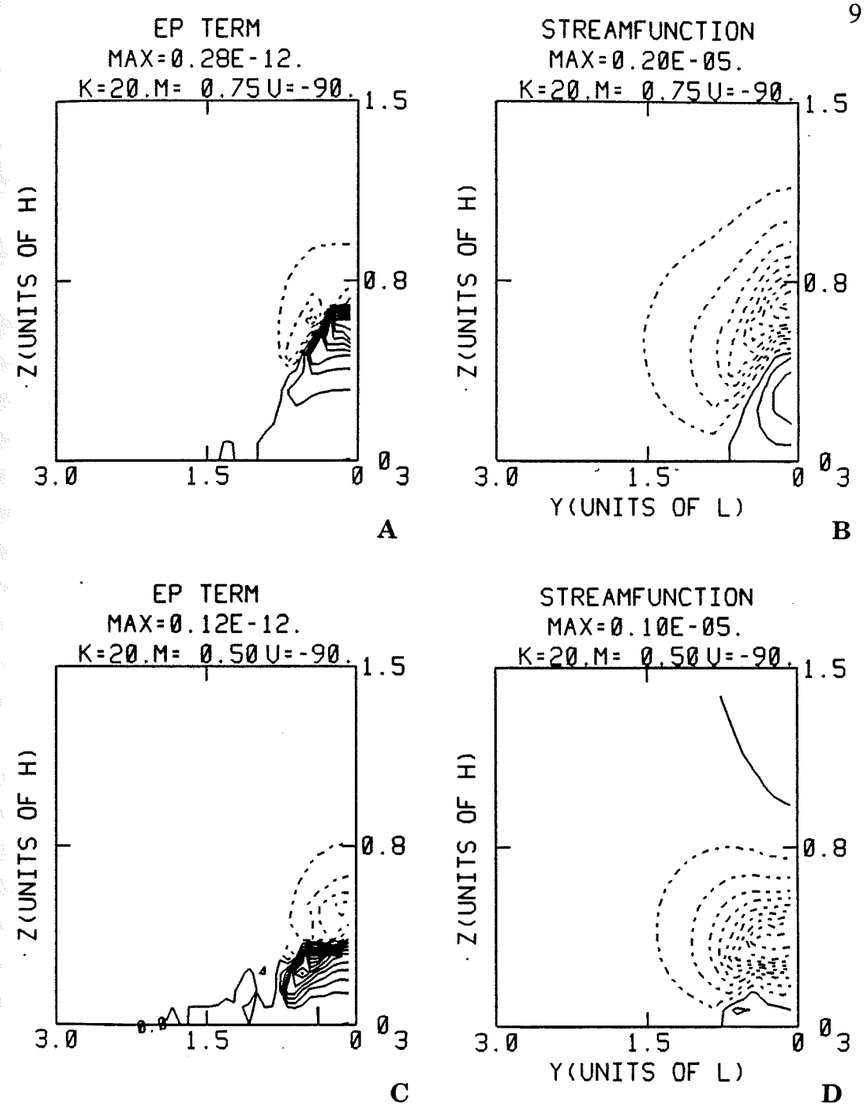

Figure 3.18: **A)** Cross-section of F for β^*=-.2 and k=20, m=.75 **B)** Cross-section of $\overline{\chi}^*$ for β^*=-.2 and k=20, m=.75 **C)** cross-section of F for β^*=-.2 and k=20, m=.5 **D)** Cross-section of $\overline{\chi}^*$ for β^*=-.2 and k=20, m=.5

CHAPTER 4 : QUASI-LINEAR MODELS

4.1. INTRODUCTION.

4.1.1. COMMENTS ON THE USE OF QUASI-LINEAR MODELS.

One of the main purposes of this work is to test the idea that the vertical decay of the zonal jets in the upper troposphere of Jupiter is controlled by inviscid large-scale instabilities. As the hypothetical deep-rooted jet system penetrates through the statically stable troposphere, it becomes unstable and instabilities arise to create a vertical shear zone and residual mean meridional circulations (RMMC). These last two consequences have successfully been reproduced in an ad hoc way by models with linear drag terms in the momentum equation (Conrath and Pirraglia, 1983; Gierasch et al., 1986). But the process we envision here does not invoke external dissipation; the large-scale barotropic instability provides the physical mechanism which a simple drag term mimics.

The linear modelling (Orsolini and Leovy, 1989b) has shown that barotropic instabilities are counteracted by vertical shears; we have looked at the structure of unstable modes, the eddy transports and eddy-induced RMMC acting to stabilize the jets. To extend these investigations to the nonlinear regime, the simplest tool is the quasi-linear model. As mentioned in Chapter 1, our basic picture of the Jovian tropospheric instabilities is quite similar to Pirraglia's (1989), who tested this concept with a different nonlinear model. He used a strongly truncated model while our model is a quasi-linear one which retains sufficient vertical and meridional resolution to represent the structure of unstable eddies. A comparison with his studies will be carried out in another section.

Quasi-linear models have gained widespread use in dynamic meteorology; they focus on the development of a single unstable wave and its coupling to the mean flow, leaving out the wave-wave nonlinear interactions. They have been applied widely in studies of stratospheric dynamics, a situation

where the atmospheric flow is thought to be well represented by a zonal flow distorted by a few waves. The quasi-linear models are able to capture some important features of these circulation systems. The relevance of these models to flows which are more reminiscent of fully developed turbulence - like the cloud-top Jovian circulation - is more questionable. The cloud-top flow on Jupiter is characterised by motions on a wide spectrum of scales and the presence of coherent vortices These may or may not originate in barotropic instability : laboratory experiments have also shown that large coherent eddies arise from jet instability in certain cases (Sommeria et al., 1989). Modelling these coherent eddies necessitates high resolution models. Recent studies have shown nicely the emergence and maintenance of such vortices in turbulent flows with or without background shears (Marcus, 1988; McWilliams, 1984). Obviously, linear and quasilinear models are far from representing these eddies, except perhaps for the gross parameters such as some relevant wavelength, meridional scale or phase speed.

The justification for using quasi-linear models to study the cloud-top circulation of Jupiter is then essentially ad hoc. It is used here because it is a relatively simple intermediate and logical step short of high resolution fully nonlinear models. The modelling of quasi-geostrophic three-dimensional turbulence is in its infancy, and the computational cost of simulating the instability of a three-dimensional flow with great resolution seems prohibitive. We believe that such a quasi-linear model allows us to test our basic picture of the Jovian troposphere and bring some useful results.

However, these quasi-linear models have compared well with the fully nonlinear models at intermediate resolutions for the determination of the vorticity transport and certain global properties, such as the enstrosphy budget. The applicability of these models has been investigated in the case of the barotropic instability of a point-jet by Nielsen and Schoeberl (1984), and by Schoeberl and Lindzen (1984). They have shown that the wave interaction distorts the most unstable mode by creating, as expected, harmonics of the basic wave. At least when the wave equilibrates to a

steady pattern, the energy content of these higher harmonics decays quite fast (Kwon and Mak, 1988). Also, the eddy potential vorticity transport $\overline{v'q'}$, which we have called F in Chapter 3, is mainly due to the leading wave. The quasi-linear model has however problems in representing the equilibration. This is due to the fact that the most unstable mode, starting from an initial small amplitude, overshoots stability (Nielsen and Schoeberl, 1984). This seems due to the inability of the model to smooth out the potential vorticity gradient properly. Apparently, wave interactions are necessary to produce smaller scales which allow faster equilibration. This is not a contradiction to the observation that the gross structure of $\overline{v'q'}$ is well represented by the leading wave; indeed one has

$$\overline{q}_{yt} = - F_{yy}.$$

Therefore, the fine structure in F is responsible for the changes in $\overline{q}_y$. Nielsen and Schoeberl (1984) indeed showed large oscillations of the $\overline{q}_y$ field in the wave-mean flow model which they correlate with the vacillations of the EPFD field; these damp out if the wave-wave interactions are included.

The vacillations encountered in the equilibrating wave-mean flow model then appear to depend strongly on the truncation. Our calculations also show that the amplitude and periods of these vacillations also depend strongly on the supercriticality of the initial mean flow. Instead of looking at the vacillations per se, one might want to examine the time-averaged changes in the mean flow and the eddy transports. Presumably, the mean flow driven by internal instability will be close to marginal stability; preliminary calculations show that the closer to the marginal stability, the smaller are the mean flow changes.

A nonlinear model which would include a few interacting waves does not seem to be appropriate for the Jovian troposphere as the flow has a wide spectrum of scales and coherent eddies. A more involved model would need high resolution to resolve the eddy structure which would arise from instability, as has been done for nonrotating fluids (Comte et al., 1987).

Quasi-linear models as the one developed in this dissertation have been used to study finite amplitude baroclinic waves (Barnes, 1986), the interaction of a forced wave with the mean flow (Holton and Mass, 1976; Barnes, 1988) among other problems. While these studies included many vertical modes, they were restricted to one mode in the meridional direction; our specific problem however requires that we keep sufficient meridional as well as vertical resolution.

4.1.2. MODEL DESCRIPTION.

In the wave-mean flow model, the zonal mean momentum $\overline{u}$ changes according to

$$\overline{u}_t = F + f\,\overline{v}^*,$$

where, as before, F is the EPFD and $\overline{v}^*$ is the residual mean meridional velocity.

In the numerical model, the right-hand side is treated semi-implicitly. We have tested that the time-evolution, in the form of vacillations of the mean quantities and the waves, is smooth and independent of the time-step length. The equation for the RMMC is solved at each time step.

In addition to the previously mentioned diagnostical quantities (such as the EPFD and the RMMC) the energetics of the problem have also been examined through the following domain-averaged quantities :

the eddy kinetic energy

$$EKE = 2\pi\,(\varepsilon/4k)\ < k^2\,|\Psi|^2 + |\Psi_y|^2 >,$$

the eddy available potential energy

$$EAPE = 2\pi\,(\varepsilon/4k)\ < (\mathbf{L}_z\,\Psi_r)^2 + (\mathbf{L}_z\,\Psi_i)^2 >,$$

the eddy enstrophy

$$EEN = 2\pi\,(\pi/4k)\ <(\mathbf{L}_k\,\Psi_r)^2 + (\mathbf{L}_k\,\Psi_i)^2>,$$

the conversion of kinetic energy from the mean flow to the wave

$$CKE = \pi\ <\ \overline{u}_y\ [\ \Psi_i\Psi_{r,y}\ -\Psi_r\Psi_{i,y}\ ]>,$$

the conversion of available potential energy from the mean flow to the wave

$$CAPE = \pi\ <\ -\varepsilon\overline{u}_z\ [\ \Psi_i\Psi_{r,z}\ -\Psi_r\Psi_{i,z}\ ]>,$$

and the zonally-averaged kinetic energy

$$ZKE = <\ \rho\ \overline{u}^2\ /\ 2\ >.$$

In these formulas, the brackets denote vertical/meridional averaging and the zonal integration has been made over one wavelength. In the following, we will neglect a constant factor $\Delta y\ \Delta z$ (essentially the surface of a vertical/meridional finite difference cell) that is common to all these expressions, so that ZKE has to be understood as proportional to the actual zonally-averaged kinetic energy; this holds for all the other expressions as well. Typically, $\Delta y\ \Delta z$ is of the order of $10^9\ m^2$. The other symbols are the same as in the previous chapers. At times, vertical profiles of horizontally-averaged similar quantities (respectively EKEH, EAPEH, EENH, CKEH, CAPEH, ZKEH) were computed.

The domain extends vertically over several scale heights and about 6 jet widths in the meridional direction, just as in the linear modelling. The vertical extent of the domain depends on the initial vertical shear but the total number of points was about 40, although a higher resolution of up to 80 points was at times used; sufficient vertical extent is needed so that the upper boundary does not interfere with the natural decay of the wave to zero. The symmetry condition at the jet core is justified in the quasi-linear approximation. The most unstable mode is symmetric and antisymmetric

modes could only be generated through wave-wave interactions which are neglected in this model (Kwon and Mak, 1988).

The initial mean flow was the same as in the linear study, i.e. a Bickley jet with some vertical modulation :

$$\overline{u}\,(y,z) = U_0\ \mathrm{sech}^2\,(y/L)\ \ \mathrm{sech}^2\,(z/mH),$$

where $U_0 = -90\ ms^{-1}$ and L=2000 km (westward jet) or $U_0 = 150\ ms^{-1}$ and L=3125 km (eastward jet); H is the scale height and m is the thickness parameter. In most cases, we have examined the evolution of an initial barotropic flow (m=100), but we also looked at the evolution of initially sheared flow close to the minimal instability (m=1). The initial wave field had the structure of a normal mode with a finite amplitude so that the initial growth rate is optimized. The energy of the initial wave is nevertheless small compared to the values reached at equilibration. The westward jets are the most interesting because they are strongly barotropically unstable; we emphasized their analysis in the following sections, demonstrating the processes at work on these cases. Eastward jets and composite jets (which include both eastward and westward jets) are later analysed.

The boundary conditions on the wave equation are the same as in the linear model. We now add the condition that the mean vertical mass flux vanishes at the top and the bottom of the layer of interest, i.e. $\overline{w}^* = 0$, whereby the modelled troposphere is decoupled from other atmospheric layers. This implies in particular that $\overline{T}_t = 0$, i.e. that $\overline{T}$ is constant at the top and the bottom pressure level. We also then have $\overline{\chi}^* = 0$ at these two levels because the no mass flux condition imposes $\overline{\chi}^*_y = 0$ and $\overline{\chi}^* = 0$ at the extremity of the domain (y=L). Another consequence is that $\overline{u}_z$ is constant at the bottom because

$$(\overline{u}_z)_t = f\overline{v}^*_z + F_z = \varepsilon\,\overline{w}^*_y.$$

The last equality results from the equation for the RMMC streamfunction. This means that the mean flow can change at z=0, as $\overline{v}^*$ is not necessarily zero, but that no vertical shear can develop. However, it turns out that $\overline{v}^*$ is small in most cases at that level because of the density weighting; the mean flow changes are then small. We also impose the symmetry condition that $\overline{\chi}^*_y = 0$ at the core of the jet.

In a recent paper, Conrath et al (1989) studied the meridional circulation driven by diabatic heating and momentum drag in the troposphere of the Outer Planets. They modelled the RMMC caused by Rayleigh friction of a steady wind pattern imposed at the lower boundary. They used $\overline{\chi}^*_z = 0 = \overline{v}^*$ at z=0. In that case, vertical shear can develop at the boundary and $\overline{T}$ is no longer constant; furthermore $\overline{w}^*$ is non zero. We anticipate little difference whether we choose $\overline{\chi}^* = 0$ or $\overline{\chi}^*_z = 0$; the RMMC cells will adjust in the lowest scale height. Our boundary condition is motivated by the fact that we wish to investigate the internal instabilities of jets. If the jets were to decay at the boundary, then the model should be interpreted to apply to jets originating below the boundary.

4.2. WESTWARD JETS.

4.2.1. EQUILIBRATION AND VACILLATIONS.

The initially unstable barotropic flow gives rise to an exponentially growing wave. After the wave has reached sufficiently large amplitude, the growth rate decreases as the eddy starts to influence the mean flow in the manner shown in the linear study; the wave acts to stabilize the flow. During such a numerical experiment with an initially barotropic flow of m=100, a shear zone develops in the lowest two scale heights[1]; the time-

[1] We also ran a simulation with an initially sheared flow close to minimal instability (m=1); the time-averaged flow remains identical to the initial flow. A slowly changing zonal mean energy cycles over a period of about 100 days, with very small changes in the actual zonal mean velocities. The eddy component is also smaller with a typical amplitude of 0.1 ms^{-1}. This is compatible with the idea that at weak supercriticality the eddies do not change the mean flow very much.

averaged vertical profile of $\overline{u}$ at the jet core is shown on figure 4.1; the standard deviation which characterizes the time fluctuations is also shown as a function of height on that figure. The standard deviation increases with height from about 8 ms^{-1} up to 15 m^{-1} in the uppermost layers, indicating that there is more time variability at higher levels. However the overall departure from the time-mean is not very large relative to the mean flow itself.

In the quasi-equilibrated regime, the flow reduces to a vertically sheared flow in the bottom layers and a barotropic component aloft; this time-averaged barotropic component aloft corresponds to a β^* of about -1. and is nearly neutral to barotropic instabilities. The time-averaged meridional profile of the jet at a height of 5H is shown in figure 4.2. The jet width, where the jet has fallen to 40% of its peak value, is about twice the initial jet width. The neutralization is accomplished by the broadening of the jet and by the weakening of its core. Note that β^* is quite sensitive to a change in the jet width since $\beta^*=\beta L^2/U_0$.

4.2.2. COMPARISON WITH PIRRAGLIA.

This mechanism for jet decay has been recently examined by Pirraglia (1989) using a truncated nonlinear model. As time evolves, an initial jet pattern which is barotropically unstable tends to stabilize toward a state in which vertical shear is created in the bottom layers. His model differs from our's in some aspects however. In Pirraglia's model, the initial flow has a sinusoidal shape in the meridional direction; it therefore contains an eastward jet and a westward jet of the same magnitude. It is also a highly truncated spectral model; in total, about 10 modes are retained and there are only 2 meridional wavenumbers allowed. In the vertical, the dynamical quantities are computed at two points only. Such a model can not represent accurately the meridional momentum spreading, i.e. the jet smoothing, involved in barotropic equilibration. In both models the dynamical processes manifest themselves in simplified but different ways; we will see however that some key results are nevertheless quite similar in the two models.

Pirraglia's model extends vertically over 4 scale heights with a constant static stability in the two bottom layers, identified as the troposphere; the static stability is also constant but larger in the two upper layers (the stratosphere). In order to compare our results with his, we perform a similar simulation with an initially barotropic flow (m=100) in a domain of the same vertical extent of 4 scale heights. Initially, his mean flow is unstable with a growth rate σ=0.4 day^{-1}; our analog value is close (σ=0.55 day^{-1}), the difference being due to a different jet profile and intensity.

With our model we are able to examine the stability of a single westward jet while his zonal flow has a meridional pattern with a westward and an eastward jet evolving together in a coupled way. Also note that in his model, $\overline{u}$ is constant at the lower boundary as a direct consequence of the wave fields being zero there. This is specific to his formalism which does not include a term like $f\overline{v}^*$.

4.2.2.1. MEAN ZONAL VELOCITIES.

The zonally-averaged velocity $\overline{u}$ may be thought of as the sum of the initial flow and a counterflow driven by the unstable eddies (Pirraglia, 1989). We plot the zonal velocity $\overline{u}$ one-half scale height above the bottom boundary as a function of time (figure 4.3); the mean zonal velocity is shown to vacillate around an average of -75 ms^{-1} after the unstable eddy has grown to sufficiently large amplitude. The period of the $\overline{u}$ fluctuations is 10-15 days and their peak-to-peak amplitude is about 15 ms^{-1}.

On figure 4.4a, the time-averaged zonal mean flow is shown along with the standard deviation at the jet core. The actual $\overline{u}$ profile is shown for several days at the end of the integration period on figure 4.4b. One can see the steady shear zone in the lowest scale heights and a more time dependent flow aloft with noticeable variations on a scale of a day. Note that the decaying profiles are taken at the jet core; because of the jet broadening at upper levels, the time-averaged zonal wind speed may increase with height in the wings of the jets.

The vertical extent of the domain does not affect much the average mean flow profile as a comparison of figure 4.4a with figure 4.1 shows. The vertical shear in the lowest two scale heights and the barotropic flow aloft have been preserved as the upper boundary is moved downward from 6 to 4 scale heights. The sharp increase of the zonal flow with height close to the upper boundary is due to interference of the top boundary with the wave decay. This should be understood as a limitation of the model and should not lead to incorrect physical interpretations.

4.2.2.2. EDDY VELOCITIES.

The eddy zonal velocity u' is much smaller than the zonally-averaged component with a typical amplitude of a few ms^{-1} at one-half width (L/2) away from the jet core; the fluctuations have a typical period of 5 days as shown on figure 4.3.

Figure 4.5b also shows the eddy meridional velocity v' at the jet core at z=1.5 H; it has a RMS value of about 15 ms^{-1}. We also displayed the RMS fluctuation of the eddy meridional velocity as a function of height (figure 4.5a).

4.2.2.3. EDDY ENERGIES AND ENERGY CONVERSIONS.

After the wave has reached a maximum amplitude, the growth rate actually becomes negative and a vacillation cycle sets in with periodic reversal of the mean-to-eddy energy conversions. The wave kinetic energy is seen to grow exponentially and then to saturate and oscillate around some mean energy level (figure 4.6a); this vacillation is noticeable in the time-evolution of the zonal kinetic energy as well.

Figure 4.6b shows the predominantly barotropic character of the vacillations with the correlation of the kinetic energy conversion to periods of wave growth; the conversion of available potential energy is negligible compared to the kinetic energy conversion. During the vacillating cycles,

the EPFD and RMMC adjust their structure along with the mean flow changes; there is a periodic reversal in the RMMC cells and the EPFD field; this is analysed in section 4.2.4.

In our model, the vacillations are coherent, in the sense that they are in phase at all levels. Figure 4.7 shows the conversions of kinetic energy at one, two and three scale heights. Note that the conversion of kinetic energy shown in figure 4.6 is vertically integrated and reflects the fact that the conversion is weighted toward a level slightly below where Ψ is maximum. The total conversion peaks at about one scale height (figure 4.8). One can also remark that not only are the energy fluctuations in phase, but the eddy velocities u' and v' oscillate in phase at all levels, due to the near-constant phase speed over the domain.

4.2.2.4. EDDY TEMPERATURE.

The typical RMS value for the temperature fluctuation is the order of 1 K (figure 4.9), consistent with the retrievals by Gierasch et al. (1986) of temperature at 270 mbars. It shows however exponential growth with height ; we also noted the same was true for the u' fluctuations. The magnitude of these fluctuations increases with height because of the exponential decrease of density with height. Indeed, one has that the eddy zonal velocity is

$$u' = \psi_y = \mathrm{Re}\,[\ \Psi_y\ \exp\{z/2H\}\ \exp\{-ikx\}\ ],$$

and the corresponding expression for the temperature also contains a factor like $e^{z/2H}$. This is a shortcoming of our simplified model; no dissipation has been introduced at this stage to prevent the amplification of velocities with height. The eddy kinetic energy is not concentrated in the uppermost layers however, because one has for example :

$$\rho u'^2 = (\ \mathrm{Re}\,[\Psi_y \exp\{-ikx\}\ ]\ )^2.$$

4.2.2.5. SUMMARY.

As a summary, our model compares with Pirraglia's in the following manner :

In his model, a vertical shear zone is seen to develop in the lower two scale heights with the zonal flow decaying to zero over the vertical domain (figure 4.10a). A similar effect can be seen in our model; however, there is a barotropically neutral component aloft that persists over the integration period. In Pirraglia's results, the near-zero stratospheric zonal wind can be seen as the small residual of large fluctuating velocities, initially of the order of the initial flow speed. This can be seen in figure 4.10b which shows the time-evolution of the zonal wind in both the stratosphere and the troposphere. In our model, the flow is neutralized in the upper layers, by spreading zonal momentum horizontally, i.e by reducing the jet amplitude and broadening it. This process cannot be represented accurately in Pirraglia's model because of the meridional truncation. There is no vertical shear involved in that process. In the lower layers, the constraint of the boundary prohibits such an equilibration.

These oscillations in the upper layers do not appear to such an extent in our model probably also because the upper boundary condition is different. Pirraglia has a condition of no perturbation potential temperature while our wave goes to zero. If the wave does not decay to zero fast enough with height, we also have noticed that the eddy velocities are amplified through the density decrease with height.

Table 4.1 and 4.2 compare typical velocities and periods in both models. Our model however corrects two shortcomings of Pirraglia's model : the eddy velocities are higher in his calculations probably as a result of his stringent truncation. He mentioned that including more modes lessened the amplitude of these fluctuations, as expected from the idea that more modes allow a smoother equilibration. Also, the stratospheric fluctuations are much less prominent in this model as our meridional resolution allows for a smooth mean flow broadening. The periods of the $\bar{u}$ fluctuations are

similar in the two models. Also, our model makes it possible to separate instablilities of eastward jets from the ones of westward jets. The instabilities of eastward jets will be analysed in another section.

4.2.3. VERTICAL SCALE SELECTION.

A strong conclusion of our modelling study is that a vertical shear zone develops over the lower two scale heights; one could wonder about the robustness of this scale estimate. Barotropic instabilities are governed by $\beta^* = \beta L^2/U_0$; if U_0 or L is changed so that β^* increases in absolute value (i.e. the flow is less unstable), then less vertical shear is needed. This is confirmed by a run for a weak jet case ($U_0 = -25$ ms^{-1}). Figure 4.11 shows the average zonal mean flow in that case; the vertical shear is much less pronounced than for the previous case which had $U_0 = -90$ ms^{-1}.

There is qualitative agreement with the stability criterion of Chapter 3; it was then seen that minimal instability corresponds to m = (L/L_D). Let us define the vertical scale in analogy with the width parameter of a Bickley jet; it is the height (in units of H) at which the zonal flow has decayed to 40% of its peak value. However, because it decays to a baroropic component, we need to take 40% of the difference between the peak value and the barotropic value. We can then see a qualitative agreement with the prediction that m=.66 for the westward jets from the zonal flow profiles of figure 4.1 and 4.11.

The stratification also plays a role in the vertical scale selection; a more stable layer (smaller Bu) would have a larger decay rate because Bu ~ N^{-2}.

4.2.4. RESIDUAL CIRCULATIONS AND EDDY DRAG.

We also examined the behavior of the residual velocities associated with the RMMC. We looked at the time-evolution of $f\overline{v}^*$ at 1.5 H above the lower boundary at the jet core; we observed that $\overline{v}^*$ fluctuates in time with a standard deviation of 3.74 10^{-5} ms^{-2} and that the time-averaged value of $f\overline{v}^*$ over the 400 days time-span of the integration is -6.82 10^{-7} ms^{-2}, which is

much smaller than the characteristic amplitude of the $f\overline{v}^*$ vacillations. The time-averaged $f\overline{v}^*$ is then a small residual; when computing the cross-section of the $\overline{\chi}^*$, we found a strong dependence upon time.

This can be understood by the following considerations : as mentioned before, there is no mean energy conversion after equilibration, and the vacillating pattern of RMMC cells, associated with the oscillating $\overline{v}^*$ and $\overline{w}^*$, follows the vacillations seen in the eddy kinetic energy or the EPFD. The alternation of phases of eddy growth and decay are associated with reversing RMMC cells. We then expect the time-averaged $\overline{v}^*$ to be zero; the small residual value of $\overline{v}^*$ is probably due to the time cut-off and averaging. We will see in a later chapter that the presence of forcing may introduce a time-averaged RMMC.

We now try to understand why barotropic instabilities act as a vertical drag term in the zonal mean momentum tendency equation. We know that in the linear case the EPFD term is like a vertical drag term in the core of the jet : it has a uniform sign in the vertical direction and is acting to reduce the jet. We examine how this property persists in the quasilinear calculations.

A look at the time evolution of the two forcing terms of the zonal mean momentum equation, $f\overline{v}^*$ and F, shows that they correlate negatively and have similar magnitudes. More precisely, one can distinguish in the time-evolution a linear regime and an equilibrated regime by looking at the relative magnitude of $f\overline{v}^*$ and F. Figure 4.12 shows the ratio of these two quantities at one jet width away from the jet core at one, two and three scale heights. One can see that $f\overline{v}^*$ is initially much smaller than the EPFD at all levels by at least a factor 10. This corresponds to the linear regime where the EPFD has a meridional dipolar structure and acts as a vertical drag term in the core of the jet (i.e. it tends to reduce the jets everywhere in the vertical), while the RMMC consists of stacked cells. During this phase, they both maintain signs predicted by the linear theory for unstable barotropic modes. After about day 28, one has an equilibrated regime with the EPFD and the RMMC balancing each other. This corresponds to the

vacillating regime and both quantities oscillate while keeping the same relative magnitude and opposite signs. Both quantities are of the order of 10^{-5} ms^{-2}. Note also that both F and $f\overline{v}^*$ increase with height giving more variability in the upper layers. The rationale is that because of the time dependence in the eddy quantities due to the overshooting, the only balance which can prevail to steady the mean flow is one in which the EPFD and the RMMC are of the same order. Note that during the vacillation $\overline{v}^*$ has a magnitude of the order 0.1 ms^{-1}. Recall however that the magnitude of the vacillating quantities depends strongly on the truncation and the supercriticality of the initial mean flow, and that time-averaged quantities should rather be examined.

The vertical decay of the zonal jet is mainly created before the equilibration, i.e. during a period of unbalance between the EPFD and the RMMC; the mean flow forcing comes essentially from the EPFD term which still acts as a drag. During this regime, the EPFD term grows from very small initial amplitudes, but figure 4.5b shows that the vertical shear zone has already formed at day 28 and will not change very much afterwards. Figure 4.13 shows the vertical shear per scale height at one and three scale heights at the jet core. One can see that at one scale height, a vertical shear of 10-15 ms^{-1} per scale height is created during this period, around day 20-28. Afterwards, it fluctuates around that value. At z=3H, the shear fluctuates and changes sign throughout the time iteration, indicating that the zonal wind sometimes increases with height as was confirmed by the plots of $\overline{u}$ on figure 4.4. These magnitudes for the vertical shear at one scale height are in agreement with those computed from the Voyager retrievals (Gierasch et al. 86), i.e. 10-15 ms^{-1} per scale height in the 150 mbar-270 mbar region.

4.2.5. ROLE OF FORCING AND DISSIPATION.

After equilibration, there is, on average, no energy conversion between the mean flow and the wave in our computations. In other words, as the mean flow has been neutralized through the growth of the instability, there is no continuous flow of energy from the mean flow to the wave. When

dissipation is introduced in the form of radiative damping acting on the wave, the wave energy decreases on a time scale equal to half of the radiative time scale. There is no time-averaged RMMC present in this case either; to explain a steady RMMC, one has to invoke a mechanism to restore the mean flow to the initial unstable configuration. Radiative damping would then tend to suppress vertical shear and drive the mean flow back to a barotropic configuration. Gravity wave emitted at the convective boundary could be provide such a forcing term as they would tend to bring the mean flow back to its value at the level where they were emitted (Leovy, personal communication). Such mechanisms will be further investigated in the next chapter. Calculations with a heuristic forcing term in the zonal mean flow equation tend to show that the wave could maintain a constant amplitude in the presence of dissipation.

The neutralisation of the barotropically unstable deep jets could explain the origin of a vertical shear zone. In the absence of forcing, the jets should maintain themselves in a state close to marginal stability with possibly disruptions due to fluctuations in the deep jet intensity or profile. There would be ensuing fluctuations in $\overline{u}$ and u'; while the fluctuations in $\overline{u}$ would have periods and magnitudes related to the forcing, the u' fluctuations would have characteristic periods and wavelengths. A dynamics of large coherent eddies can prevail in such a neutral flow (Sommeria et al., 1989) with a source of energy that can be at small scales.

However, the presence of steady rings of eddies and permanent quasi-steady RMMC, both of which could originate in instabilities, seems to indicate that another hypothesis is that there is a mean flow balance between a forcing to an unstable state and a relaxation to a neutral state, leaving behind near-steady eddies.

Table 4.1 : Typical zonal velocities (units of ms^{-1}).

TROPOSPHERE

	Pirraglia's	Our model
U_0 (initial flow)	60	90
eddy-induced $\overline{u}$	10-15	10 (at jet core)
u' (eddy velocity)	10-20	4 (at jet core)
time-averaged $\overline{u}$	20	65

STRATOSPHERE

	Pirraglia's	Our model
U_0 (initial flow)	60	90
eddy-induced $\overline{u}$	10-30	15 (at jet core)
u' (eddy velocity)	20-30	
time-averaged $\overline{u}$	-3	60

Table 4.2 : Typical periods of the fluctuations(in Jovian days).

TROPOSPHERE

	Pirraglia's	Our model
$\overline{u}$	30-40	30-45
u'	15	

STRATOSPHERE

	Pirraglia's	Our model
$\overline{u}$	20-30	30-45
u'	15	

4.3. EASTWARD JETS.

A similar experiment was run for an initially unstable eastward jet. The jet width and intensity were chosen to be the same as in the linear study, i.e. U_0 = 150 ms^{-1} and L = 3125 km. The initial flow was barotropic (m = 100).

The most unstable linear modes were shown to have critical lines at high levels; for example, the mode for m = 10 had a phase speed of 49 ms^{-1}, i.e. $c_r/U_0 \sim .3$, so that the critical level is slightly above 10 H. This dictated that the computational domain extends over many scale heights.

One can see from the numerical experiment that the mean flow is readily stabilized; this is seen in the time evolution of EKE and ZKE (figure 4.14) which shows that EKE grows to a much smaller fraction of ZKE than in the westward jet case. As expected from the linear study, a thick shear zone stabilizes the flow : the numerical experiment shows that the vertical shear zone forms only above 6 H (figure 4.15); the flow remains barotropic below that height. There is a lot of variability in the upper layers, with the RMS deviation from the time-mean being of order of 100 ms^{-1}. This can be understood as a consequence of the fact that through the exponential decrease in density, small eddy energies can give rise to large amplitudes and residual velocities which create tremendous fluctuations in the mean flow. This is a non-Boussinesq effect and the behavior is influenced by the upper boundary, as was encountered before. There is nevertheless good agreement between the structure of the linear mode and the developing eddy in the nonlinear case (figure 4.16).

We have not proceed by analyzing the eddy quantities in great detail as we did for the westward jets. It is clear that in this case the above mentioned non-Boussinesq and boundary effects introduce quite unrealistic magnitudes. This nonlinear experiment confirms nevertheless the results of the linear study; it suggests that strong eastward jets can possibly penetrate the stable layer. Observations however suggest that the shears

above eastward jets are as strong as the ones above the westward jets. We will see in the next section how instabilities of westward jets can propagate meridionally and affect the stability of eastward jets.

4.4. COMPOSITE JETS.

4.4.1. DESCRIPTION OF THE COMPOSITE JET STRUCTURE.

We have so far looked at the stability of eastward and westward Bickley jets. These zonal winds had a constant direction over the whole domain. We want now to consider the case where an eastward jet and a westward jet are close together so that, through meridional propagation, the potential instabilities of one may influence the other one.

Within the framework of the numerical model developed in this work, we have looked at the following family of zonal wind profiles : these profiles have an eastward Bickley jet, $U_0\ \mathrm{sech}^2\ (y/L)$, centered at the origin, patched with a westward Bickley jet of the same width and intensity, centered at y_0 : $-U_0\ \mathrm{sech}^2\ [(y-y_0)/L]$. The patching is done in the following manner : one chooses a distance y_1, away from the origin, at which the eastward jet profile is replaced by a linear interpolation up to the point y_0-y_1; beyond that point, the profile follows the previously mentioned westward Bickley jet. The interpolation is made by choosing the slope of the straight line equal to the jet slope at $y = y_1$; by symmetry, the slope of the straight line is also equal to the jet slope at $y = y_0$-y_1. Typically, y_1 is chosen between .75L and 2L, where L is the Bickley jet width parameter.

Note that this is a one-parameter family of profiles once U_0 and L have been chosen; for example, once y_1 is chosen, the distance at which the westward jet peaks, y_0, is determined by the relation

$$y_0 = -2\,b/a\ +\ 2\,y_1,$$

where $b= U_0\ \mathrm{sech}^2\ (y_1/L)$ and $a= d/dy\ \{U_0\ \mathrm{sech}^2\ (y/L)\}\ |\ y_1$. This can be seen

from the wind matching condition at $y = y_0 - y_1$:

$$a(y_0 - 2y_1) + b = -b.$$

This profile satisfies the same symmetry conditions as the profiles used earlier in the study of Bickley jets : the zonal wind is symmetric at the origin of the domain and goes to zero at the other side. Figure 4.17 shows three profiles with y_1=.5L, .75L and 2L. When y_1=2L, one can think that the jets are well apart; when y_1=.75L, the jets come closer to each other. When y_1 decreases below that value, the separation between the jets increases again.

Note that no instability is supposed to develop in the region separating the jets because the interpolation is linear. At the matching points, there is continuity of the wind and its first derivative, but there are discontinuities of the second derivatives (see figure 4.22). We have not found any effect of these discontinuities in the nonlinear runs as these narrow regions of variations of the potential vorticity gradient $\overline{q}_y$ are smoothed out rapidly during the nonlinear equilibration. Due to the computational burden, we used 51 points in the meridional direction.

We have run two quasi-linear experiments, one with y_1=2L and one with y_1=.75L. In these simulations, we chose U_0=90 ms^{-1}, L=2000 km and the other parameters equal to those used in previous experiments. One starts with a barotropic flow (m=100); the zonal wavenumber is k=20. Our numerical linear stability analysis of Bickley jets shows that the westward jet is more unstable than the eastward jet for all k; the intensity of the eastward jet was then 150 ms^{-1} and its width 3125 km, so that it had a non-dimensional beta $\beta^* \sim 0.3$. With the current parameters, i.e. a width L of 2000 km and an intensity of 90 ms^{-1}, one has $\beta^* \sim 0.2$ so that the eastward jet is more unstable than in the previous numerical runs. Nevertheless, inspection of a linear stability diagram for Bickley jets indicates that the westward jets are still more unstable (Haltiner and Williams, 1980). Consequently we choose k so as to maximize the growth rate of the unstable disturbances of the westward jet.

FJ/L/9

jet.

One can notice that in previous studies (Conrath and Pirraglia, 1983; Gierasch et al., 1986; Conrath et al., 1990), the Rayleigh drag generates mean meridional circulations which are "zone-like" (upwelling in anticyclonic shear zones), while in this study, the introduction of a Rayleigh forcing has created an additional circulation of the opposite sense. This apparent contradiction can be resolved by looking at a more general form of S_0, the source term of the mean meridional circulation. In presence of a Rayleigh drag $\alpha\,(\overline{u}_0(y) - \overline{u})$ and radiative damping (with $\alpha_R = t_R^{-1}$) but neglecting the contribution of the eddies, one has

$$S_0 = -\,(f/N^2)\;\rho_0\,[\,\partial_z\,(\,\alpha\;\overline{u}_0) + (R\alpha_R/fH)\,\partial_y\,T_{eq} + \partial_z\,(\,(\alpha_R - \alpha)\,\overline{u}\,)\,].$$

We further assume for simplicity that α and α_R are independent of height. It was assumed in the studies mentionned above that

1) $\alpha_R \sim \alpha$, i.e. that the radiative time scale and the drag time scale are equal.

2) T_{eq} has no meridional variation on the scale of the jets.

One has then that S_0 reduces to

$$S_0 = -\,(f/N^2)\;\rho_0\;\partial_z\,(\,\alpha\;\overline{u}_0).$$

For a decaying westward jet, $\partial_z\,(\,\alpha\;\overline{u}_0) > 0$ and $S_0 < 0$; this implies a "zone-like" meridional circulation. The physical explanation of the balance is described for example in Conrath and Pirraglia (1983). Through thermal wind balance, a decaying westward jet is associated with a meridional circulation that produces heating through downwelling on the equatorward (cyclonic) side of the jet and cooling through upwelling on the poleward (anticyclonic) side; cooling and heating are compensated by radiative damping, so that a negative meridional temperature gradient is

maintained. In our model however, a different balance exists. We have neglected the effect of radiative damping on the mean flow; instead, a Rayleigh drag was introduced with an adjustable time constant. In our case, $\partial_z \overline{u}0 = 0$, so that S_0 reduces to :

$$S_0 = - (f/N^2)\ \rho_0\ \partial_z (- \alpha\ \overline{u}).$$

As shown before, this implies a meridional circulation with upwelling on the equatorward side. The introduction of an explicit forcing has therefore modified the shape and structure of the mean meridional circulation driven by the instabilities.

When $\alpha^{-1} \sim 50$ days, maximum vertical velocities associated with $\overline{\chi}^*$ are of the order of $5\ 10^{-10}$ H/s; they also scale as α. These vertical velocities, a fraction of a scale height per orbital period, are quite small. Nevertheless, vertical velocities of this magnitude compare well with the value derived from the heat balance at 270 mbar by Gierasch et al. (1986). They derived a meridional profile of $\overline{w}^*$ from the thermodynamic equation assuming constant values for radiative time constant, static stability and radiative equilibrium temperature, so that $\overline{w}^*$ is essentially linearly proportional to $\overline{T}$. Their meridional profile of $\overline{w}^*$ coincides nicely with concentration of ammonia and cloud optical depths, suggesting that the RMMC is responsible for the tracer transports and not the eddies. The RMMC on the scale of the jets has to be linked with the instabilities as the radiatively driven RMMC is very small in the upper troposphere (Conrath et al., 1989).

The argument of Gierasch et al. (1986) was based on the assumption that the balance for the zonal mean temperature is

$$\overline{w}^* (N^2 H/R) = (\overline{T} - \overline{T}_e)/ t_R$$

where t_R is the radiative time scale, typically 10^8 s in the upper troposphere. On the jet scale, this implies meridional temperature contrast

$$\Delta T = (N^2 H/R)\, w^* t_R$$

where w* is an estimate of the residual mean vertical velocity. Temperature gradients on the scale of the jets are of the order of a few K; a $\Delta T \sim 1$ K imposes $w^* \sim 10^{-9}$ H/s. It should be noted that we performed our numerical experiments with a radiative time constant of 100 days, a value three times smaller than the value representative of the actual radiative time constant used in Gierasch et al. (1986); the value of α necessary to provide a steady-state should then be appropriately rescaled. Such small vertical velocities, fractions of a scale height per orbital period, can give rise to such temperature differences because of the long radiative time scale on Jupiter.

5.5. IMPLICATIONS.

The quantities that are probably relevant to the real atmosphere of Jupiter are the averaged amount of eddy energy and the flow profile. In many cases, the time-evolution of the eddy energy has a regular vacillation the period of which does not depend on the presence of forcing. These vacillations are ubiquitous in quasi-linear models; they do probably not represent real phenomena however. They depend strongly on the truncation, and the process that gives rise to them - shearing of a eddy leaning relative to the mean shear - is a crude representation of real situations, and it is not well represented by a simple wave-mean flow decomposition. Let us examine some consequences of the two cases of $\alpha^{-1} = t_R$ and $\alpha^{-1} < t_R$.

The case of $\alpha^{-1} = t_R$ shows life-cycles of a length of several t_R. On Jupiter, the corresponding time span of such life-cycles would be many terrestrial years ($t_R \sim 2$ years). There is no steady pattern of RMMC during that cycle as periods of wave growth correspond to a RMMC pattern with a bottom cell having upwelling on the poleward side of the jet (i.e. a zone-like behavior), while the decay phase of the cycle would show a reverse pattern. There would be abrupt switchings from one pattern to the other, occuring episodically at intervals of several years.

When the forcing is faster, i.e when $\alpha^{-1} < t_R/2$, there is a time-averaged pattern of eddy fluxes, as well as a small but definite residual mean meridional circulation. These circulations are quite complex : there are ascending motions in regions of anticyclonic shear (i.e. a "zone-like" behavior) induced by the instabilities, but opposite cells are also generated by the Rayleigh forcing. The residual vertical velocities are quite small but they are not incompatible with the observations. The Rayleigh forcing introduced in this model is not equivalent to the Newtonian radiative damping of the mean flow however.

The bands of Jupiter are probably a shallow phenomenon, the evidences for which disappear below 2 bars, as is suggested by the NH_3 observations (De Pater, 1986). This means that they span a region of three scale heights, from the 2-bar level to the tropopause region. The residual circulations of figure 5.12 also span two or three scale heights, and with the bottom boundary at the 2-bar level, the associated vertical velocity field would extend over sufficiently deep layers to influence the formation of the NH_3 and NH_4SH cloud layers.

The observed structure of the bands of Jupiter suggests that they irregularly changes with time, with a time scale of a few years; sometimes these changes are quite fast. In a possibly similar context, one can remark the striking case of the planet Saturn on which the rapid development of a gigangic storm has been observed in the fall of 1990. Depending of the strength of the forcing, the model developed here displays a regime of eddy life-cycles with residual circulations that are only briefly generated, or a regime of weak steady residual circulations.

When the forcing is faster, i.e when $\alpha^{-1} < t_R/2$, there is a time-averaged pattern of eddy fluxes, as well as a small but definite residual mean meridional circulation. These circulations are quite complex : there are ascending motions in regions of anticyclonic shear (i.e. a "zone-like" behavior) induced by the instabilities, but opposite cells are also generated by the Rayleigh forcing. The residual vertical velocities are quite small but they are not incompatible with the observations. The Rayleigh forcing introduced in this model is not equivalent to the Newtonian radiative damping of the mean flow however.

The bands of Jupiter are probably a shallow phenomenon, the evidences for which disappear below 2 bars, as is suggested by the NH_3 observations (De Pater, 1986). This means that they span a region of three scale heights, from the 2-bar level to the tropopause region. The residual circulations of figure 5.12 also span two or three scale heights, and with the bottom boundary at the 2-bar level, the associated vertical velocity field would extend over sufficiently deep layers to influence the formation of the NH_3 and NH_4SH cloud layers.

The observed structure of the bands of Jupiter suggests that they irregularly changes with time, with a time scale of a few years; sometimes these changes are quite fast. In a possibly similar context, one can remark the striking case of the planet Saturn on which the rapid development of a gigangic storm has been observed in the fall of 1990. Depending of the strength of the forcing, the model developed here displays a regime of eddy life-cycles with residual circulations that are only briefly generated, or a regime of weak steady residual circulations.

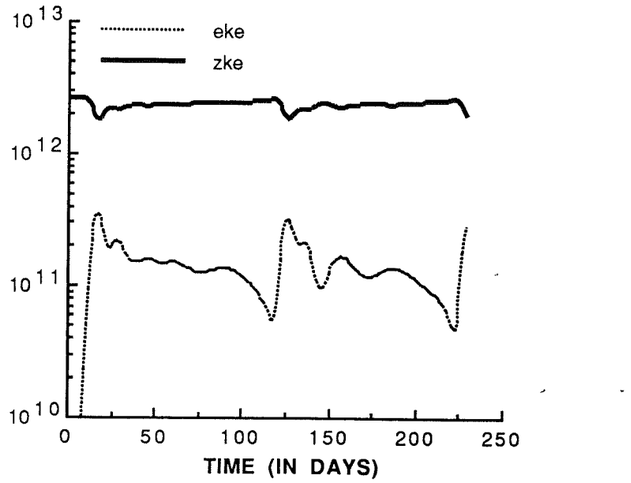

Figure 5.1: Eddy kinetic energy (EKE) and zonal mean kinetic energy (ZKE) as a function of time for $\alpha^{-1} = t_R = 10$ days.

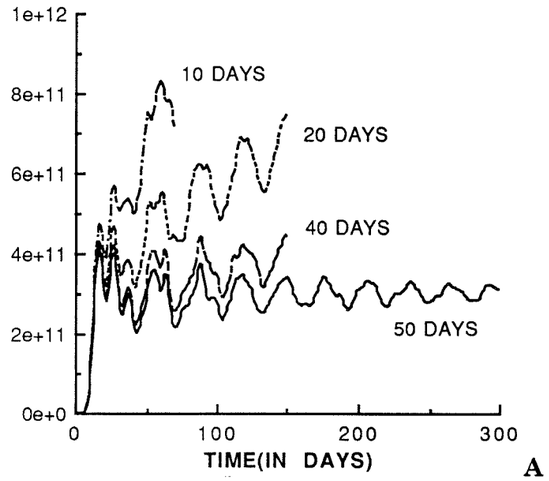

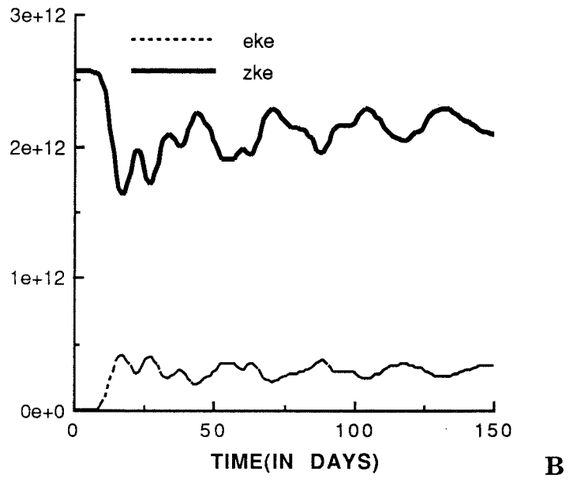

Figure 5.2: **A)** Eddy kinetic energy (EKE) as a function of time for various α^{-1}. (t_R = 100 days). **B)** Eddy kinetic energy (EKE) and zonal mean kinetic energy (ZKE) as a function of time for α^{-1} = 50 days and t_R= 100 days.

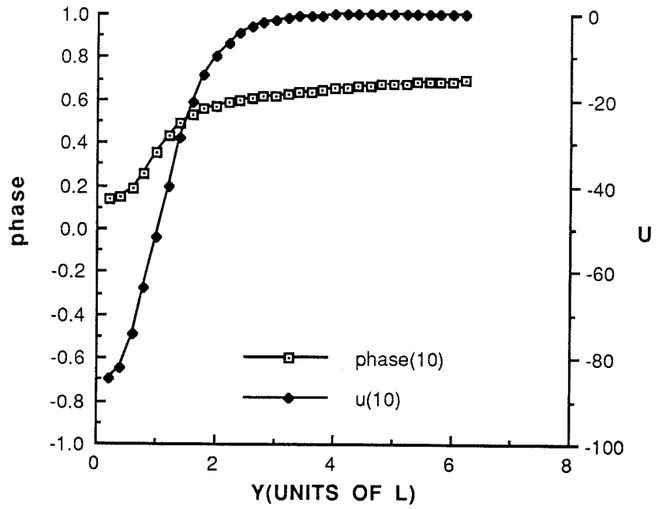

Figure 5.3: Meridional profile of the phase of the wave and of the mean flow at z= 1.5 H after 10 days (for $\alpha^{-1} = t_R = 10$ days).

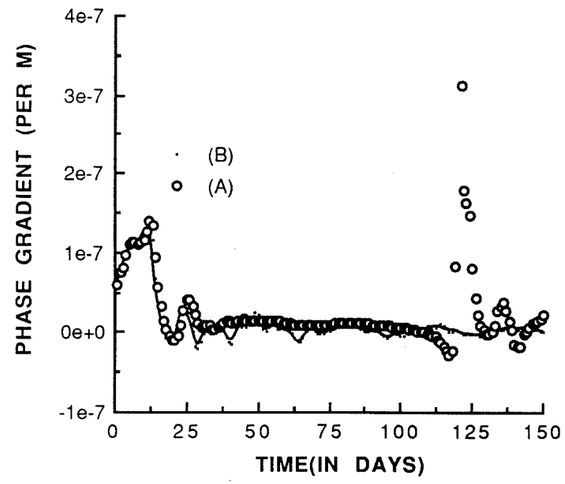

Figure 5.4: Meridional phase gradient at y=L as a function of time for $\alpha^{-1} = t_R$ = 10 days (A), and for α^{-1} = 20 days and t_R = 100 days (B). The phase is at z= 1.5 H.

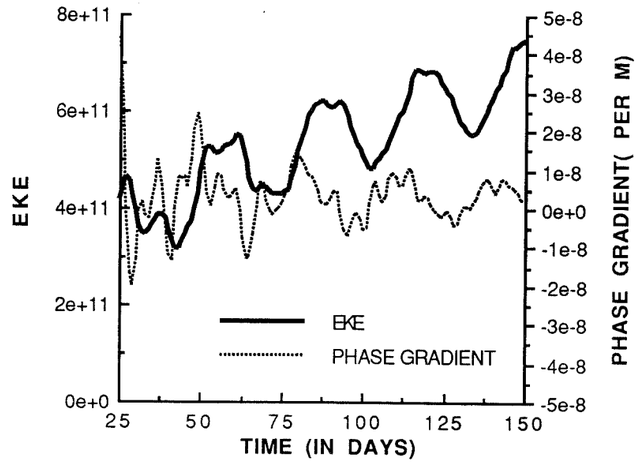

Figure 5.5: Eddy kinetic energy (EKE) and meridional phase gradient as a function of time for α^{-1} = 20 days, t_R = 100 days.

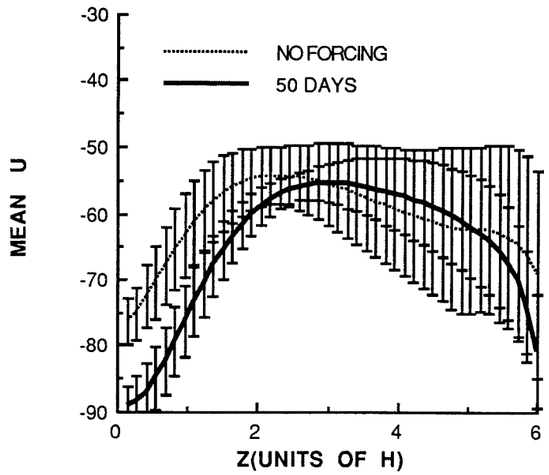

Figure 5.6: Vertical profile of the time-averaged mean flow at the jet core for the undamped case and for α^{-1} = 50 days. Also shown are the RMS deviations.

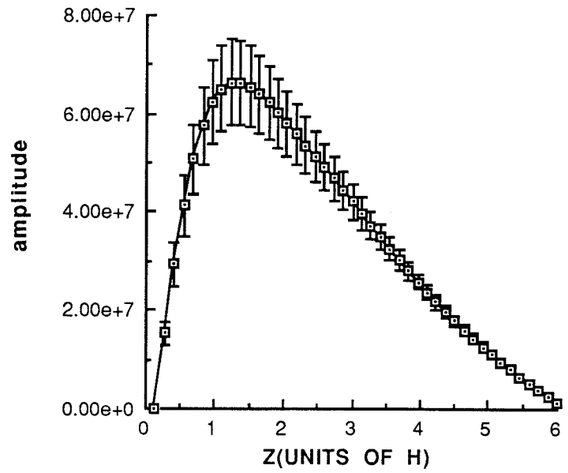

Figure 5.7: Vertical profile of the time-averaged eddy amplitude ($|\Psi|$) at the jet core for α^{-1} = 10 days, t_R = 100 days. The standard deviation is also shown.

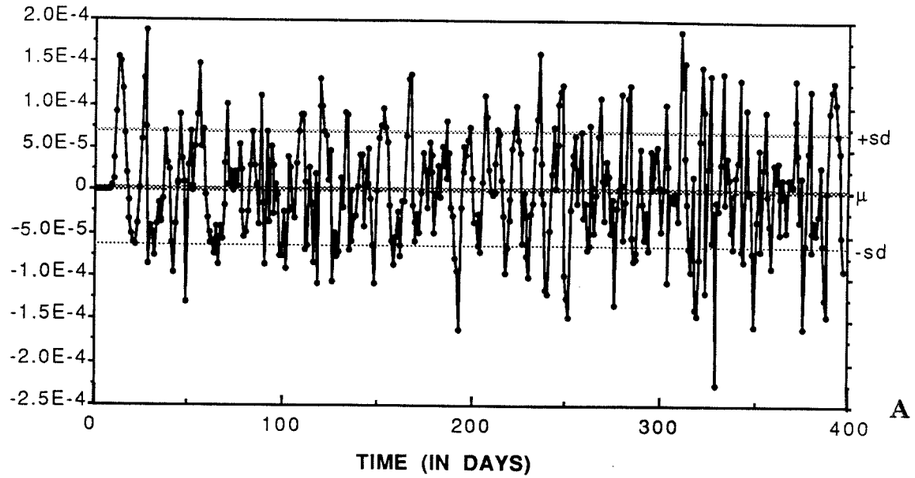

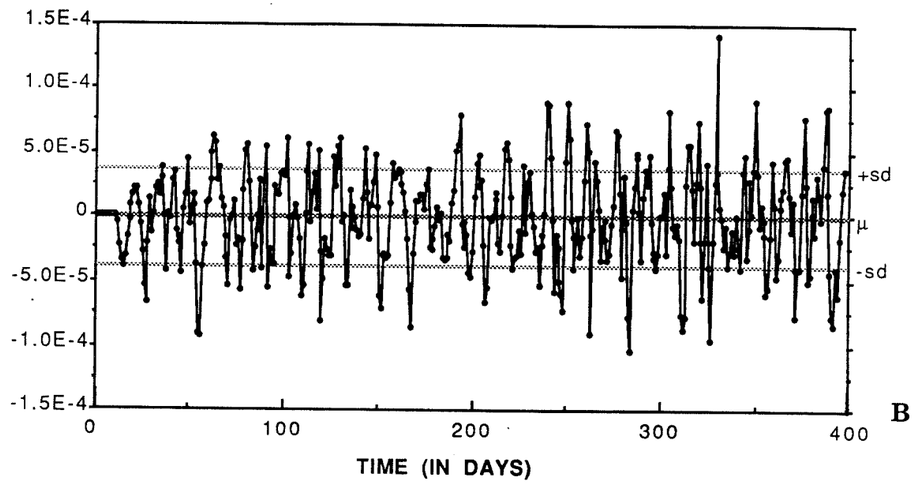

Figure 5.8: **A)** Time-evolution of F at z=1.5 H at the jet core for undamped case. **B)** Time-evolution of $\overline{fv}^*$ at z=1.5 H at the jet core in same case. μ is the time-average and sd is the standard deviation; their values are indicated on table 5.1

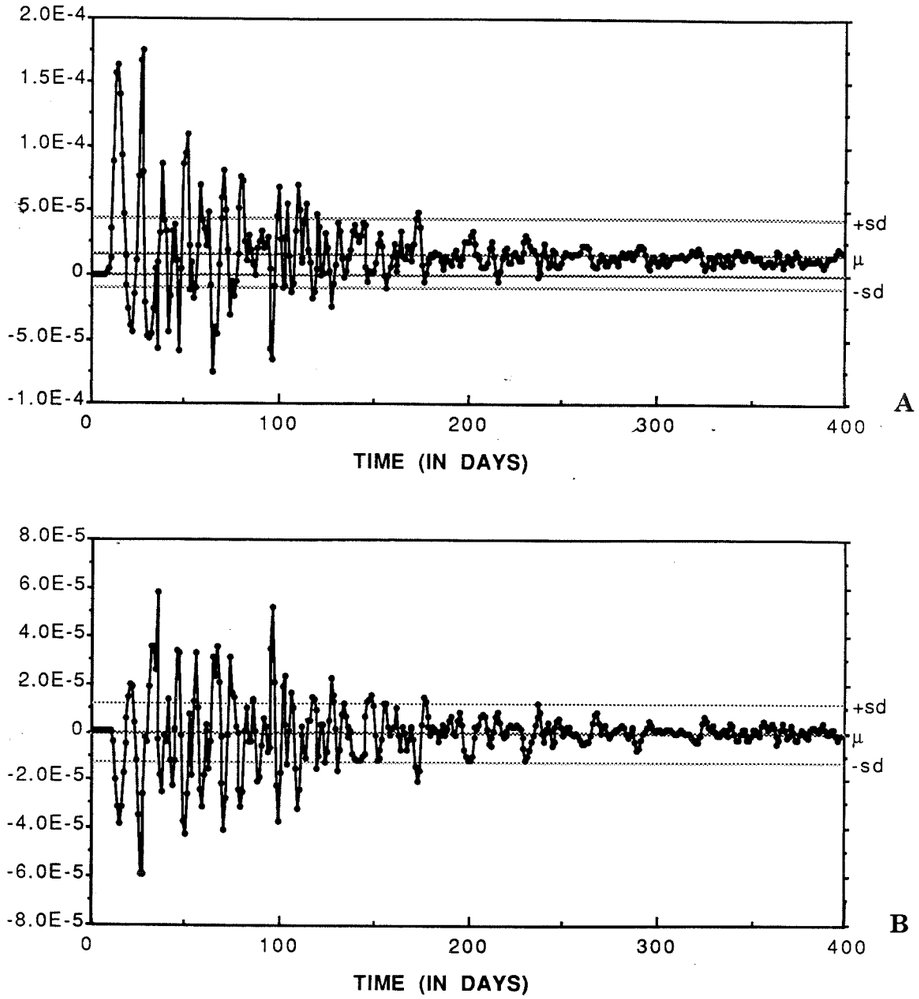

Figure 5.9: **A)** Time-evolution of F at z=1.5 H at the jet core for α^{-1}= 20 days. **B)** Time-evolution of $\overline{fv}^*$at z=1.5 H at the jet core in same case. μ is the time-average and sd is the standard deviation; their values are indicated on table 5.1

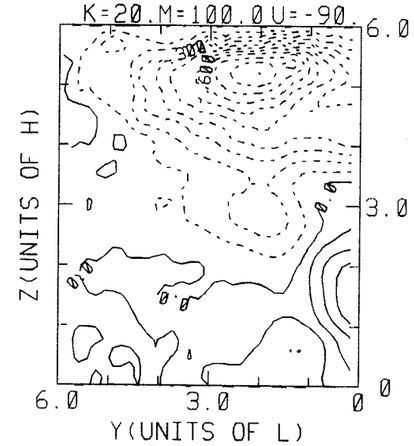

A

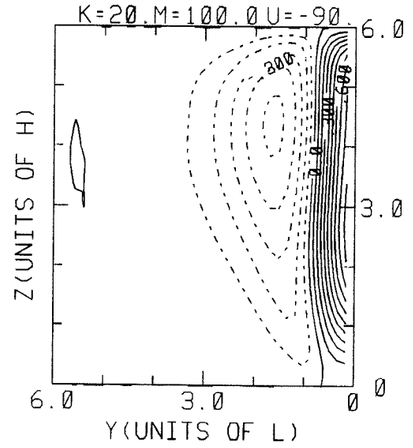

B

Figure 5.10: **A)** Cross-section of F in the y-z plane for the undamped case. **B)** Cross-section of F for α^{-1}= 20 days. **C)** Same for α^{-1}= 50 days.

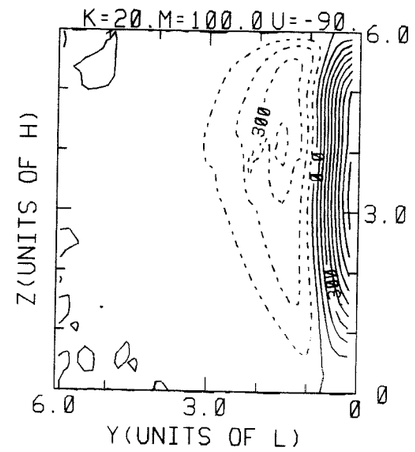

C

Figure 5.10: (continued)

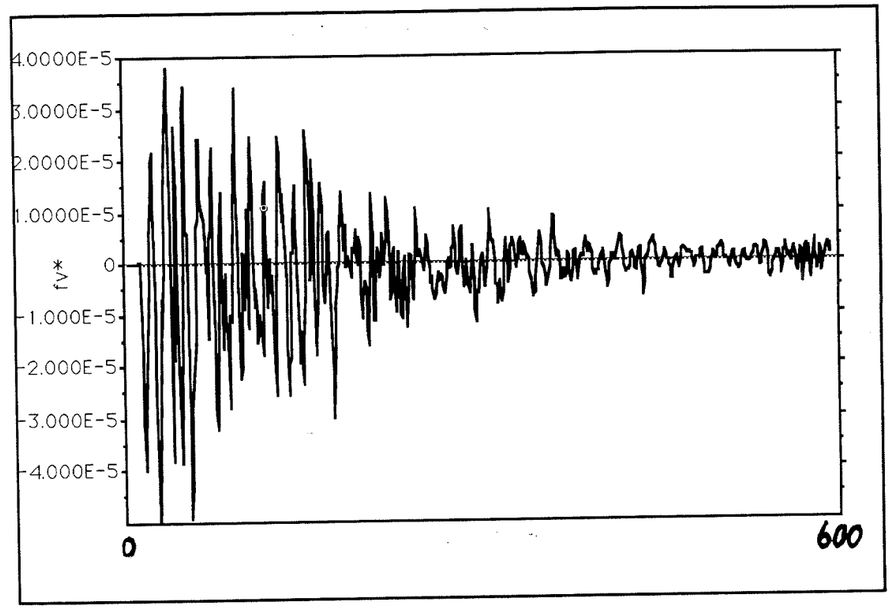

Figure 5.11: Time-evolution of fv^{*} at z=1.5 H at the jet core for α^{-1}= 50 days.

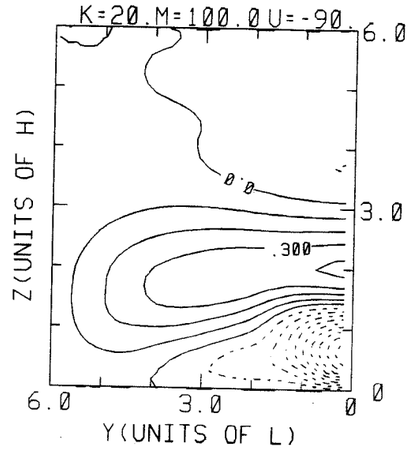

A

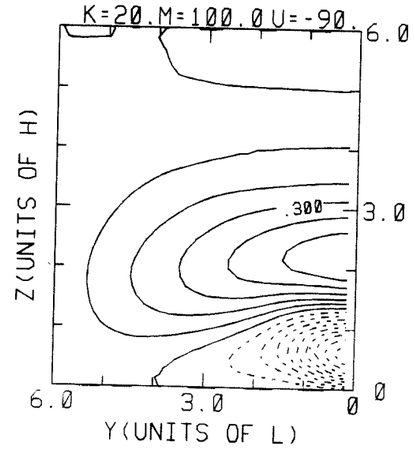

B

Figure 5.12: **A)** Cross-section of $\overline{\chi}^*$ in the y-z plane for α^{-1}= 50 days, averaged from day 400 to day 500. **B)** Same from day 400 to day 600.

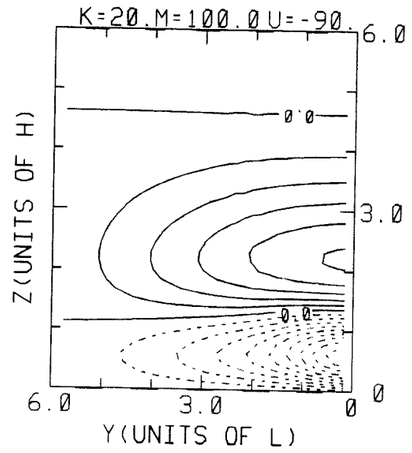

Figure 5.13: Cross-section of $\overline{\chi}^*$ in the y-z plane for α^{-1}= 20 days.

CHAPTER 6 : CONCLUSION

6.1. INTRODUCTION.

One of the major goal of this study was to explain the existence of the vertical shear layer that has been observed to cap the jets above the clouds of Jupiter. The analysis of Voyager temperature data has shown that both eastward and westward jets decay with height with nearly monotonic shear magnitudes. Our framework has been a capping layer model of the Jovian upper troposphere which relies on the hypothesis that the jets observed at the cloud-top originate in the deep atmosphere; we further suppose that they reach there a state of neutral stability. As the jets penetrate the stably stratified portion of the atmosphere, they may become barotropically unstable. Within the context of that model, the vertical shear layer arises as a natural response to the instability that ultimately stabilizes the flow.

To examine this conceptual framework requires the use of a three-dimensional model, as we are dealing with barotropic instability in presence of vertical shear. Due to the three-dimensional nature of the problem, we are forced to use a low-resolution model which represents barotropic instability in a simple way. By low-resolution model, we mean that we do not have enough meridional and zonal resolution to look at problems such as the fine structure of eddies or the nonlinear interactions of many zonal scales.

Our method has been to look at the linear modes of instability and their feedback on the mean flow.

Spectacular progress has been made in the last decade in the understanding of the emergence of coherent vortices and their coexistence with fully-developed turbulence; some of these important results have been applied to the Jovian vortices (Sommeria et al., 1989; Marcus, 1987). Our purpose has been quite different and by no mean contradictory to these studies. As barotropic instability possibly plays a role in generating the

eddies of Jupiter, even a simple linear stability analysis can give useful results about the relevant scales, namely the zonal wavenumber and the eddy meridional scale. With the hypothesis that the most untable mode feedback on the mean flow is a good, albeit rough, representation of the eddy feedback that actually brings the jet to a neutral state, the wave-mean flow problem ought to give an indication of the vertical shear structure required to stabilitize the flow.

Our approach has been to take a simple analytic jet profile with an intensity thought to be representative of a strong deep jet.

6.2. RESULTS OF THE LINEAR MODELLING.

The principal results of the linear study are that there is a regime for which jets of width that is representative of the cloud-top jets of Jupiter are indeed barotropically unstable. Moreover, one has that:

+) The relevant zonal wavenumbers are in the range 20 to 40.

+) A vertical shear such that the jets decay with height tends to stabilize the jets, and the most stable mean flows tend to have a Burger number Bu of the order of one at the most.

+) Westward jets are more unstable and eastward jets can thus penetrate to higher levels in the atmosphere while maintaining the strong zonal wind magnitude characteristic of the deep levels.

+) The eddy fluxes are such as to broaden the jets meridionally and to act as a vertical drag in the core of the jets. They drive meridional circulations with stacked cells of subsiding and rising motions. The bottom cell has rising motions on the anticyclonic shear side of the jet, consistent with the classical view of rising and sinking motions in zones and belts respectively.

+) The phase speeds of the unstable modes are about .6 of the jet maximal speed for westward jets, and .4 for the eastward jets.

6.3. RESULTS OF THE QUASI-LINEAR MODELLING.

In this model, the eddies grow until a state of equilibration is reached for which the eddy quantities have finite amplitude and the mean flow is stable. That regime is such that :

+) The eddy kinetic energy is about 20% of the mean-flow kinetic energy. Temperature fluctuations associated with these eddies have a RMS amplitude of the order of 1 K.

+) The mean flow vertical scale selection derived in the linear study, that Bu ~ 1, is preserved here provided that we take into account that the jets decay to a non-zero barotropic flow.

+) In the absence of forcing and damping, there are no permanent residual mean meridional circulations or eddy fluxes.

+) For adjacent eastward and westward jets, unstable modes associated with the westward jet can propagate meridionally into the core of eastward jet; they can generate mean vertical shears which reduce the eastward jet strength even if it is stable.

Our results compare well with the results of Pirraglia's (1989) who treated a quite similar problem with a strongly truncated nonlinear model. The vertical shearing of the mean flow proceeds similarly in his model, although we have in our model a strong barotropic component which extends into the uppermost layers; this did not appear in Pirraglia's model. This could be due to the vertically variable stratification he introduced in his model; it also depends somewhat on the jet profile. The observed Jovian jets do indeed seem to decay to smaller values than our barotropic component; in our standard experiment, we had a jet intensity (U_0) of - 90 ms^{-1} and a jet width (L) of 2000 km and, in the core of the jet, the zonal velocity decays to about -55 ms^{-1}. That value obviously depends on the jet width L; thinner jets should be more unstable and the jets should then be

characterized by a smaller value of the barotropic component. For jets with L=1000 km, one get a time-averaged zonal velocity profile shown in figure 6.1. The barotropic component is now about - 40 ms^{-1}. Note that the vertical shear layer is now thinner also; it has $L/L_D \sim 1/3$ in agreement with Bu ~ 1. This value of the barotropic component is closer to the cloud-top wind magnitudes.

6.4. THE ROLE OF FORCING AND RADIATIVE DAMPING.

The presence of damping and forcing determines the flow of energy through the eddy/mean-flow system, i.e. when the above-mentioned instabilities are active. The presence of radiative damping acting on the eddies and a Rayleigh forcing of the mean flow toward the barotropic state with a time scale α^{-1} have been included in the model. The conclusions are the following :

+) For $t_R/2 < \alpha^{-1} < t_R$, one finds an asymmetric life-cycle behavior with abrupts changes from short periods of eddy growth to long periods of eddy decay. The eddy fluxes and residual circulations accordingly adjust to the periods of growth and decay.

+) The steady-state is reached for $\alpha^{-1} \sim t_R/2$ (for $\alpha^{-1} < t_R/2$, one has a growing eddy). One founds in this case a steady pattern of eddy flux which balances the eddy against radiative damping. A weak residual mean meridional circulation is present, but there is an explicit contribution of the ad hoc forcing term.

6.5. FUTURE DIRECTIONS.

Future work could proceed along several directions :

+) Owing to the resemblance of the atmospheres of Saturn and Jupiter, one could try to draw parallel results for the corresponding conditions of Saturn.

+) The effect of a height-dependent static stability parameter, and vertical changes in the forcing/damping time scales could be investigated. The presence of a strongly stratified upper layer (i.e. a stratosphere) might modify the mean flow profile. The time-averaged Eliassen-Palm flux divergence, F, that appears in the case of strongly forced case, has a vertical structure that is going to depend on height variations in the forcing time scale and consequently, the residual mean meridional circulations are going to be altered.

+) Modelling ought to be carried out with more sophisticated models. The generation of eddies and vortices by a barotropically unstable forced jet should be performed for a comparison with the Jovian atmosphere, where we know that turbulent motions coexist with strong near-steady jets. The three-dimensional nature of the problem treated here might however render this task quite formidable from the computational point of view.

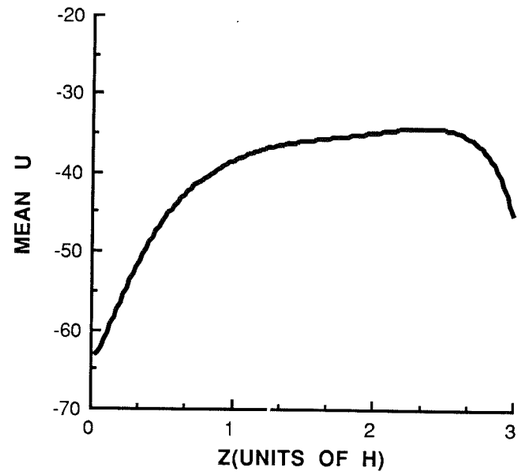

Figure 6.1: Vertical profile of the time-averaged zonal mean flow at the jet core for L=1000 km.

BIBLIOGRAPHY

Achterberg R. K. and Ingersoll A. P., 1989: A normal-mode approach to Jovian atmospheric dynamics. *J. Atmos. Sci.*, **46**, 2448-2462.

Allison M. D. and P.J. Gierasch, 1982: Jovian atmospheric dynamics: shear stability control of diabatically forced, weakly stratified zonal flow (abstract), *Bull Am. Astron. Soc.*, **14**, 722.

Andrews D. G., J. R. Holton and C. B. Leovy, 1987: Middle atmosphere dynamics. Academic Press, New York.

Atreya S.K. and P.N. Romani, 1985: Photochemistry and clouds of Jupiter, Saturn and Uranus. in *Recent advances in planetary meteorology* (G. E. Hunt, Ed.), Cambridge Univ. Press.

Barnes J.R., 1986: Finite-amplitude behavior of a single baroclinic wave with multiple vertical modes: effects of thermal damping, *J. Atmos. Sci.*, **43**, 58-71.

—— and J.L.Hollingsworth, 1987: Dynamical modeling of a planetary wave mechanism for a martian polar warming, *Icarus*, **71,** 313-334.

Bjoraker G. L. et al., 1986: The abundance and distribution of water vapor in Jupiter's atmosphere. *Ap. J.*, **311**, 1058-1072.

Busse, F. H., 1976: A simple model of convection in the Jovian atmosphere. *Icarus*, **29**, 255-260.

——, 1983: Convection-Driven zonal flows in the major planets. *PAGEOPH*, **121**, 375-390.

——, and L. L. Hood, 1982: Differential rotation driven by convection in a rapidly rotating anulus. *Geophys. Astrophys. Fluid Dyn.*, **21**, 59-74.

Caldwell J.R. et al, 1979: Temporal characteristics of the Jovian atmosphere, *Ap. J.*, 234: L155-158.

Charney J. G. and J. Pedlosky, 1963: On the trapping of unstable planetary wave in the atmosphere. *J. Geophys. Res.*, **68**, 6441-6442.

Comte P. et al., 1987: Simulation numérique d'un jet plan turbulent. *C. R. Acad. Sci. Paris*, **305**, Serie II, 1037-1044.

Conrath B. J., 1986: Parahydrogen equilibration in the atmosphere of the outer planets. Conference on the Jovian atmospheres, M. Allison and L.D. Travis, Eds., NASA Conference Publication 2441.

——, and P. J. Gierasch,1984: Global variation of the parahydrogen fraction in Jupiter's atmosphere and implications for dynamics on the outer planets. *Icarus*, **57**, 184-204.

—— and J. A. Pirraglia, 1983: Thermal structure of Saturn from Voyager infrared measurements : implications for atmospheric dynamics. *Icarus*, **53**, 286-292.

—— et al., 1981: Stability of zonal flows on Jupiter. *Icarus*, **48**, 256-282.

—— et al., 1990: Temperature and circulations in the stratosphere of the outer planets, *Icarus*, **83**, 255-281.

de Pater I., 1986: Jupiter's zone-belt structure at radio wavelengths. 2. Comparison of observations with model atmosphere calculations. *Icarus*, **68**, 344-365.

Dickinson R. E., 1973: Baroclinic instability of an unbounded zonal shear flow in a compressible atmosphere. *J. Atmos. Sci.*, **30**, 1520-1527.

Drazin P.G. and L. N. Howard,1966: Hydrodynamic stability of parallel flow of inviscid fluid. Advances in Applied Mechanics, **9**, 1-89.

Drossart P. et al., 1987: Variations in the Jovian atmospheric composition and chemistry. In *Time-variable phenomena in the Jovian system*. NASA SP-494.

Encrenaz T., 1990: Remote sensing of the atmospheres of Jupiter, Saturn and Titan, *Rep. Prog. Phys.*, **53**, 793-836.

Eshleman V.R. et al, 1979: Radio Science with Voyager 1 at Jupiter : preliminary profiles of the atmosphere and ionosphere, *Science*, **204**, 976-978.

Farrell B.F., 1982: Modal and non-modal baroclinic waves, *J. Atmos.Sci.*, **41**, 668-673.

Fegley B. and R. G. Prinn, 1987: Chemical constraints on the water and total oxygen abundances in the deep atmosphere of Jupiter. *Ap. J.*, **324**, 621-625.

Flasar F. M., 1986: Global dynamics and thermal structure of Jupiter's atmosphere. *Icarus*, **65**, 280-303.

——, 1987: Temporal behavior of Jupiter's meteorology. In *Time-variable phenomena in the Jovian system*. NASA SP-494.

—— and P.J.Gierasch, 1986: Mesoscale waves as a probe of Jupiter's deep atmosphere, *J. Atmos. Sci.*, **43**, 2683-2707.

—— et al., 1987: Voyager infrared observations of Uranus' atmosphere : thermal structure and dynamics, *J. Geophys. Res.*, **92**,15011-15018.

Gautier D. and T. Owen, 1989: The composition of outer planet atmospheres. In *Origin and evolution of planetary and satellite atmospheres* (Atreya S.K. et al, Eds.). University of Arizona press, Tuscon.

Geisler J.E and R. G. Garcia, 1976: Baroclinic instability at long wavelengths on a β-plane simulation of barotropic instability. *J. Atmos. Sci.*, **34**, 311-321.

Gierasch P. J. et al., 1979: Baroclinic instabilities in Jupiter's zonal flow. *Icarus*, **40**, 205-212.

—— et al., 1986: Zonal mean properties of Jupiter's upper troposphere from Voyager infrared observations. *Icarus*, **67**, 456-483.

Glatzmaier G. A., and P. A. Gilman, 1981: Possible convection in a rotating spherical shell. Solar Phenomena in Stars and Stellar Systems, R. M. Bonnet and A. K. Dupree, Eds., Reidel Publishing Company.

Haltiner G. J. and Williams R. T., 1980: Numerical prediction and dynamical meteorology. 2nd edition. John Wiley & Sons Publishers.

Hanel R. et al., 1979a: Infrared observations of the jovian system from Voyager 1. *Science*, **204**, 972-976.

Hanel R. et al., 1979b: Infrared observations of the Jovian system from Voyager 2. *Science*, **206**, 952-956.

Hart J. E. et al., 1986: Space-laboratory and numerical simulations of thermal convection in a rotating hemispherical shell with radial gravity.*J. Fluid Mech.*, **173**, 519-544.

Hatzes A. et al., 1981: Oscillations and velocity structure of a long-lived cyclonic spot. *J. Geophys. Res.*, **86**,8745-8749.

Hess, S. L. and H. A. Panofsky, 1951: The atmospheres of the outer planets. Compendium of Meteorology, 391-400. American Meteorological Society, Boston.

Holton, J. R., 1974: On the trapping of unstable baroclinic waves. *J. Atmos. Sci.*, **31**, 2220-2222.

——, 1982: The role of gravity wave induced drag and diffusion in the momentum budget of the mesosphere, *J. Atmos. Sci.*, **39**, 791-799.

——, 1986: Meridional distribution of stratospheric trace constituents, *J. Atmos. Sci.*, **43**, 1238-1242.

—— and C. Mass, 1976: Stratospheric vacillation cycles, *J. Atmos. Sci.*, **33**, 2218-2225.

Hunten D. M. et al., 1986: Atmospheric science on the Galileo mission. *Space Science Reviews*, **44**, 191-240.

Ingersoll, A. P. and J.N. Cuzzi, 1969: Dynamics of Jupiter's cloud bands. *J. Atmos. Sci.*, **26**, 981-985.

—— and D. Miller, 1986: Motion in the interiors and atmospheres of Jupiter and Saturn: 2. Barotropic instabilities and normal modes of an adiabatic planet. *Icarus*,**65**, 370-382.

—— and D. Pollard, 1982: Motion in the interiors and atmospheres of Jupiter and Saturn: Scale analysis, anelastic equations, barotropic stability criterion. *Icarus*,**52**, 62-80.

—— et al., 1979: Zonal velocity and texture in the jovian atmosphere inferred from Voyager images. *Nature*, **280**, 773-775.

—— et al., 1981: Interaction of eddies and mean zonal flow on Jupiter as inferred from Voyager 1 and 2 images. *J. Geophys. Res.*,**86**, 8733-8743.

—— et al., 1984: Structure and dynamics of Saturn's atmosphere. In *Saturn*, (T. Gerhels and M. S. Matthews, Eds.), 197-205. Univ. of Arizona Press, Tucson.

James I. N. and B. J. Hoskins, 1985: Some comparisons of atmospheric internal and boundary baroclinic instability. *J. Atmos. Sci.*, **42**, 2142-2155.

Kuo K. L. ,1973: Dynamics of quasi-geostrophic flows and instability theory. Advances in Applied Mechanics, **13**, 247-330.

Lellouch E. et al., 1989: A new analysis of the Jovian 5-um Voyager/IRIS spectra. *Icarus*, **77**,457-465.

Leovy C. B., 1964: Simple models of thermally driven mesospheric circulations. *J. Atmos. Sci.*, **21**, 327-341.

——, 1986: Eddy processes in the general circulation of the Jovian atmospheres. Conference on the Jovian atmospheres, M. Allison and L.D. Travis, Eds., NASA Conference Publication 2441.

Lewis J. S., 1969: The clouds of Jupiter and the NH_3-H_2O and NH_3-H_2S system. *Icarus*, **10**, 365-378

Liebacher and Stein, 1981: Wave generation. In *The Sun as a star.* (S. Jordan, Ed.). NASA SP-450.

Limaye S. S., 1986: Jupiter: new estimates of the mean zonal flow at the cloud level. *Icarus*, **65**,335-352.

—— , 1987: Jupiter: short-term variations of the mean zonal flow at the cloud level. In *Time-variable phenomena in the Jovian system*. NASA SP-494.

Lindal G. F. et al, 1981: The atmosphere of Jupiter: an analysis of Voyager radio occultation measurements. *J. Geophys. Res.*, **86**, 8721-8727.

Lindzen R. S., 1981: Turbulence and stress due to gravity wave and tidal breakdown. *J. Geophys. Res.*, **86**, 9707-9714.

Lindzen R. S. and K.L. Kuo, 1969: A reliable method for the numerical integration of a large class of ordinary and partial differential equations, *Mon. Wea. Rev.*, **96**, 732-734.

Lipps F., 1962: The barotropic stability of the mean winds of the atmosphere. *J. of Fluid Mech.*, **12**,397-407.

Lunine J. I. and Hunten D. M., 1987: Moist convection and the abundance of water in the troposphere of Jupiter. *Icarus*, **69**, 566-570.

Marcus P.S., 1988: Numerical simulation of Jupiter's great red spot, *Nature*, **331**, 693-696.

Massie S. T. and D. M. Hunten, 1982: Conversion of para and ortho hydrogen in the Jovian planets. *Icarus*, **49**, 213-226.

Matsuno T., 1970: Vertical propagation of stationary planetary waves in winter northern hemisphere, *J. Atmos. Sci.,* **27,** 871-883.

McWilliams J. C., 1989: Statistical properties of decaying geostrophic turbulence. *J. Fluid Mech.*, **198**, 199-230.

Mitchell J. L., 1982: The nature of large-scale turbulence in the Jovian atmosphere. JPL Publication 82-34.

Nielsen J.E. and M.R. Schoeberl, 1984: A numerical simulation of barotropic instability. Part II: Wave-wave interaction, *J. Atmos. Sci.*, **41**, 2869-2881.

Orsolini, Y. and C.B. Leovy, 1989a: Large-scale instabilities in a model of the Jovian troposphere. (abstract), XIVth EGS General Assembly. *Annales Geophysicae*,Special Issue, 271.

Orsolini, Y. and C.B. Leovy, 1989b, Linear eddies of a Jovian atmosphere forced by deep jets. *Geophys. Res. Letters.* **16.**, 1245-48.

Owen T. and Terrile, 1981:Colors on Jupiter. *J. Geophys. Res.*, **86**, 8797-8814.

Peek B. M., 1958: The planet Jupiter. Faber, London, 1958.

Pfister L., 1979: A theoretical study of three dimensional barotropic instability with applications to the upper stratosphere. *J. Atmos. Sci.*, **36**, 908-920.

Pirraglia J. A., 1989: Dissipationless decay of Jovian jets. *Icarus*, **79**, 196-207.

—— et al., 1981: Thermal structure and dynamics of Saturn and Jupiter. *Nature*, **292**, 677-679.

Read P. L., 1988: On the scale of baroclinic instability in deep compressible atmospheres. *Quart. J. R. Met. Soc.*, **114**, 421-437.

Sanchez-La Vega A., 1987: Great Scale changes in the belts and zones of Jupiter : the outbursts of activity and disturbances in the SEB and NTrZ-NTBs regions. In *Time-variable phenomena in the Jovian system*. NASA SP-494.

Schoeberl M. R. and R.S. Lindzen, 1984: A numerical simulation of barotropic instability. Part I: Wave-mean flow interaction, *J. Atmos. Sci.*, **41**, 1368-1379.

Sommeria J. et al., 1989: Experiments on vortices and Rossby waves in eastward and westward jets. In *Nonlinear Topics in Ocean Physics*. (Osborne A., ed.), North-Holland, Amsterdam.

Sromosky L. A. et al., 1982: Jovian winds from Voyager 2. Part II: Analysis of eddy transports. *J. Atmos. Sci.*, **39**, 1433-1445.

Sromovsky L. A. et al., 1985: Cloud-top meridional momentum transports on Saturn and Jupiter.Conference on the Jovian atmospheres, M. Allison and L.D. Travis, Eds., NASA Conference Publication.

Weidenschilling S. J. and J.S. Lewis, 1973: Atmosphere and cloud structures of the Jovian planets, *Icarus*, **20**, 465-476.

West R. et al., 1986: Clouds, aerosols and photochemistry in the Jovian atmosphere. *Icarus*, **65**, 161-217.

Williams G. P., 1978: Planetary circulations : 1. Barotropic representation of Jovian and Terrestrial turbulence. *J. Atmos. Sci.*, **35**, 1399-1426.

——, 1979: Planetary circulations : 2. The Jovian quasi-geostrophic regime. *J. Atmos. Sci.*, **36**, 932-968.

APPENDIX A : FINITE DIFFERENCE FORMULATION

In the absence of radiative damping, the equation for the wave ψ is written as

$$(\partial_t + ik\,\overline{u})\ \mathbf{L}_k(\psi) + ik\,\overline{q}_y\,\psi = 0$$

where

$$\mathbf{L}_k = (-k^2 + \partial_{yy}) + \varepsilon\,(\partial_{zz} - 1/4H^2).$$

If we write $\varphi = \partial_t\,\psi$, then the following equation needs to be inverted :

$$\mathbf{L}_k(\varphi) = -ik\ [\,\overline{u}\,\mathbf{L}_k(\psi) + \overline{q}_y\,\psi]$$

Using second-order differencing, the wave operator $\mathbf{L}_k$ acting on φ can be written in finite difference form as

$$\mathbf{L}_k\,\varphi_{i,j} = W^1\,\varphi_{i,j+1} + W^2\,\varphi_{i,j-1} + W^3\,\varphi_{i,j} + W^4\,\varphi_{i+1,j} + W^5\,\varphi_{i-1,j} \qquad (1)$$

where

$$W^1 = 1./\Delta y^2$$
$$W^2 = 1./\Delta y^2$$
$$W^3 = -k^2 - 2/\Delta y^2 - 2\varepsilon/\Delta z^2 - \varepsilon/4H^2$$
$$W^4 = \varepsilon/\Delta z^2$$
$$W^5 = \varepsilon/\Delta z^2$$

and $\varphi_{i,j}$ represents any interior point. We may write the RHS of (1) in a matrix form

APPENDIX A : FINITE DIFFERENCE FORMULATION

In the absence of radiative damping, the equation for the wave ψ is written as

$$(\partial_t + ik\,\overline{u})\ \mathbf{L}_k(\psi) + ik\overline{q}_y\,\psi = 0$$

where

$$\mathbf{L}_k = (-k^2 + \partial_{yy}) + \varepsilon\,(\partial_{zz} - 1/4H^2).$$

If we write $\varphi = \partial_t\,\psi$, then the following equation needs to be inverted :

$$\mathbf{L}_k(\varphi) = -ik\ [\,\overline{u}\,\mathbf{L}_k(\psi) + \overline{q}_y\,\psi]$$

Using second-order differencing, the wave operator $\mathbf{L}_k$ acting on φ can be written in finite difference form as

$$\mathbf{L}_k\,\varphi_{i,j} = W^1\,\varphi_{i,j+1} + W^2\,\varphi_{i,j-1} + W^3\,\varphi_{i,j} + W^4\,\varphi_{i+1,j} + W^5\,\varphi_{i-1,j} \qquad (1)$$

where

$$W^1 = 1./\Delta y^2$$
$$W^2 = 1./\Delta y^2$$
$$W^3 = -k^2 - 2/\Delta y^2 - 2\varepsilon/\Delta z^2 - \varepsilon/4H^2$$
$$W^4 = \varepsilon/\Delta z^2$$
$$W^5 = \varepsilon/\Delta z^2$$

and $\varphi_{i,j}$ represents any interior point. We may write the RHS of (1) in a matrix form

$$A_i F_i + B_i F_{i+1} + C_i F_{i-1}$$

where F_i are vectors formed with the components $\varphi_{i,j}$ (j = 1,...J) and the 3 sets of matrices A_i, B_i, C_i (i = 0,...I) have non-zero elements

$$[A_i]_{j,j} = W^3 \qquad [A_i]_{j,j+1} = W^1 \qquad [A_i]_{j,j-1} = W^2$$
$$[B_i]_{j,j} = W^4 \qquad [C_i]_{j,j} = W^5 .$$

The matrices A_i, B_i, C_i are (JxJ) matrices. Including the source term, the wave equation in finite difference form is cast in (I+1) matrix relations

$$A_i F_i + B_i F_{i+1} + C_i F_{i-1} = D_i$$

with D_i a J-dimensional vector. Following the algorithm of Lindzen and Kuo (1969), solutions are sought of the form

$$F_i = \alpha_i F_{i+1} + \beta_i . \qquad (2)$$

We then get recursion relations

$$\alpha_i = - (C_i \alpha_{i-1} + A_i)^{-1} B_i$$
$$\beta_i = (C_i \alpha_{i-1} + A_i)^{-1} (D_i - C_i \beta_{i-1}). \qquad (3)$$

These recursion relations must be initialized using a lower boundary condition. At the lower boundary, we have $F_0 = 0$; comparing with (2) for i = 0, we get

$$\alpha_0 = 0$$
$$\beta_0 = 0$$

The top boundary condition at i=I is also of the form $F_I = 0$. Combining the finite difference form of this equation with the recursion relation between

φ_I and φ_{I-1}, we get

$$F_I = 0$$
$$F_{I-1} = \beta_{I-1}$$

At each time-step, one computes first α_i,β_i from i=0 to I-1 using the recursion relation (3). Then F_I is computed and the recursion relation (2) applied backward from i = I to i = 0. The matrices α_i are time-independent,but the vectors β_i include the time-dependent factors through D_i, the source term of the wave equation.

For interior points, the jth component of D_i is written

$$[D_i]_j = - ik\overline{u}_{i,j} [W^1 \varphi_{i,j+1} + W^2 \varphi_{i,j-1} + W^3 \varphi_{i,j} + W^4 \varphi_{i+1,j} + W^5 \varphi_{i-1,j}]$$

$$- ik\varphi_{i,j} [\beta a - (\overline{u}_{i,j+1} - 2\overline{u}_{i,j} + \overline{u}_{i,j-1})/\Delta y^2 + (\overline{u}_{i,j+1} - \overline{u}_{i,j-1})/2\Delta y + 2\,\overline{u}_{i,j}$$

$$+ f\,\{(\overline{u}_{i+1,j} - 2\,\overline{u}_{i,j} + \overline{u}_{i-1,j})/N^2\Delta y^2 + (\overline{u}_{i+1,j} - \overline{u}_{i-1,j})/2\Delta z$$

$$(1./HN^2)\}].$$

In the presence of radiative damping, one has

$$(\partial_t + ik\,\overline{u})\ \mathbf{L}_k(\psi) + ik\overline{q}_y\,\psi = D$$

with the height-dependent radiative damping operator written as

$$D(\psi) = \varepsilon\,[\,\alpha\,\psi_{zz} + \alpha_z\,(\psi_z + \psi/2H) - \alpha\psi/4H^2\,].$$

The damping operator is treated semi-implicitely as usual; let us write

$$\varphi = (\psi^+ - \psi^-)\,/\,2\Delta t$$

where ψ^+ denotes ψ at the next time step and ψ^- denotes ψ at the previous time step. One needs to invert the operator equation

$$\mathbf{L}_k^{damp}(\varphi) = -ik\,[\,\overline{u}\,\mathbf{L}_k^{damp}(\psi) + \overline{q}_y\,\psi] - D(\psi^-)$$

The procedure is exactly identical to the undamped case provided that one modifies some W factors according to :

$$W^3 = -k^2 - 2/\Delta y^2 - \varepsilon\,(2/\Delta z^2 + 1./4H^2) + \varepsilon\,\Delta t\,(\alpha_z/2H - \alpha/4H^2 - 2\alpha/\Delta z^2)$$

$$W^4 = \varepsilon/\Delta z^2 + \varepsilon\,\Delta t\,(\alpha_z/2\Delta z + \alpha/\Delta z^2)$$

$$W^5 = \varepsilon/\Delta z^2 - \varepsilon\,\Delta t\,(\alpha_z/2\Delta z - \alpha/\Delta z^2).$$

The time scheme is a leapfrog scheme with a periodic use of a restart mode to damp the computational mode; usually the time step is 3600 sec. and the restart procedure is applied every 24-hours.

In the wave-mean flow problem, on has to also solve for the residual mean circulation. It obeys the following equation :

$$\mathbf{L}'\,[\chi^*] = S_0.$$

where the operator $\mathbf{L}'$ is defined as

$$\mathbf{L}' = \partial_{yy} + \varepsilon\,\rho_0\,\partial_z\,(\rho_0^{-1}\,\partial_z);$$

With the W factors appropriately chosen, we solve that equation in the same manner as the equation for the wave potential vorticity. We need to take the following W' :

$$W'^1 = W^1$$

$$W'^2 = W^2$$

$$W'^3 = k^2 + \varepsilon/4H^2 + W^3$$

$$W'^4 = W^4 + \varepsilon / 2H\Delta z$$

$$W'^5 = W^5 - \varepsilon / 2H\Delta z.$$

The boundary conditions are introduced appropriately. Once χ^* has been computed at each time-step, the derived residual velocities are used to compute the change in the zonal mean momentum :

$$\overline{u}_t = F + f\overline{v}^* - \alpha (\overline{u} - \overline{u}_0). \qquad (4)$$

We use a semi-implicit treatment of the right-hand side; the zonal mean velocity is updated according to :

$$\overline{u}+ = \overline{u} \; [(2 + \alpha \Delta t) / (2 - \alpha \Delta t)] + S^* [2 \; \Delta t / (2 - \alpha \Delta t)]$$

where $\overline{u}+$ is the zonal mean velocity at time $t+\Delta t$. S^* denotes the sum of all the terms in the right-hand side of (4) which are independent of $\overline{u}$ and the "*" indicates that this term is evaluated semi-implicitely.

The meridional resolution was chosen so that the growth rate become nearly independent of the horizontal grid spacing. In most cases, 31 points were used spanning 6 jet widths (6L). Figure A.1a compares the time-evolution of the wave energy for different grid spacings during the initial regime of exponential growth. The curves are nearly parallel, and the growth rate, computed between day 5 and day 6, is .542 $\pm$ .001 per day for the three curves. After about 10 days, one enters the equilibration regime, and one can see in figure A.1b that the wave equilibrates at a kinetic energy level of 20% of the mean kinetic energy in the three cases. The number of

grid points in the meridional direction largely determines the computational burden, so we determined that taking 31 points was representing the barotropic instability accurately enough for this problem.

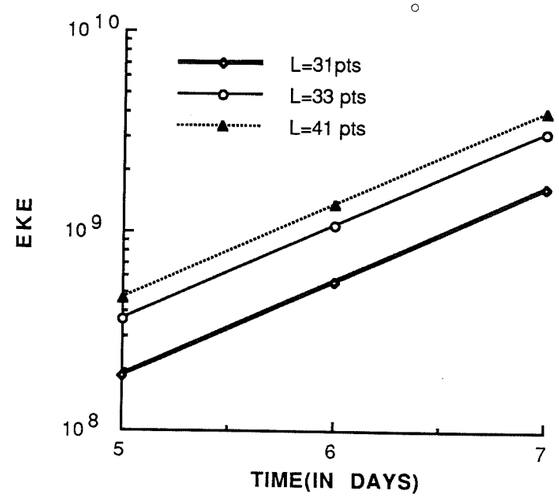

A

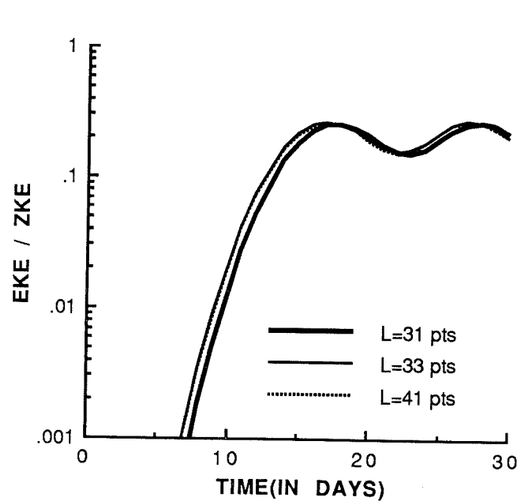

B

Figure A.1: **A)** Eddy kinetic energy (EKE) as a function of time for various meridional resolutions in the exponential growth regime. **B)** Ratio of eddy kinetic energy (EKE) to zonal mean kinetic energy (ZKE) as a function of time.

APPENDIX B : THE BOTTOM BOUNDARY CONDITION

The appropriate bottom boundary condition for quasi-geostrophic motions in a stable shallow layer bounded at its bottom by a deep adiabatic layer has been established by several authors (Gierasch et al., 1979; Conrath et al., 1981; Achterberg and Ingersoll, 1989). We will here closely follow the derivation of Achterberg and Ingersoll.

Consider a shallow quasi-geostrophic layer bounded at its bottom by a deep adiabatic layer in which the motions are also geostrophic.

In each layer, the usual quasi-geostrophic equations are :

$$D_t (\Delta_H \psi + f) - f \mathbf{L}_z(w) = 0 \quad (1)$$
$$D_t (\psi_z) + (f L_D^2 / H^2) w = 0 \quad (2)$$

where $\mathbf{L}_z = \rho^{-1} \partial_z(\rho)$, Δ_H the horizontal laplacian, D_t the material derivative, ψ the geostrophic streamfunction,w the vertical velocity, H the scale height and L_D the Rossby radius of deformation, NH/f. The density decreases exponentially as : $\rho = \rho_0 \exp\{-z/H\}$.

In the interior layer, extending from z_0 to z_1 , we linearize around a state of no motions on the β-plane; we suppose that the geostrophic streamfunction behaves as

$$\psi(x,y,z,t) = \Psi(z) \, e^{i(kx+ly)} \, e^{ikct} ,$$

where k is the zonal wavenumber, l the meridional wavenumber and c the phase speed. As the lower layer is adiabatic, we let N go to zero; equation (2) becomes

$$ikc \, \Psi_z = 0,$$

so that Ψ is independent of z. With that simplification, (1) becomes

$$ikc\,(k^2+l^2)\,\lambda\,\Psi - f\,\mathbf{L}_z(w) = 0 \qquad (3)$$

where we define the nondimensional number λ as

$$\lambda = -\,1 + \beta/(k^2+l^2)\,c$$

We then integrate (3) from the bottom z_0 to the top z_1 using the condition that the vertical velocity be zero at the bottom. With $D = z_1 - z_0$ being the depth of the bottom layer, we have that

$$w_1 = i\,(kc/f)\,(k^2+l^2)\,\lambda\,\Psi\,H\,(e^{D/H} - 1) \qquad (4).$$

This formula gives an expression for the vertical velocity at $z=z_1$.

In the upper layer, equation (2) gives

$$ikc\,\Psi_z + (f\,L_D^2/H^2)\,w = 0 \qquad (5)$$

Applying the continuity of vertical velocity at $z=z_1$, i.e. comparing (5) at $z=z_1$ and (4), we have

$$\Psi_z + \{L_D^2\,(k^2+l^2)\,\lambda\,H^{-1}\,(e^{D/H} - 1)\}\,\Psi = 0, \qquad (6)$$

where ψ and ψ_z have to be evaluated at $z=z_1$. The quantity $(e^{D/H} - 1)$ is a very large number, the bottom layer being very deep. Let us suppose that $L_D^2\,(k^2+l^2)\,\lambda\,H^{-1}$ is not too small; then (6) is a relation of the sort of

$$\Psi_z + (\Psi/\varepsilon) = 0 \qquad (7)$$

where ε is a small number. It imposes the condition that the only physically acceptable solution has ψ of order ε, and ψ_z of order 1. Equation (7) then requires that ψ be very small at $z=z_1$ at the lowest (zero) order in ε.

This result holds provided that

$$L_D^2 \ (k^2+l^2) \ \lambda H^{-1}$$

is not too small; this number has the dimension of m^{-1}. Note that λ is related to eigenvalues of the vertical structure equation. In the upper layer, the quasi-geostrophic equations lead to a vertical structure equation for an eigenmode $\Psi(z)$:

$$\mathbf{L}_z (\Psi_z) + \Lambda^2 \ \Psi = 0 \qquad (8)$$

One has $\Lambda^2 = [\lambda (k^2+l^2) L_D^2 / H^2]$; Λ also has the dimension of m^{-1}. One has then to show that for all modes, $H\Lambda^2$ is not too small. For a shallow incompressible upper layer where the static stability is constant, one has eigenvalues of (8)

$$\Lambda_n = n\pi / d \qquad (9),$$

where d is the depth of the upper layer. For the barotropic mode, n is zero and Ψ is independent of height ; for the baroclinic modes for which Λ_n is given by (9), equation (7) is then valid provided that

$$H\Lambda_n^2 = H (n\pi / d)^2$$

is not too small. Recall that d of the order of a few scale heights; $H\Lambda_n^2$ is minimum for the lowest baroclinic mode (n=1) and will be higher for higher baroclinic modes. That minimum value is about H^{-1} ; the factor $e^{D/H}$ is sufficiently large to ensure that equation (7) applies. The more oscillations the vertical structure has in the upper layer, the better this condition will be obeyed.

The conclusion is that Ψ is near-zero for the baroclinic modes. The barotropic mode has a constant Ψ throughout the two layers. The only motions which can extend at great depths are the barotropic motions.

Physically, the law of conservation of vorticity expressed in (1) requires that vertical stretching of the entire fluid column balances the local variation of vorticity; this would create unacceptably large vertical velocity at the interface if baroclinic motions would extend to great depths.

APPENDIX C : ON THE POSSIBLE ROLE OF GRAVITY WAVES

Drag and diffusion terms have been used in the mean momentum equation as a parametrization of macroscopic fluid mechanical processes decelerating or accelerating the zonal mean flow. A simple linear drag term (Rayleigh friction) has long ago been used in modelling the effects of wave drag in the mesosphere (Leovy, 1964); recently, more sophisticated parametrizations have been used to model the effect of breaking gravity waves (Lindzen, 1981; Holton, 1982).

Gravity waves are suspected to provide a crucial wave drag in the terrestrial middle atmosphere. Upward propagating gravity waves, produced in the troposphere, have growing amplitude because of the density stratification of the atmosphere. At some point, the temperature perturbation produced by the wave may become large enough to produce a superadiabatic lapse rate; waves then become unstable and are said to break. Under the saturation hypothesis formulated by Lindzen (1981), they produce the right amount of turbulent diffusion to keep a constant amplitude above that breaking level, thereby exerting a drag on the mean flow.

In a general manner, whatever the damping mechanism is (breaking, radiative damping,...), gravity waves tend to drive the mean flow to their phase speeds wherever they dissipate.

On Jupiter, gravity waves are most certainly generated by penetrative convection at the base of the stable layer. Understanding how penetrative turbulent convection will generate waves is a formidable problem; this 3-D turbulence will be strongly affected by the stratification, and its is a complex task to determine how energy will be converted the form of 2-D turbulent motions, vortices or emitted in gravity waves. Numerical simulations of these complex fluid dynamical motions are far beyond our scope. Nevertheless, crude estimates of wave fluxes generated by turbulence have

been useful in situations where the coupling between turbulent motions and waves is weak, i.e. when the typical wave velocity amplitude is much smaller than the convective velocity. This is sometimes the case in the coupling of turbulent motions with acoustic waves; the turbulence can then be treated as an external forcing (this is often called the Lighthill mechanism), and the power radiated in forms of acoustic waves can then be estimated (Liebacher and Stein, 1981). This result has been extensively used in solar physics to estimate the amount of acoustic waves generated at the top of the convective layer of the Sun. In the case of gravity waves, this result is not believed to apply as the wave velocities are of the order of the convective velocities.

In what follows, we proceed by making a crude estimation of the possible gravity wave amplitudes; some guesses on what kind of waves will be emitted can lead to an estimate for the breaking levels and drags.

To estimate a typical convective velocity at the base of the stable layer of Jupiter, one usely relies on a mixing length hypothesis; the convective heat flux F_I is then related to a convective velocity u_{conv} by :

$$F_I = \rho C_p u_{conv} \; bl$$

where C_p is the heat capacity by unit mass, l is a mixing length and b is the deviation of the temperature vertical gradient from its adiabatic value. Converting the work of the buoyancy force, gbl/T, into kinetic energy with efficiency one :

$$\rho \, u_{conv}^2 / 2 \; = \rho \, bgl^2 / 2T,$$

gives a convective velocity

$$u_{conv} = l \, (gb/T)^{1/2}.$$

Alternatively, u_{conv} can be expressed in terms of F_I :

$$u_{conv} = F_I / \rho C_p bl = (glF_I/ \rho C_p T)^{1/3}.$$

With the following values chosen for Jupiter : g = 24.4 ms^{-2}, F_I = 5.44 W m^{-2}, l = H, C_p = 1.3 10^4 J K^{-1} kg^{-1}, and $\rho T=p/R= 10^2/3.71$, one has an upper bound for the convective velocity

$$u_{conv} \sim 2\ ms^{-1}.$$

This corresponds to a convective time scale, l/u_{conv}, of 10^4 s, and to b = 67 10^{-9} Km^{-1}. Also one can see that the departure from an adiabatic temperature gradient required is quite small : $bC_p/g \sim 3.5\ 10^{-5}$.

Asking if breaking might be a relevant mechanism, we estimate the height at which such wave may break and exert a drag on the mean flow. According to the model of Holton (1982) the breaking level z_B is given by

$$\frac{z_B}{H} = 3 \ln \frac{| \overline{u}-c |}{\left[\frac{BN}{k | \overline{u}_0-c |^{1/2}} \right]^{2/3}}$$

and the drag F_B above the breaking level by

$$F_B = - (k/2N) (\overline{u}-c)^3 \{ 1/H - 3 \overline{u}_z/(\overline{u}-c) \}.$$

In these formulae, B is the gravity wave velocity amplitude, $\overline{u}_0$ is the mean flow velocity at the level of emission, c the wave phase speed and the other symbols have their usual meaning. As a value for static stability at the 1-bar level, we choose N=.001 according to Conrath and Gierasch (1984). This value is much smaller than the value chosen for our numerical models, where a typical value for the upper troposphere (N=.013) was chosen. The wind profile was of the kind obtained in our nonlinear equilibration experiments. We suppose that the wave phase speed is very close to $\overline{u}_0$ and further use $k=H^{-1}$. The breaking level then only depends on the wave amplitude B. We have taken B = 2 ms^{-1}, 1 ms^{-1}, .5 ms^{-1} and solved for the breaking level; for B = 2 ms^{-1}, the equation for F_B has no solutions, indicating that the wave "has broken" below the level of

emission, i.e. that the wave amplitude is too large. The estimate of u_{conv} was an upper bound anyway. We computed that a wave with an amplitude of 1 ms^{-1} will break at about 1 H; obviously, it will break at higher levels if the amplitude is smaller. Breaking levels are then likely in the portion of the upper troposphere we are modelling (1 to 4 H) if we believe that the wave velocities are as large as 1 ms^{-1}.

To get an estimate of the magnitude of the drag, we first notice that the first term in the expression for F_B is by far the largest; we then get

$$| F_B | \sim (k / 2NH^2) | \overline{u} - \overline{u}_0 |^3 .$$

In the upper layers, the mean flow is nearly barotropic, so that we can estimate F_B by taking $(\overline{u} - \overline{u}_0) \sim 30$ ms^{-1}. This formula gives a strong gravity wave drag, of the order of 5 ms^{-1} per day. This would correspond to a Rayleigh drag with a characteristic time scale of 6 days.

Taking into consideration our limited knowledge of the gravity wave emission mechanism and the gravity wave spectra these mechanisms will generate, we did not find it useful to incorporate in our model the parametrization of their drag as described by F_B, and we have kept a simple Rayleigh friction as our drag term. For one thing, the mean flow being nearly barotropic above two scale heights, the parametrization of Holton (1982) is equivalent to a Rayleigh damping with an appropriate drag coefficient, so that the results will probably not depend qualitatively on the form of the parametrization.

The above remarks just indicate that gravity wave breaking is a mechanism worth considering with more elaborate models. In our models we have also considered highly idealistic situations with simple atmospheric parameters. A forcing mechanism such as penetrative convection might also excite resonant modes (Flasar and Gierasch, 1987), the nature of which will depend on the precise static stability profile, which is not well known.

VITA

Yvan Joseph Orsolini was born on February 2, 1961 in Charleroi, Belgium and graduated from the Saint-Michel high school in 1978. He received the degree of Licence en Sciences Physiques (option théorique) from the Free University of Brussels in 1983. He entered the University of Illinois at Urbana-Champaign in 1984 from which he graduated in 1986 with a M.S. in Atmospheric Sciences. He then joined the Geophysics Program at the University of Washington. From September to December 1989, he was a research assistant at the NATO Undersea Research Centre in La Spezia, Italy. In 1990, he was awarded the Johnston Memorial Fellowship of the Geophysics Program.

63 TH 31365 05/26/92
234/68 43659 CPP IDI